Program and Abstract Volume

LUNAR AND PLANETARY INSTITUTE

LPI Contribution No. 1552

SECOND INTERNATIONAL PLANETARY DUNES WORKSHOP:

Planetary Analogs — Integrating Models, Remote Sensing, and Field Data

May 18–21, 2010

Alamosa, Colorado

Sponsors

Lunar and Planetary Institute
NASA's Mars Exploration Program

Convener

Timothy Titus
U.S. Geological Survey

Scientific Organizing Committee

Timothy Titus
U.S. Geological Survey
Mary Bourke
Planetary Science Institute
Lori Fenton
NASA Ames Research Center
Rose Hayward
U.S. Geological Survey
Nick Lancaster
Desert Research Institute
Andrew Valdez
Great Sand Dunes National Park

Lunar and Planetary Institute 3600 Bay Area Boulevard Houston TX 77058-1113

LPI Contribution No. 1552

Compiled in 2010 by
LUNAR AND PLANETARY INSTITUTE

The Lunar and Planetary Institute is operated by the Universities Space Research Association under a cooperative agreement with the Science Mission Directorate of the National Aeronautics and Space Administration.

Abstracts in this volume may be cited as

Author A. B. (2010) Title of abstract. In *Second International Planetary Dunes Workshop: Planetary Analogs — Integrating Models, Remote Sensing, and Field Data*, p. XX. LPI Contribution No. 1552, Lunar and Planetary Institute, Houston.

This volume is distributed by

ORDER DEPARTMENT
Lunar and Planetary Institute
3600 Bay Area Boulevard
Houston TX 77058-1113, USA
Phone: 281-486-2172
Fax: 281-486-2186
E-mail: order@lpi.usra.edu

A limited number of copies are available for the cost of shipping and handling.
Visit the LPI Online Store at https://www.lpi.usra.edu/store/products.cfm.

ISSN No. 0161-5297

Preface

This volume contains abstracts that have been accepted for presentation at the Second International Dunes Workshop: Planetary Analogs — Integrating Models, Remote Sensing, and Field Data, May 18–21, 2010, Alamosa, Colorado.

Administration and publications support for this meeting were provided by the staff of the Publications and Program Services Department at the Lunar and Planetary Institute.

Contents

Program

Tuesday, May 18, 2010
AEOLIAN GRAINS: SOURCES AND TRANSPORT
8:30 a.m. Rio Grande/Santa Fe Room

Chairs: **Margaret H. Redsteer**
Briony Horgan

8:30 a.m. Fenton L. K. *
Welcome and Introduction

8:45 a.m. Bourke M. *
Keynote: *Developments and Emerging Trends in Planetary Dune Studies*

9:00 a.m. Sullivan R. * Geissler P. Herkenhoff K. Landis G. Vaughan A.
Mars Exploration Rover Observations of Sand Saltation and Sand-Sized Dust Aggregates **[#2036]**

9:30 a.m. Vixie G. * Barnes J. W.
Sand Sources and Transport Mechanics on Titan **[#2031]**

10:00 a.m. Scheidt S. P. * Lancaster N. Ramsey M. S.
Sand Composition of the Gran Desierto: A Terrestrial Analogue for Thermal Infrared Imaging and Spectroscopy Techniques **[#2010]**

10:30 a.m. Aleinikoff J. N. Muhs D. R. *
Isotopic Evidence for South Platte River and Bedrock Sources for Eastern Colorado Dune Fields **[#2006]**

11:00 a.m. Tirsch D. * Craddock R. A. Jaumann R.
Spectral Analysis of Dark Dunes in Ka'u Desert (Hawai'i): Initially Altered Terrestrial Analogs to Dark Dunes on Mars **[#2022]**

11:30 a.m. DISCUSSION

12:00 p.m. LUNCH

Tuesday, May 18, 2010
DUNES, WATER AND ICE
1:00 p.m. Rio Grande/Santa Fe Room

Chairs: **Timothy Titus**
Charles Bristow

1:00 p.m. Putzig N. E. * Mellon M. T. Herkenhoff K. E. Phillips R. J. Davis B. J. Ewer K. J.
Thermal Anomaly in Martian North Polar Erg Likely Due to Near-Surface Ice **[#2037]**

1:30 p.m. Wood S. E. * Griffiths S. D. Bourke M. C.
Subsurface Thermal Effects of Dune Migration on Mars: Implications for Ground Ice Stability **[#2035]**

2:00 p.m. Kreslavsky M. A. *
Characteristic Time Scales of Dune-related Processes in Polar Regions of Mars **[#2033]**

2:30 p.m. Diniega S. * Byrne S. Glasner K.
Connecting Aeolian and Nivean Processes with Martian Polar Dune Morphology **[#2005]**

3:00 p.m. BREAK

3:30 p.m. Bristow C. S. * Augustinus P. Jol H. M. Wallis I. C. Rhodes E.
Topographic Steering and Dune Morphology in a Polar Desert, Analogues for Mars from the McMurdo Dry Valleys of Antarctica **[#2007]**

4:00 p.m. Horgan B. * Bell J. F. III Bourke M. C.
Ice and Sulfate Induration in the Martian North Polar Sand Sea **[#2023]**

4:30 p.m. Gardin E. * Bourke M. C. Allemand P. Quantin C.
Bright Footprints Suggest Possible Dune Migration on Mars **[#2032]**

5:00 p.m. DISCUSSION

5:30 p.m. FIELD TRIP REVIEW

6:00 p.m. POSTER REVIEWS

Tuesday, May 18, 2010
POSTER SESSION: PLANETARY DUNES:
MIGRATION, MINERALOGY, MODELING, MORPHOLOGY, AND ANALOGS
7:00 p.m. Alamosa Room

Bridges N. T.
Martian Bedforms Changes and Textures as Seen by HiRISE **[#2040]**

Kochemasov G. G.
Eolian Features on Mars and Titan: Resemblance and Difference **[#2001]**

Lorenz R. D.
Dunes as Streamlines: Modeling Topographic Diversion and Blocking of Linear Dunes with Potential Flow Theory **[#2019]**

Scheidt S. P. Lancaster N.
Sensitivity of Automatic Determination of Sand Transport Direction and Rate to Dune Morphology in the Namib Sand Sea **[#2024]**

Bogle R. C. Vogel J. M. Velasco M. Redsteer M. H.
Sand Dune Migration Monitoring on the Navajo Nation, Southwestern United States **[#2012]**

Hayward R. K. Zimbelman J. R. Fenton L. K. Titus T. N. Cushing G. E.
Mars Analog: Grand Falls Dune Field, Arizona **[#2004]**

Hooper D. M. McGinnis R. N. Necsoiu M. Dinwiddie C. L. Basu D.
Volcaniclastic Aeolian Deposits at Sunset Crater Volcano, Arizona: Applications for Martian Analogs **[#2011]**

Cardinale M. Komatsu G.
Aeolian Events in the Moreux Crater: Analysis of Diverse Dune Fields **[#2017]**

Cornwall C. Titus T. N.
Compositional Analysis of 21 Martian Equatorial Dune Fields and Possible Sand Sources **[#2016]**

Mangold N. Baratoux D. Arnalds O. Bardintzeff J.-M. Platvoët B. Grégoire M. Pinet P.
Segregation of Olivine Grains in Volcanic Sands in Iceland — Implications for Mars **[#2008]**

Bristow C. S. Aston A.
Morphology, Petrology and Structure of Basaltic Volcanic-Clastic Sand Dunes at Kvensödull in Iceland **[#2002]**

Titus T. N. Cushing G. E.
Thermal Inertia Characterization of Possible Niveo-Aeolian Formation in Oympia Undae, Mars **[#2034]**

Dinwiddie C. L. McGinnis R. N. Jr. Stillman D. E. Hooper D. M. Michaels T. I.
Bjella K. L. Grimm R. E. Necsoiu M.
Sand, Wind, and Ice: Mars Analog Aeolian Studies at the Great Kobuk Sand Dunes, Alaska **[#2029]**

Rudoy A. N. Chernomorets S. S.
Giant Current Ripple Marks: Remote Sensing of New Locations on the Earth **[#2009]**

Thursday, May 20, 2010
BEDFORM ACTIVITY I: (NON)DETECTION AND MONITORING
9:00 a.m. Rio Grande/Santa Fe Room

Chairs: **Lori Fenton**
Mark Bishop

9:00 a.m. Redsteer M. H. * Bogle R. Vogel J.
Active Dune Fields of the Navajo Nation, Southwestern United States **[#2039]**

9:30 a.m. Chojnacki M. * Burr D. M. Moersch J. E.
Evidence of Bed Form Deflation, Modification and Transport at Endeavour Crater, Meridiani Planum, Mars, from Orbital Observations **[#2028]**

10:00 a.m. Silvestro S. * Fenton L. K. Vaz D. A. Bridges N. Ori G. G.
Ripple Migration on Active Dark Dunes in Nili Patera (Mars) **[#2003]**

10:30 a.m. Kerber L. * Head J. W. III
A Progression of Induration in Medusae Fossae Formation Dunes **[#2027]**

11:00 a.m. DISCUSSION

12:00 p.m. LUNCH

Thursday, May 20, 2010
BEDFORM MORPHOLOGY: ENVIRONMENTAL CONTROLS AND PATTERNS
1:00 p.m. Rio Grande/Santa Fe Room

Chairs: **Mary Bourke**
Nick Lancaster

1:00 p.m. Lancaster N. *
Assessing Dune-forming Winds on Planetary Surfaces — Application of the Gross Bedform Normal Concept **[#2030]**

1:30 p.m. Reffet E. * Fulchignoni M.
Planetary Dunes Analogs Using Laboratory Experiments and Numerical Simulations **[#2025]**

2:00 p.m. Radebaugh J. * Savage C. J. Lorenz R. D. Lancaster N. Wall S. D. Stofan E. R. Lunine J. I. Kirk R. L. Le Gall A. Farr T. G.
Dunes on Titan: Wind Directions, Behavior, and Evolution from Statistical and Morphological Studies **[#2038]**

2:30 p.m. Lorenz R. D. * Radebaugh J. Claudin P. Andreotti B. Tokano T.
Huygens Boundary Layer Data Explain the ~3 km Spacing of Titan's Dunes **[#2014]**

3:00 p.m. BREAK

3:30 p.m. Zimbelman J. R. * Williams S. H. Johnston A. K.
Cross-Sectional Profiles of Ripples, Megaripples, and Dunes: A Method for Discriminating Between Formational Mechanisms **[#2013]**

4:00 p.m. Shockey K. M. * Zimbelman J. R.
Transverse Aeolian Ridges as Seen in HiRISE Images **[#2018]**

4:30 p.m. Lorenz R. D. * Bridges N. T. Rosenthal A. A.
Elevation Dependence of Bedform Wavelength on Tharsis Montes, Mars **[#2015]**

5:00 p.m. DISCUSSION

Friday, May 21, 2010
BEDFORM ACTIVITY II: IMPROVING (NON)DETECTION AND MONITORING
8:30 a.m. Rio Grande/Santa Fe Room

Chair: Lori Fenton

8:30 a.m. Bishop M. A. *
Obstacle Marks: Evidence of Variable Wind Erosion and Sediment Transport, Hellespontus, Mars **[#2020]**

9:00 a.m. Bandeira L. * Marques J. S. Saraiva J. Pina P.
Martian Dune Fields Detection by Automated Approaches **[#2021]**

9:30 a.m. Michaels T. I. *
Obtaining Relevant Atmospheric Contexts for Dune Studies **[#2041]**

10:00 a.m. Fenton L. K. * Michaels T. I.
Modeling Aeolian Erosion Potential on Mars with the MRAMS LES **[#2026]**

10:30 a.m. DISCUSSION

11:00 a.m. SESSION REVIEW

11:30 a.m. TOP 10 THINGS TO TAKE AWAY

12:00 p.m. MEETING ADJOURNS

ISOTOPIC EVIDENCE FOR SOUTH PLATTE RIVER AND BEDROCK SOURCES FOR EASTERN COLORADO DUNE FIELDS. J.N. Aleinikoff[1] and D.R. Muhs[2], [1]U.S. Geological Survey, MS 963, Box 25046, Federal Center, Denver CO 80225 (jaleinikoff@usgs.gov), [2]U.S. Geological Survey, MS 980, Box 25046, Federal Center, Denver, CO (dmuhs@usgs.gov).

Introduction: One of the requirements for the development of sand dunes and sand seas is an ample supply of loose, unconsolidated sand. Many investigators [1], [2], [3], [4], [5] have emphasized the importance of fluvial sediments as sources for dune growth, because such particles are loose, well-sorted, and available for eolian entrainment from channel bars and at least temporarily unvegetated floodplains. Less certain is the role that direct eolian entrainment of bedrock sources can play in dune origins. However, for planetary geologic studies, this process is important to consider because fluvial sources may not be available in extraterrestrial settings. Here we report new isotopic and geochemical data on the complex role played by the South Platte River and bedrock sources in the origin of dune fields in northeastern Colorado.

Study Area: Holocene and Pleistocene eolian sand is extensive in northeastern Colorado and covers an estimated 12,000 km^2. In the westernmost part of this region, two dune fields are situated north (Greeley) and south (Fort Morgan) of the South Platte River (Fig. 1). Winds are dominantly from the northwest at present and apparently were similar during much or all of the Holocene. Thus, we hypothesize that the Fort Morgan dune field originated from South Platte River sediments. The origin of the Greeley dune field is less apparent because of its location upwind of the South Platte River. Nevertheless, late Holocene paleowinds in this dune field were from the northwest, similar to the Fort Morgan dune field. A possible source for the Greeley dune field is sand from the Cretaceous Laramie Formation, a mineralogically mature sandstone that crops out extensively to the northwest of the dunes [6]. We test this hypothesis here.

Methods: Detrital zircons were separated from samples of eolian sands of the Fort Morgan and Greeley dune fields and from fine-to-medium sands of the South Platte River and the Laramie Formation. U-Pb microanalysis by sensitive high resolution ion microprobe (SHRIMP) provides ages of individual zircons. The spectrum of U-Pb ages of detrital zircons from each provenance is a "fingerprint" that can be used to identify source(s) of sand in dune fields [7]. In addition, we conducted major element geochemical analyses of sands from the source sediments and dune fields, which reflect the bulk mineralogy in each sediment body.

Results: U-Pb ages of zircons from the South Platte River and Laramie Formation (two potential sources) are distinctive (Fig. 2). The South Platte River and tributaries head in Precambrian crystalline rocks of the Front Range. As expected, South Platte River sediments contain zircons derived from the three major Precambrian igneous rock suites that make up much of the Front Range, including rocks that are ~1.7 Ga (Routt suite), ~1.4 Ga (Berthoud suite), and ~1.0 Ga (Pikes Peak batholith). Tertiary-age zircons are also present. In contrast, the Laramie Formation lacks zircons derived from the Pikes Peak batholith, but does contain 1.7 Ga, 1.4 Ga, and Tertiary zircons. Zircons from the Fort Morgan dune field have an age spectrum that is very similar to ages of zircons from South Platte River sands, confirming the fluvial source of this dune field. The Greeley dune field, however, has a zircon age spectrum that more closely matches that of the Laramie Formation, highlighted by the lack of ~1.0 Ga zircons.

Mineralogical data, derived from major element geochemistry, support the interpretations of dune field origins from the U-Pb zircon ages (Fig. 3). On geochemical plots, SiO_2 is a proxy for quartz, and $K_2O+Na_2O+Al_2O_3$ is a proxy for plagioclase and K-feldspar, the dominant minerals in most dune fields. Although eolian sand from the Fort Morgan dune field overlaps the compositional field of the Laramie Formation slightly, most of the dune samples plot well within the field of feldspar-rich South Platte River sands. In contrast, sands from the Greeley dune field all plot within the field for the quartz-rich Laramie Formation and outside the field for the South Platte River. Sands from both dune fields fall outside the range of the feldspar-rich Ogallala Formation, another potential bedrock source.

Discussion and Conclusions: Results presented here show that adjacent dune fields that formed at the same time and under similar wind conditions can have very different origins. The Fort Morgan dune field was derived from a major fluvial source, the South Platte River that is immediately upwind, whereas the Greeley dune field apparently received little or no input from the South Platte. The Laramie Formation apparently was the major source for the Greeley dune field, thus documenting that bedrock sources can supply sediment to eolian sand bodies. Where we have examined it in the field, the Laramie Formation is

weakly consolidated and often weathered to residuum, which may account for the ease of its entrainment. We note that the South Platte River played a role in the origin of the Greeley dune field in an opposite sense of the Fort Morgan dune field. Downwind growth and migration of the Greeley dune field may have been stopped by the presence of the South Platte River valley. Filling of river valleys and even formation of dune dams have both been documented in Nebraska [8]. In northeastern Colorado, however, while the South Platte River served as a source for the Fort Mogran dunes, it supplied little or nothing to the Greeley dunes. Identification of a non-fluvial source for a dune field (Greeley) is unusual and has significance for dune fields on other planets, where fluvial sources either do not exist or have not been capable of supplying sediment for a long time.

References: [1] Cooke, R. et al. (1993) *Desert Geomorphology*, UCL Press Limited, London, 526 pp. [2] Fryberger, S.G. and Ahlbrandt, T.S., 1979) *Zeit. Geomorph., 23*, 440–460. [3] Pye, K. and Tsoar, H. (1990) *Aeolian Sand and Sand Dunes*, Unwin Hyman, London, 396 pp. [4] Wilson, I.G. (1973) *Sed. Geol., 10*, 77-106. [5] Muhs et al. (2003) *Quat Int.,* 104, 3-18. [6] Muhs et al. (1996) *Geomorph*., 17, 129-149. [7] Aleinikoff et al. (2008) *GSA Bull., 120*, 1362-1377. [8] Muhs et al. (2000) *Quat. Res., 53*, 214-222.

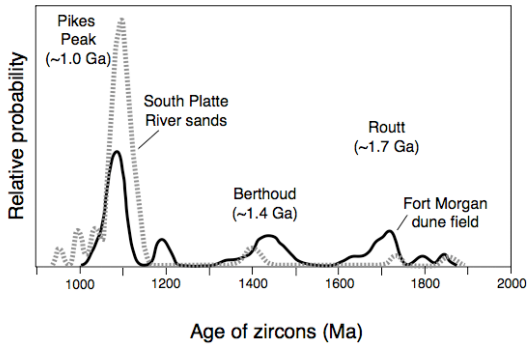

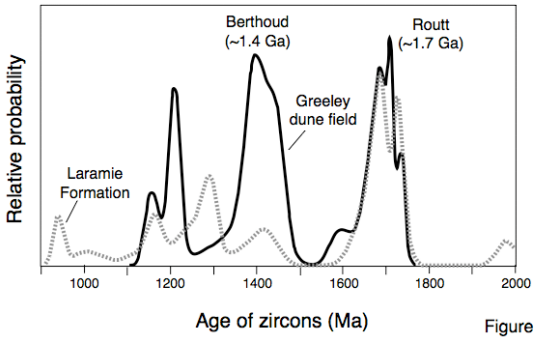

Figure 2

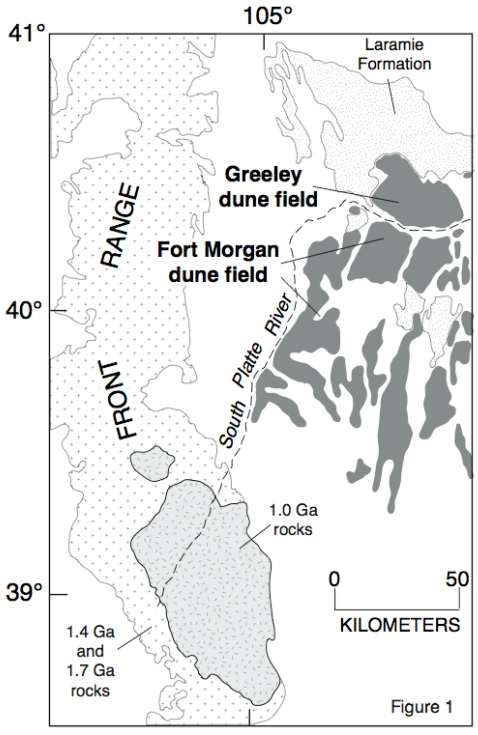

Figure 1

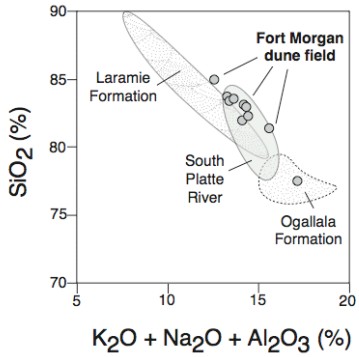

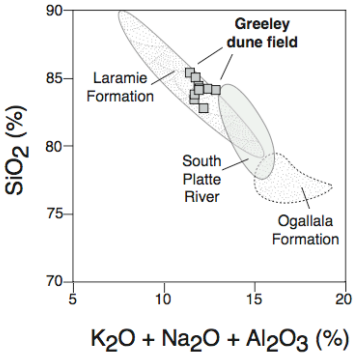

Figure 3

MARTIAN DUNE FIELDS DETECTION BY AUTOMATED APPROACHES. L. Bandeira[1] , J. S. Marques[2], J. Saraiva[1] and P. Pina[1], [1]CERENA, Instituto Superior Técnico, Av. Rovisco Pais, 1049-001 Lisboa, Portugal (lpcbandeira@ist.utl.pt, jose.saraiva@ist.utl.pt, ppina@ist.utl.pt), [2] ISR, Instituto Superior Técnico, Av. Rovisco Pais, 1049-001 Lisboa, Portugal (jsm@isr.ist.utl.pt).

Introduction: Dunes are the most frequent aeolian features on the Martian surface, and their study contributes to the understanding of the interactions between the atmosphere and the surface of the planet, of the way the climate has evolved along the history of Mars and of how it works currently [1]. At the time of writing, the catalogue of dune fields identified on the surface of Mars by the Mars Dune Consortium [2] contains information about the area between latitudes 65ºS and 90ºN, which is available online in a geographical database, the MGD[3]-Mars Global Digital Dune Database [3, 4]. This represents many hours of manual detection and mapping of aeolian features on thousands of images of the surface of Mars. However, many small fields have yet to be identified and studied in detail.

The development of an automated method for the delineation and characterization of dune fields, capable not only of mapping them on remotely sensed images at different scales and moments in time, but also of detecting changes in the characteristics of these dynamic aeolian features, would thus constitute an important improvement in their study. In the last years, some techniques to automatically detect structures on planetary surfaces have been tried, but, so far, only the field of impact crater studies has achieved some maturity. When it comes to aeolian features, there is as yet no automated approach to deal with their identification, although we have already performed some preliminary tests to verify the adequacy of different automated methods on the detection of ripples [5] and sand dunes [6-7].

Thus, our objective is to use recent and up-to-date machine learning methodologies for the detection of aeolian dunes on remotely sensed images of Mars. This work is partly inspired on some of our previous strategies and algorithmic sequences used for automated crater detection [8].

Methodology: For the purpose now considered, we have selected two types of features that work best in the extraction of the directional and periodic characteristics of the dunes (gradient and histogram-of-oriented-gradients [9] features), and which were both used on Boosting [10] and SVM-Support Vector Machine [11] classifiers to indicate if a given region of the image contains dunes. The performance of those methods is evaluated with a set of high spatial resolution images which reflect the diversity of Martian dune types. A detailed description of these features and of the classifiers can be consulted in [7].

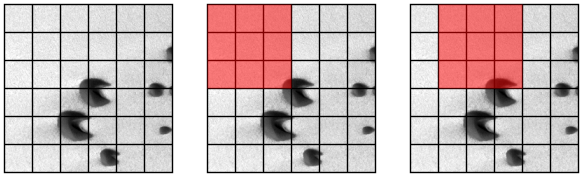

Fig. 1. Principle of evaluation of an image: Tiling in (a) cells and (b) blocks (3x3 cells), in red; (c) Block displacement with overlapping. This region corresponds to a sample of image E02-01086 [image credits: MSSS/NASA/JPL].

Experimental results: To test our approach, we have selected a set of 20 remotely sensed images captured by the Mars Orbiter Camera of the Mars Global Surveyor probe, in N/A mode, from different locations on the planet, covering a total area of about 1320 km^2 and that are representative of the diversity of the most frequent type of dunes (barchan). For each image we constructed ground-truth information, by manually delineating the dunes therein contained, thus indicating the 'dune' and 'not-dune' regions. In the tiling of the ground-truth into cells only the ones containing more than 30% of dune area were considered as 'dune', whereas the cells with less than 10% of dune area were considered as 'not-dune'. The cells with dune areas comprised in the interval 10-30% were not considered.

Every classifier was tested with each of the set of features using a 5-fold cross-validation, i.e., the total number of image blocks was divided into five subsets of the same size: four of them were used for training, the remaining one was used for testing. This procedure was repeated five times, so that each subset is used once for testing.

The performance of each classifier with each set of features is evaluated through the computation of the probabilities of false negatives ($p_{FN} = FN/(FN+TP)$), false positives ($p_{FP} = FP/(FP+TN)$) and of a global error ($p_{error} = p_N \cdot p_{FP} + p_P \cdot p_{FN}$), where FN stands for the number of false negative blocks, TN the number of true negative blocks, FP the number of false positive blocks, TP the number of true positive blocks, N the total number of negative blocks and P the total number of positive blocks.

The classification output is illustrated in Fig. 2 with two distinct MOC images. The overall performances obtained for the whole set of images are very good, with the majority of situations presenting probabilities of error (p_{error}) below 0.025.

Conclusions and future work: The major conclusion put forth is the adequacy of automated methods to deal with the diversity of sand dunes on the Martian surface, since many correct detections with significant performances were achieved. Although a set of powerful features and classifiers were successfully used on representative samples of the large diversity of Martian dune fields, we must keep in mind that this is only a preliminary study. We have dealt with dune fields composed by individuals of different sizes, shapes and densities in distinct illumination conditions, but we are aware that many more different situations will have to be faced, namely considering the scale and the diversity of the Martian landscape where many other geomorphological features can and will sometimes be present. Nonetheless, we believe that the adaptive and learning nature of the methods we are using will be able to deal with those different circumstances.

In future work we intend to greatly expand the datasets by incorporating images of every type of Martian dunes and testing on them the approaches we have employed here; we will also test additional types of features and classifiers. Moreover, and with the ultimate goal of making available a robust tool to be used in the cartography of Martian dunes at a planetary scale, we also intend to automatically classify the Martian dunes according to the scheme used in the classification of analogue terrestrial structures [13].

References: [1] Greeley R. et al. (2001) *Spa. Sci. Rev.* 96, 393-404. [2] Hayward R. K. et al. (2007) JGR, 112, E1107. [3] Hayward R. K. et al. (2008) Dunes2008 Abs. # 7013. [4] Hayward R. K. (2010) *LPS XLI* Abs. # 1109. [5] Pina et al. (2004) *LPS XXXV*, abs # 1621. [6] Bandeira et al. (2009) *LPS XL* Abs. # 1288. [7] Bandeira et al. (2010) *LNCS* (in press). [8] Martins R. et al. (2009) *IEEE GRSL* 6(1), 127-131. [9] Dalal N., Triggs B. (2005) *CVPR2005* 886-893, IEEE Press. [10] Viola P., Jones M. (2004) *Int. J. Comp. Vis.* 57(2), 137–154. [11] Vapnik V. N. (1995) *The nature of statistical learning theory*, Springer. [12] Joachims T. (2000) *ICML'2000* 431-438, Morgan Kaufmann Pub. [13] McKee E. D. (1979) *A study of global sand seas*, 1-19, University Press of the Pacific.

Acknowledgements: This work was partially supported by FCT Portugal under the pluriannual fundings of CERENA and ISR. JS (SFRH/BD/37735/2007) and LB (SFRH/BD/40395/2007) acknowledge financial support by FCT Portugal.

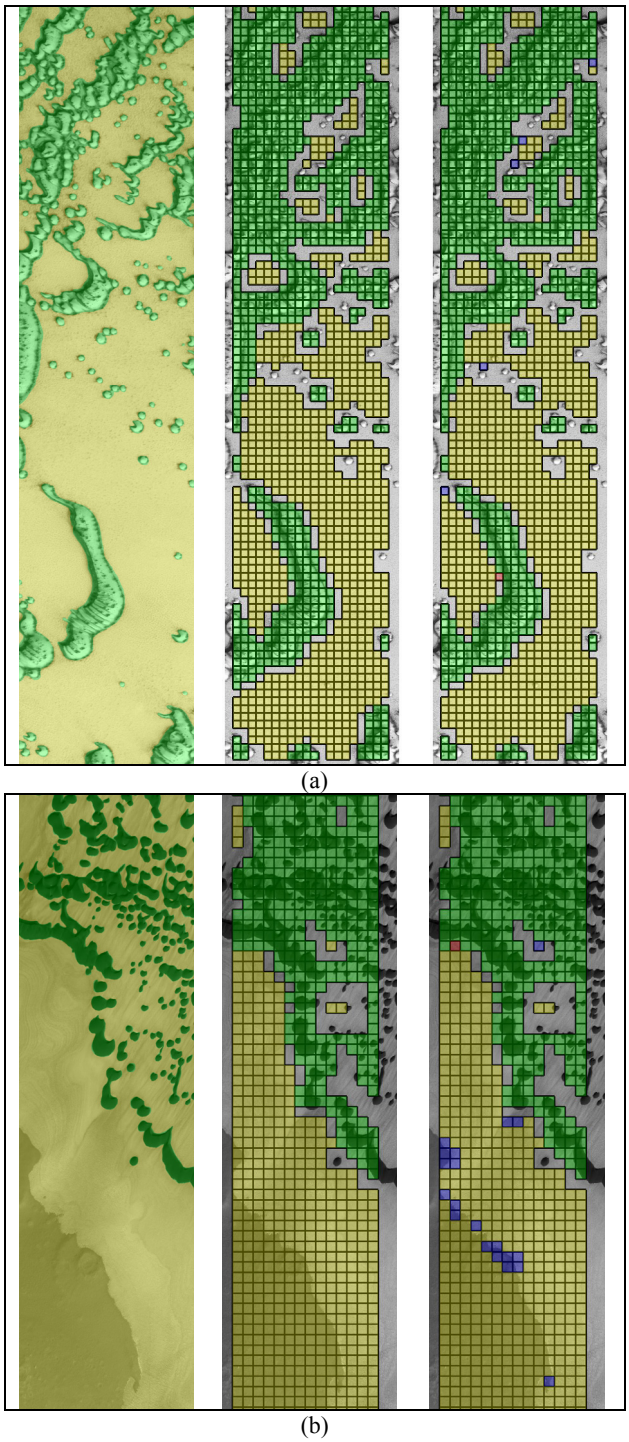

Fig. 2. Examples of automated dune classification on parts of the images: (a) S01-00925 and (b) R17-00333 (*TP* in green, *TN* in yellow, *FN* in red and *FP* in blue). The images correspond to: (left) input with overlapping of manual ground-truth; (center) ground-truth tiling in cells; (right) output of the classifier [image credits: MSSS/NASA/JPL].

OBSTACLE MARKS: EVIDENCE OF VARIABLE WIND EROSION AND SEDIMENT TRANSPORT, HELLESPONTUS, MARS. Mark A. Bishop[1,2] [1]Barbara Hardy Centre [Terrain Analogue Understanding (TAU) research], School of Natural and Built Environments, University of South Australia, Adelaide, SA, 5000, Australia, mark.bishop@unisa.edu.au [2]Planetary Science Institute, 1700 E. Fort Lowell, Suite 106 Tucson, AZ 85719-2395, USA, bishop@psi.edu.

Introduction:
Obstacle marks, specifically current crescents [1] or scour flutes formed by aeolian erosion, have not been previously identified from orbit on Mars. Apart from the recognition of scour zones around boulders at the Viking 1 and Mars Pathfinder sites [2] and at 'Home Plate' during the traverse by Mars Exploration Rover (MER) Spirit into the Columbia Hills [3], no further appraisal of such features has occurred. However in a recent acquisition from the Extended Science Phase (ESP) for the High Resolution Imaging Science Experiment (HiRISE) camera, images of an unnamed intracrater dune field within the Hellespontus region have shown innumerable scour flutes around fine and medium grade blocks [4]. The types, relative numbers and distributions of scour features can be used collectively by proxy to determine the modes of surface wind-direction and pathways of sediment transport across the crater floor. It is therefore the purpose of this letter to demonstrate the feasibility of meter-scale aeolian current crescents as indicators of recent wind activity (erosion and transport) within an intracrater setting in the Hellespontus region of Mars.

Methods:
From a random selection of blocks and scours (n = 124) across HiRISE image ESP_016036_1370, feature outlines were digitized using ArcGIS 9.3® (Fig. 1). This platform allowed for the determination of centroids for each block and the subsequent measurement of scour orientation (azimuth) from these. The sample for each of U-, R- and O-type taxonomies was 61%, 32% and 7%, respectively. For those scours of U-type morphology (n = 74) the angle of mid-scour was plotted upon a circular histogram and the circular statistics for reference direction and dispersion of modal groups were calculated (Fig. 2).

Results:
Data from the HiRISE camera offers an orbital perspective of Mars at a spatial resolution (25.5 cm/pixel) that capably identifies large-scale (mega-) ripples and scour around obstacles such as boulders and blocks (Fig. 1). Image ESP_06036_1370 comprises an intracrater dunefield (42.7°S, 38.0°E) that shows a wealth of sedimentological features, in particular, aeolian scours. The sediment-limited, block strewn intracrater setting offers an ideal environment in which obstacle marks can form. Most scours identified in this sample cluster into two localities.

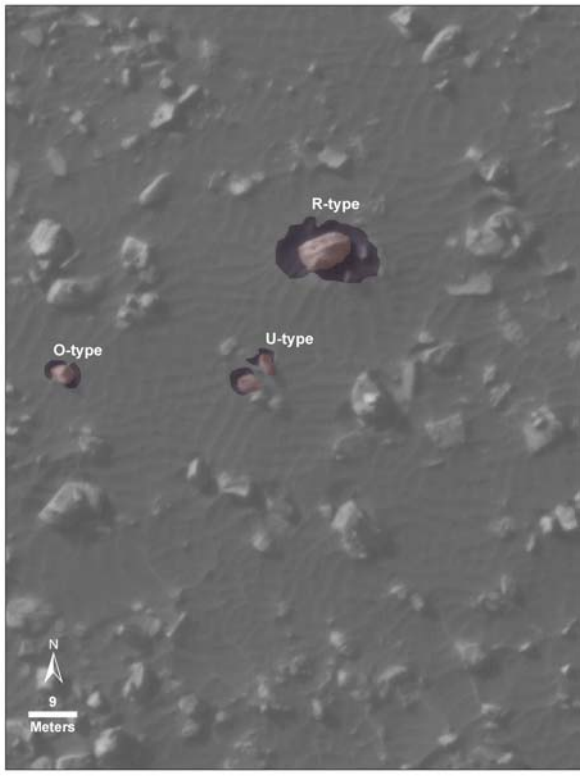

Fig. 1. Scour types (purple outline) across the block laden floor of an unnamed crater in Hellespontus (Ls = 29.8°, southern autumn). The taxonomy of U-, O-, and R-type scours recognises unidirectional, oscillatory (reversing) and rotational (multi-directional) air flow, respectively (adapted from Allen [5]). (Image: ESP_06036_1370_RED, NASA/JPL/University of Arizona).

The largest groups occur in the north-west of the image, where block fields coexist with 'patches' of unconsolidated aeolian sediment, while a second grouping occurs upon the interdune and lower plinths of dunes in the south-east. Although numerous scour flutes have occurred across the region; a ubiquitous wind current moves from the north-west producing the zone of widest and deepest scour. The statistics for scour distribution have collectively shown that U-type forms are orientated with a mean vector of 326° (median of 322°). The null hypothesis of distribution

regularity is rejected, as a high value (0.79) for the length of the mean vector was determined. High length values within the theoretical range (0, 1) imply the sample to be clustered closely around the mean [6]. This observation is further supported by the sample's circular variance (V) where $0 \leq V \leq 1$, and a small value ($V = 0.21$) as found here, implies the existence of a concentrated distribution. Furthermore, the statistic of concentration ($\kappa = 2.75$) where uniformity is shown by $\kappa = 0$, also endorses an increasing concentration about the reference direction [6]. Simply, the distribution of U-type current crescents is not isotropic, but recognizes a preferred orientation.

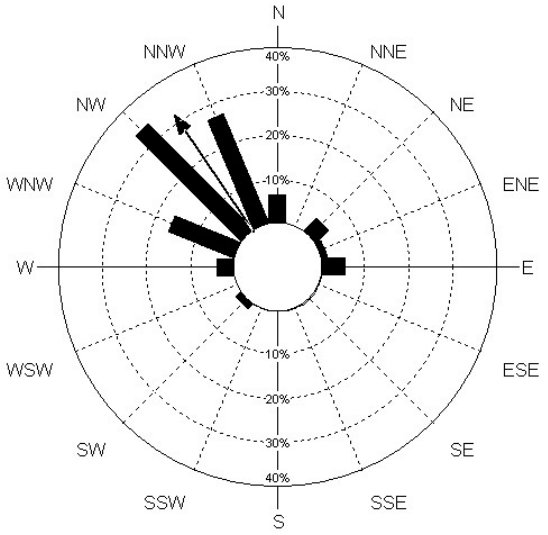

Fig. 2. Circular histogram showing the reference direction (arrow) and modal distribution of U-type scours.

Discussion:

The overarching character of the dune field is crescentic, and exhibits a transverse morphology. However it is the linear-like characteristic of the dune field which best gives a sense of a bi-modal wind system at the regional scale. The preferred orientation of the U-type scours is normal from the direction of the dunes' leeward slopes, hence direction of migration, and implies that the dunes have formed under winds that are primarily from the south-west. The southern portion of the dunefield also shows a suite of ripple trains which are oriented both parallel and orthogonal to the direction of the dunes. The dominance of the north-westerly reference direction for the scour flutes, as well as the south-easterly orientation of the dunes, and corresponding orientations of large-scale ripples supports the existence of two major modes of air flow capable of significant sand transport. In addition, the dominance of a preferred orientation for U-type scours infers that substantial surficial erosion and sediment transport occurs towards the south-east. Accordingly, this may explain why many of the dunes are relatively low, symmetrical forms with poorly developed slip-faces, and in part, a transitional morphology between crescentic and longitudinal.

Conclusions:

The orientation of U-type scour flutes across the intracrater dunefield indicates a dominant north-westerly air stream that is not identified by dune orientation. The coexistence of bedforms (dunes and ripples) and scour features with both equivalent and contrasting orientations implies that the intracrater wind regime has two major directions, one that is north-westerly, and the other south-westerly. Furthermore, the considerable numbers of R-type scours as well as the orientation of ripple trains and their interference patterns denote the likely interaction of transitional winds, either seasonal or diurnal.

In the absence of 'in-field' measurements of wind directions and strengths, surficial sedimentary structures such as scour flutes, offer detailed data from which planetary boundary conditions at the surface-air interface can be better interpreted. Moreover, this data can be used for conducting risk analyses for the siting and operation of landers and rovers on planetary surfaces. Monitoring studies of scour features and ripples would also better define aeolian erosion rates and sediment mobility for Mars, than does dune monitoring alone.

References: [1] Peabody F.E. (1947) *J. Sediment. Petrol.* 17, 73-76. [2] Greeley R. et al. (2002) *JGR* 107 (E1) 5005. [3] Greeley R. et al. (2008) *JGR*, 113, E06S06. [4] Blair T.C. and J.G. McPherson (1999) *J. Sediment. Petrol.* 69 (1) 6-19. [5] Allen J.R.L. (1984) *Sedimentary Structures: Their Character and Physical Basis*. Developments in Sedimentology, Amsterdam: Elsevier. [6] Fisher, N.I. (1995) *Statistical analysis of circular data*. Cambridge University Press.

SAND DUNE MIGRATION MONITORING ON THE NAVAJO NATION, SOUTHWESTERN UNITED STATES. R. C. Bogle[2], J. M. Vogel[2], M. Velasco[2], and M. H. Redsteer[2] [2]U.S. Geological Survey, 2255 N Gemini Drive, Flagstaff, AZ 86001 rbogle@usgs.gov

Native Americans of the southwest United States live on ecologically sensitive arid to semiarid lands, with increasing temperatures, decreasing precipitation, and fluctuating wind regimes transforming the landscape in ways that negatively impact its inhabitants. Annual rainfall in the western Navajo Nation has fallen below 80mm/year during the recent drought, directly contributing to an increasing areal extent of sand susceptible to mobilization and reactivating formerly stabilized dunes. Reservation housing and road networks are threatened by this increase in dune movement, while native plants and grazing lands are made more vulnerable.

As part of our research effort on the Navajo Nation, we have registered historical aerial photography, dating from the 1950s through the 1980s, to more recent orthorectified aerial photography. Using this collection of georeferenced aerial photographs, along with on-going high precision (+-5mm) GPS surveys, we have mapped the 60 year migration of entire dune fields as well as more recent, high precision, migration rates of smaller dune groups. While migration rates vary widely by year and location, preliminary findings demonstrate that some dunes in the southwest Navajo Nation advanced over 70m between 2007 and 2009.

Additionally, we are developing and testing a variety of methodologies and instruments to facilitate high-temporal precision measurement and monitoring of morphological changes in a dune field. These include: (1) The use of terrestrial LiDAR surveys of sample dunes to create volumetric models of the dunes, accurate to less than a centimeter, several times a year; (2) Establishing an automated digital imaging system, which records daily images as well as captures images of the dunes when wind speed averages exceed saltation thresholds. This imagery will provide us with a record of effects of individual storm events as well as a time-lapse record of dune migration. We are also using the imagery to assess the use of photogrammetric techniques as a low-cost alternative to performing terrestrial LiDAR surveys; (3) Establishing meteorological and climate variability measures through the use of multiple sensor sites in the dune field; and (4) Developing a low-cost alternative to the Sensit sensor that will be capable of recording the number of seconds each day in which particles saltate at various locations in the dune field.

This research, combined with data compiled from co-located weather instruments and other sensors, will provide a more sophisticated understanding of the processes driving dune migration, and provide mitigation options to the challenges that dune migration poses to the Navajo Nation.

MARTIAN BEDFORMS CHANGES AND TEXTURES AS SEEN BY HIRISE

N.T. Bridges, Applied Physics Laboratory, 11100 Johns Hopkins Road, Laurel, MD 20723 (nathan.bridges@jhuapl.edu)

Introduction

HiRISE has been observing Mars in its primary science orbit since November, 2006, during which the full range of seasons in both hemispheres has been documented over 1.5 Martian years. Over 14,000 images have been acquired, showing a wealth of detail and diversity that have provided fundamental data for numerous investigations. Almost all HiRISE images show dunes, ripples, and transverse aeolian ridges (TARs), with over 500 specifically targeted to observe aeolian features. Here we provide a summary of HiRISE studies of bedforms, focusing on evidence or lack thereof for changes and surface textures. Some of this work, in particular the studies of change detection, is a summary of investigations by other researchers, with this abstract intended as a venue for discussion.

Major Themes

Change Detection

Many HiRISE observations have been taken one Mars year or more apart to look for changes in dune and ripple positions. A recent study found that the 2nd order ripples on dunes in Nili Patera moved 2 m in 2.5 months [1]. This represents apparently very rapid movement and is a surprising finding. On Earth, 2nd and 3rd order ripples can form on time scales as short as a day, so the findings that the Nili Patera ripples are moving on such rapid time scales, as opposed to the overall dunes, is consistent. Such movement also agrees with current sand migration in the Columbia Hills, as evidenced by the trend of ventifact abrasion features that are aligned with 2nd order ripples [2].

Evidence for deflation or abrasion of sand (as opposed to migration) is more common. For example, bedforms in Endeavour Crater in Terra Meridiani have been documented to disappear and shrink over a period of 7 years as seen by MOC and then HiRISE [3]. Similarly, MOC data has documented the shrinkage and disappearance of ice-cored dome dunes in the North Polar Erg [4], indicating an active saltation-induced process of sand transport and probably abrasion of ice-cemented sand, perhaps assisted by sublimation of interstitial ice, or a combination of the two. HiRISE images of the same area show no changes over a period of slightly more than 3 years [5]. Combined studies by MER and HiRISE indicate that basaltic sand is currently being blown out of Victoria Crater by northern summer winds, forming the prominent windstreaks projecting north of the crater [5]. Similarly, many HiRISE images show changes in sand-dust patterns , but whether sand or dust is moving cannot be ascertained.

Besides the Nili Patera case, there is no definitive evidence for a change in the position of dune or ripple crests that would indicate migration by the wind. This is consistent with past studies, albeit with lower resolution instruments, that also failed to document any changes [6-8]. It therefore seems that Mars is largely static, but with notable exceptions. A combination of high wind shear, loosely bound particles, and perhaps low particle size are favorable for saltation.

Reticulate Textures: Part Two

A reticulated texture down to scales of a few meters is common in many low thermal inertia regions and has been interpreted as intersecting ripple sets in a thick dust aggregate mantle [9]. Supporting a dust aggregate origin, a “fresh” crater with dark, radial ejecta, shows thick reticulated material in its interior in a recent HiRISE image (ESP_015962_1695). This crater,

located south of Noctis Labynthus in a low thermal inertia area, may be filled with dust aggregates that have accumulated and become trapped. A more enigmatic example is seen in a recent HiRISE image of barchanoid dunes on Arsia Mons (originally identified by MOC) that show a texture confined to the stoss slopes (ESP_016068_1720). If the reticulate texture is redistributed mantle material, the mantle must have been stripped off the non-dune areas. Alternatively, this could represent some sort of sculpted abrasion texture on cemented dunes. More work is needed to assess the full range and characteristics of this texture outside of the Tharsis region that was initially studied.

Note: Figures were removed from this abstract due to file size limitations. They will be presented at the conference.

References [1] Silvestro, S. et al. (2010). *Lunar Planet. Sci. XLI*, 1820. [2] Thomson, B.H. et al. (2008), *J. Geophys. Res., 113*, E08010, doi:10.1029/2007JE003018. [3] Chojnacki et al. (2010), *Lunar Planet. Sci. XLI*, 2326. [4] Bourke, M.C. et al. (2008), *Geomorphology,* 94, 247–255. [5] Bourke, M.C. et al. (2009), *Lunar Planet. Sci. XL*, 1748. [5] Geissler, P.E. et al. (2008), *J. Geophys. Res.*, *113*, E12S31, doi:10.1029/2008JE003102. [6] Edgett, K.S. and M.C. Malin (2000), *J. Geophys. Res., 105*, 1623-1650. [7] Zimbelman, J.R. (2000), *Geophy. Res. Lett., 27*, 106901972. [8] Malin, M.C. and K.S. Edgett (2001), *J. Geophys. Res., 112*. 23,429-23,570. [9] Bridges, N.T. et al. (2010), *Icarus*, doi:10.1016/j.icarus.2009.05.017

Morphology, Petrology and Structure of Basaltic Volcanic-Clastic Sand Dunes at Kvensödull in Iceland

C. S. Bristow[1] and A. Aston[1], [1] Department of Earth and Planetary Sciences, Birkbeck and UCL Joint Research School, Gower Street, London WC1E 6BT c.bristow@ucl.ac.uk

Introduction: Sand dunes with a variety of morphologies have been imaged on the surface of Mars [1, 2, 3]. Dunes on Mars are generally dark hued and their sand is believed to be derived from the erosion of volcanic rocks which due to the geology of Mars is most likely to be composed of basalt [4]. Further studies of Martian meteorites, plus recent data from landers, rovers and remote sensing data confirm that the Martian crust is predominantly composed of basalt with some areas interpreted as andesite or weathered basalt [e.g. 5]. Although Iceland has been identified as a suitable analogue for Mars, and Iceland is reputed to have the world's largest volcaniclastic sand fields [6], there is very little published information on the sand dunes of Iceland. The review by Edgett and Lancaster [4] contains little information on the dune morphology in Iceland and no information on the dune composition.

In this paper we describe the results of a geophysical and petrological investigation of a basaltic volcanic-clastic sand dune in Iceland. The sands are fine to medium grained and poorly sorted. They are composed largely of volcanic glass, average 60%, with around 35% lithic clasts. The percentage of volcanic glass is greater than previously described from other volcanic-clastic dune sands. Despite this difference in composition, the bulk density of the sands is similar to that of desert sands from the Sahara. The dune morphology is influenced by local wind regime as well as the local topography. The dune appears to be barchanoid in planform but lacks a slipface. The lack of a slipface is attributed to the variable wind regime. GPR profiles reveal that the internal structure is dominated by low-angle strata which dip towards the north, confirming that the dune has not had a slipface in the past, and that it has accreted in a northward direction. The east-west alignment of the dune crest and the northward dipping strata indicate that this is a transverse dune. The barchanoid morphology is due to valleys and ridges in the underlying topography that influence the width and thickness of the dune which is wider and thicker within the valleys and narrower and thinner across the ridges.

References:

[1] Hayward, R.K., et al. Mars global digital dune database and initial science results. USGS Open-file report #2007-1158, p.57.

[2] Parteli E.J.R., and Herrmann, H.J., 2007, Dune formation on the present Mars. Physical Review E 76, 041307

[3] Bourke, M., and Goudie, A., 2009, Varieties of barchan dune form in the Namib Desert and on Mars. Aeolian Research.

[4] Edgett, K.S., and Lancaster N., 1993, Volcaniclastic aeolian dunes: terrestrial examples and application to martian sands. Journal of Arid Environments 25, p.271-297.

[5] Mustard, J.F., Poulet, F., Gendrin, A., Bibring, J-P., Langevin, Y., Gondet, B., Mangold, N., Belluci, G., and Altieri, F., Olivine and pyroxene diversity in the crust of Mars. Science 307, p.1594-1597.

[6] Arnalds, O., Gisladottir, F.O., Sigurjonsson, H., 2001, Sandy deserts of Iceland: an overview. Journal of Arid Environments 47, p.359-371.

Topographic Steering and Dune Morphology in a Polar Desert, Analogues for Mars from the McMurdo Dry Valleys of Antarctica C. S. Bristow [1], P. Augustinus [2], H.M. Jol [3], I. Wallis [2], E. Rhodes [4].

[1] School of Earth Sciences, Birkbeck College, University of London, Malet Street, London WC1E 7HX c.bristow@ucl.ac.uk

[2] Department of Geography and Anthropology, University of Wisconsin Eau-Claire, 105 Garfield Avenue, Eau Claire, WI 54702-4004, USA.

[3] School of Geography, Geology and Environmental Science, The University of Auckland, Private Bag 92019, Auckland, New Zealand

[4] Department of Earth and Space Sciences, University of California, Los Angeles, 595 Charles Young Drive East, Box 951567, Los Angeles, CA 90095-1567, U.S.A.

Introduction: The McMurdo Dry Valleys of Antarctica are recognised as one of the best Earth analogues for the surface of the planet Mars due to the low temperatures, lack of liquid water and absence of vegetation. The Victoria Valley is the northernmost of the McMurdo Dry Valleys of Antarctica and contains three areas of sand dunes that demonstrate a strong topographic control on dune morphology and dune migration. The valley is aligned roughly East to West and the local wind regime, which is essentially bimodal, is topographically constrained [1]. Easterly winds blow up the valley from the Ross Sea while westerly föehn and katabatic winds blow down the valley from the polar icecap. The relative strength and duration of these winds, combined with topographic steering and shear against the valley wall, control aeolian sand transport, dune morphology and dune migration within the Lower Victoria Valley. Local changes in the wind regime within the valley are reflected in the dune morphology and the sedimentary structures preserved within the dunes.

Packard Dune Field

The Packard Dune Field is located on the northern side of the Lower Victoria Valley, beneath the Packard Glacier (Fig. 1). It is around 4km long and 0.5km wide covering an area of 2km^2 [2]. The dunes which include barchans, transverse barchanoid, reversing dunes and climbing dunes are up to 13m high. The dune crests are aligned roughly Northeast-Southwest to North-South, with slipfaces facing west in response to the summer winds that blow up the valley from the East [3]. GPR profiles through the dunes shows that net migration is from east to west with many reactivation surfaces formed when the dune is reshaped by the reversing winds [1]. In addition, the reversing wind regime influences the dune morphology with the formation of flat-topped dunes. Optical dating of the Packard dunes indicates that they are up to 1,300 years old. The ages are used to calculate end-point migration rates that vary from 0.05 to 1.3 m/yr [1] but generally less than the rates derived from field measurements and from the analysis of aerial photographs [2].

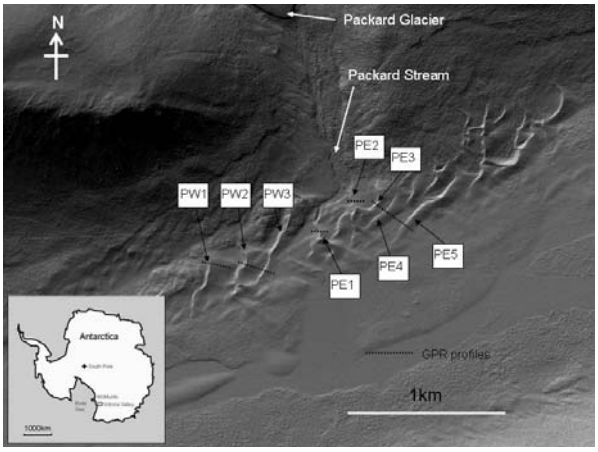

Figure 1. LiDAR image of the Packard dune field which included barchanoid, transverse, reversing and climbing dunes located along the north side of the Lower Victoria valley beneath the Packard Glacier.

Whaleback dunes

Whaleback dunes in the Victoria Valley lie on the valley floor and are aligned sub-parallel with the valley walls (Fig. 2). The dunes are aligned obliquely across the valley and although Selby et al. [3] suggest that their alignment and shape may be partly controlled by the underlying moraine it appears that the dunes are aeolian landforms and only locally influenced by the underlying fluvial and glacial topography [4]. The whaleback dunes are up to 1 ikm in length and around 100 m in width, and lack slipfaces. GPR profiles through one 800m long whaleback dune reveal low angle inclined reflections interpreted as dune bedding [4]. The bedding primarily dips towards the east indicating that the dune has extended from west to east in response to westerly winds. Bedding also dips towards the south indicating that the dune is expanding across the valley at the same time as extending along the valley.

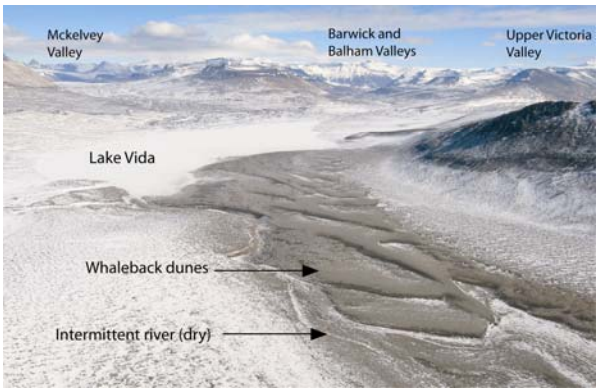

Figure 2. Oblique aerial photograph of whaleback dunes on the floor of the Lower Victoria Valley. View towards the west with Lake Vida and the McKelvey, Barwick and Balham valleys in the background. Westerly winds funnelled through the Lower Victoria Valley appear to control the orientation and migration of the whaleback dunes [4].

Lake Vida Dune

The Lake Vida dune stands on a debris lobe that projects south into the valley toward Lake Vida (Fig. 3a). The dune has a barchanoid morphology and is over 80m high, and over 800m wide, much higher and wider than any other dunes in the Victoria valley. GPR profiles across the dune show inclined reflections dipping towards the east (Fig. 3c), which indicates that the dune is migrating from west to east driven by westerly winds. This is the opposite direction to that which would be expected from the barchan like morphology. One possible explanation is that ice cement is stabilising the arms of the dune so that it is taking on a parabolic form. The depth of penetration by the GPR is greater than predicted for Quaternary sediments, most likely because of the absence of liquid water.

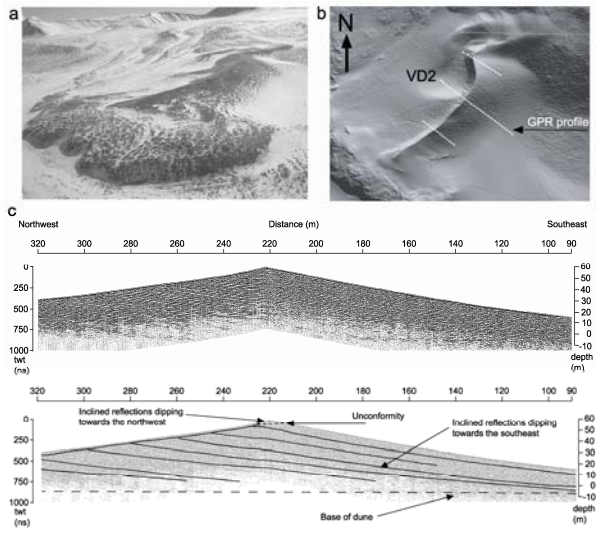

Figure 3. a, North facing oblique aerial view of Vida Dune standing on debris lobe. b, LIDAR image showing location of GPR profile, c, 100 MHz GPR profile across Vida Dune showing bedding dipping from left to right towards the east which indicates that the dune has been accreting towards the east.

The three areas of dunes in the Lower Victoria Valley show contrast in dune morphology and migration direction within a distance of 10km along the valley. Sedimentary structures revealed by GPR within two of the dunes, a whaleback dune and the Lake Vida dune indicate net migration towards the east. In contrast, GPR profiles across the Packard dunes indicate net migration towards the west (Fig. 4). Dune migration from east to west is driven by easterly winds that blow onshore from the Ross Sea. These sea-breezes are generated by solar radiation heating the valley floor and are therefore more common in the summer months. Dune migration from west to east is driven by westerly winds that are föehn and Katabatic winds that are more common and more powerful during the winter months.

The Lake Vida dune which stands on a debris flow lobe is elevated above the valley floor and exposed to the westerly winds. It is probably partially sheltered from the easterly winds due to the change in orientation of the Lower Victoria Valley as the valley opens out to the west.. The whaleback dunes lie on the valley floor and are exposed to both the easterly and westerly winds. This axial position and exposure to both winds has probably influenced the dune morphology which is elongate and lacks slipfaces. The dominance of east dipping strata within the dune indicates that the westerly winds are dominant dune forming winds in the middle of the valley. Sedimentary structures revealed by GPR profiles across the Packard dunes indicate net migration towards the west and thus in this area the easterly winds are the dominant dune forming wind. The Packard dune field lies along the northern edge of the valley beneath the Packard glacier and in this location the dunes are partially sheltered from the westerly winds. Thus the location of the dunes within the valley determines their morphology and migration direction due to their relative exposure to, or shelter from, the winds that are steered along the valley by the mountainous topography.

References:

[1] Bristow, C.S., Augustinus, P.C., Wallis, I.C., Jol, H.M., Rhodes, E.J., 2010a, Investigation of the age and migration of reversing dunes in Antarctica using GPR and OSL with implications for GPR on Mars. Earth and Planetary Science Letters, v. 289, p.30-40.

[2] Bourke, M.C., Ewing, R.C., Finnegan, D. & McGowan, H.A., 2009, Sand dune movement in the Victoria Valley, Antarctica. Geomorphology, v. 109, p.148-160.

[3] Selby, M.J., Rains, R.B., & Palmer, R.W.P., 1974, Eolian deposits of the ice free Victoria Valley, southern Victoria Land, Antractica. New Zealand Journal of Geology and Geophysics 17, p.543-562.

[4] Bristow, C.S., Jol, H.M., Augustinus, P., Wallis, I.C., 2010b, Slipfaceless whaleback dunes in a polar desert, Victoria Valley, Antarctica: insights from ground penetrating radar. Geomorphology, v.114, p.361-372.

AEOLIAN EVENTS IN THE MOREUX CRATER: ANALYSIS OF DIVERSE DUNE FIELDS.

Marco Cardinale[1], Goro Komatsu[1], [1]International Research School of Planetary Sciences, Università D'Annunzio, Viale Pindaro 42, 65127 Pescara, Italy (cardinal@irsps.unich.it).

Introduction:

The Moreux crater is a 138 km-diameter impact basin located at the edge of a plateau of southern highlands, and its southern portion representing the dichotomy boundary, disrupts the regional scarp [1]. Features associated with the interior of the crater suggest that Moreux crater's appearance has been shaped by the action of glaciers at first, but wind also played an important role for the formation of the depositional and erosional structures that we observed inside the crater. Hummocks, swirls and ridges are found on the floor of the crater [2].

Large Dark Dunes (LDD)[3], and Transverse Aeolian Ridges (TARs) [4][5] are both visible all around the central peak. So We performed a geomorphological analysis of aeolian features inside the crater using CTX and HIRISE datasets, allowing us to conclude that multi-directional winds influenced the geomorphological features of the crater.

Methodology:

THEMIS visible images, provide a good coverage of the study area and the necessary spatial resolutions to identify dark ergs.

CTX images allow us to resolve dune slip face orientations. All the datasets have been processed using ISIS and VICAR software and then integrate into a GIS project.

We produced a geomorphological map of the Moreux crater highlighting the aeolian units (Fig.1).

Aeolian features:

In the Moreux crater we described mainly two different types of aeolian features; in addition sand sheets surround the dunes and cover knobs, hills, and ridges on the crater floor.

The dune morphology of *Dark dunes* was classified using McKee 's criteria [6]; we recognized ergs consisting of barchans, barchanoids and transverse dunes. Star dunes, domes and linear dunes (Fig.2) are also observed.

We classified linear dunes which evolve from barchan horns. We used the trend of wind streaks [7] to constrain the wind regime responsible for the connection of the ergs all around the central peak.

A multi-directional wind regime influences the ergs around the crater, forming a sand transport system; furthermore the topographic setting of the crater could also explain the presence of these dune fields on the floor.

We identified *Bright bedforms*, which are also called Transverse Aeolian Ridges (TARs)[4][5].

Conclusions:

Our morphological analysis suggests that Aeolian features analyzed developed under a multi-directional wind regime; dune morphology suggests several episodes of aeolian deposition sustained by changes in wind direction.

As suggested by the presence of complex dune fields [8] formed by the convergence of different wind directions; the topographic setting of the crater lead to the formation of long sand corridors made of barchans and barchanoid dunes. Dark dunes are developed over bright bedforms, and they may represent the last episode of aeolian activity . Deposition of the TARs developed also in different times is indicated by variable degree of degradation of these features as in other areas on Mars [9].

To understand the local dynamics of aeolian processes, we will try to compare these features with wind data from meso-scale wind models..

References: [1] Marchant D. et al. (2007) LPS XXXVII, #1425. [2] Head J. and Marchant, D. (2006) LPS XXXVII, #1127. [3] Hayward R.L. et al. (2007) JGR, 112, E11007, doi:10.1029/2007JE002943. [4] Balme M. et al. (2008) Geomorphology, 101, 703-720. [5] Zimbelman J.R. (2009), Geomorphology, in press. [5] [6] McKee E. D. (1979) *U.S.Geol. Surv.Prof. Pap., 1052*, 3-17. [7] Thomas P. et al. (1981) Icarus, 45, 124-15. [8] Silvestro S. (2009) LPSC XV, #1862. [9] Silvestro S. (2010) LPSC XVI, #1838.

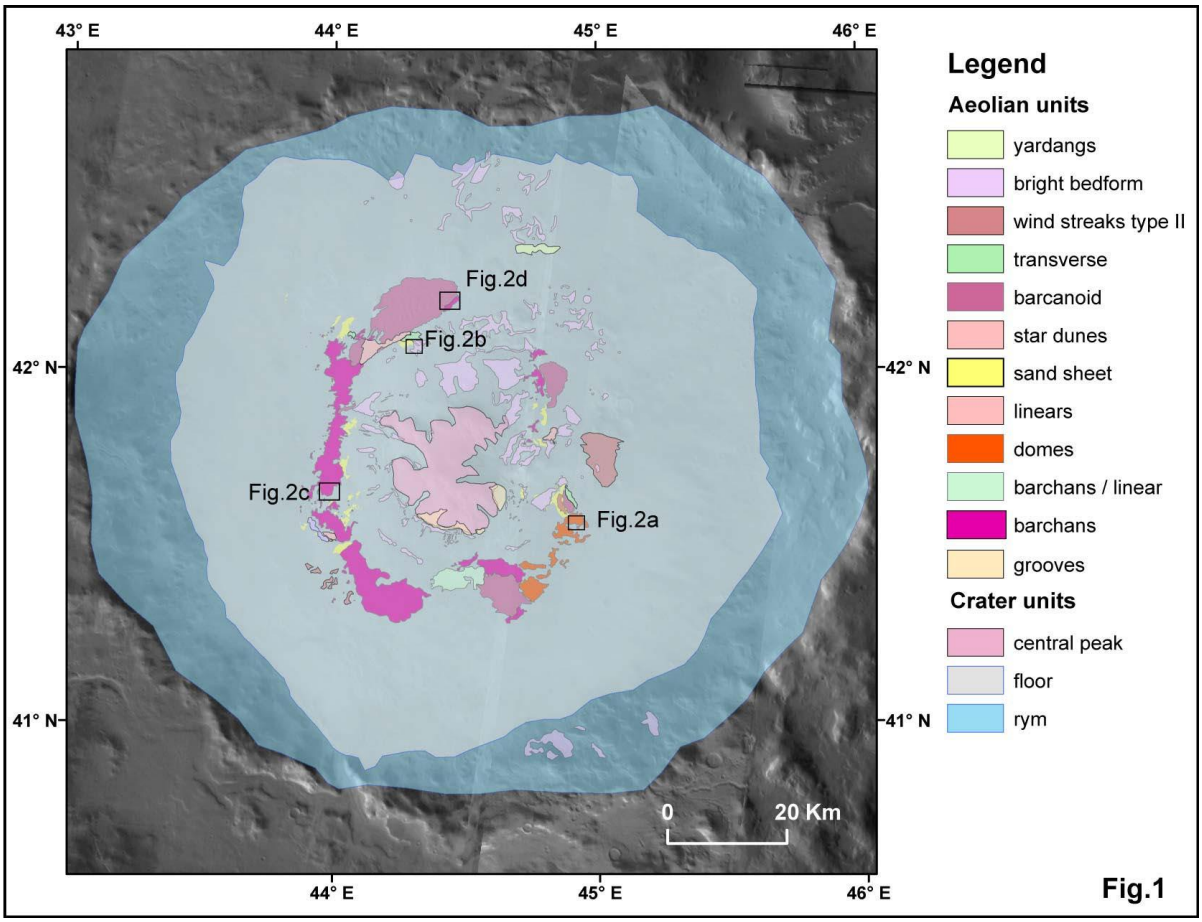

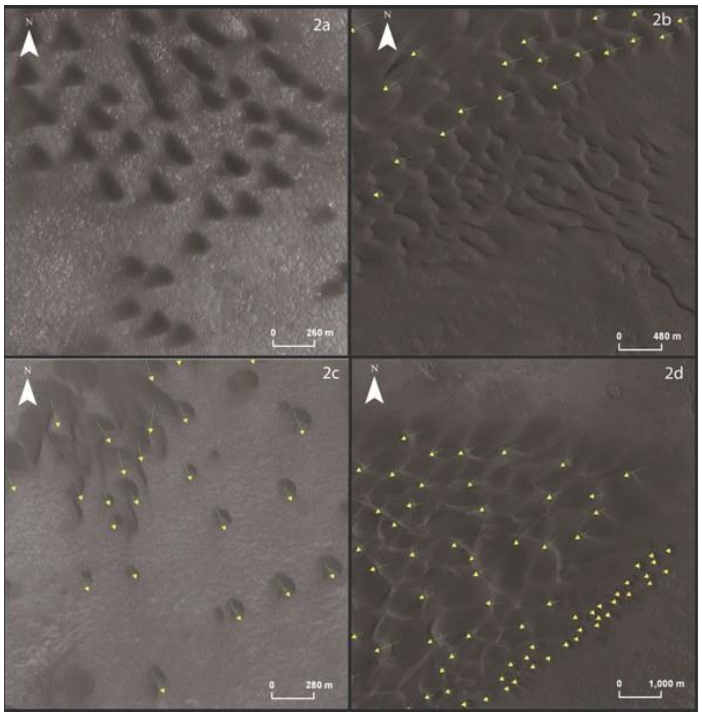

Figure 1: Geomorphological map of the Moreux crater showing aeolian features overlain over a THEMIS-IR day mosaic.

Figure 2: a) domes in the center of the image, b) star dunes, barchanoid ridges and the inferred wind directions (green and yellow arrows), c) barchans and the inferred wind directions (green and yellow arrows), d) barchanoid ridges and barchans dunes with the inferred wind directions (green and yellow arrows), (HiRISE PSP_001735_2220 for figure 2a, CTX P03_002098_2220_XI_42315W for figures 2b, 2c, 2d).

EVIDENCE OF BED FORM DEFLATION, MODIFICATION AND TRANSPORT AT ENDEAVOUR CRATER, MERIDIANI PLANUM, MARS, FROM ORBITAL OBSERVATIONS. M. Chojnacki[1], D. M. Burr[1], and J. E. Moersch[1], [1]Planetary Geosciences Institute, Department of Earth and Planetary Sciences, 306 EPS Building, University of Tennessee, Knoxville, TN 37996 (chojan1@utk.edu).

Introduction: Meridiani Planum, Mars, exhibits ample evidence in orbital images and ground-based observations, by the Mars Exploration Rover Opportunity, for aeolian activity with dunes, ripples and dark streaks [1-2]. The next major campaign for Opportunity is the investigation of the ~20-km-diameter Endeavour crater, ~13 km southeast of the rover's position in March 2010 (Figure 1). Here we expand on the recent documentation [1] that aeolian bed forms in Endeavour crater have been active in the span of the past decade.

Background: Contemporary dune activity has been a long-sought goal of Martian aeolian remote sensing. *Bourke et al* [3] used repeat MGS data (1999-2004) to show the disappearance of two, small (~1000 m^2) dome dunes, although no bed form migration was observed. More recently, high-resolution images have shown modification of ripples and dune edges in less than a Martian season [4]. These events demonstrate that the threshold wind speed for entrainment was exceeded under current conditions in these locations.

Evidence for modern day aeolian activity at rover landing sites was found with ripple modification, sand movement and dark streak activity [2, 5]. However, no associated bed form change has been detected from orbital observations.

Methods: For our investigation of surface change, we used narrow-angle images from the Mars Orbiter Camera (MOC) [6] to compare with data from the Context Camera (CTX) [7] and the High Resolution Imaging Science Experiment (HiRISE) [8].

Aeolian Activity: Endeavour crater has two main populations of dune bed forms. Well-formed barchans and transverse dunes are found in the western portions of crater, whereas less-developed, degraded bed forms populate the eastern half. The eastern bed forms resemble transverse and small dome dunes, but appear to lack slipfaces and to have low relief. Slip face orientations and sand streamers suggest a wind flow to the south-southeast, consistent with mesoscale wind modeling [9]. Recent thermophysical analysis [10] using THEMIS thermal inertia data [11-12] show the eastern dunes have a thermal inertia of 150-190 $Jm^{-2}K^{-1}s^{-1/2}$, consistent with 50-130 µm particle sizes (very fine sand). These derived grain size values are in good agreement for the optimal particle sizes (~100 µm) thought capable of being moved by the Martian atmosphere [13].

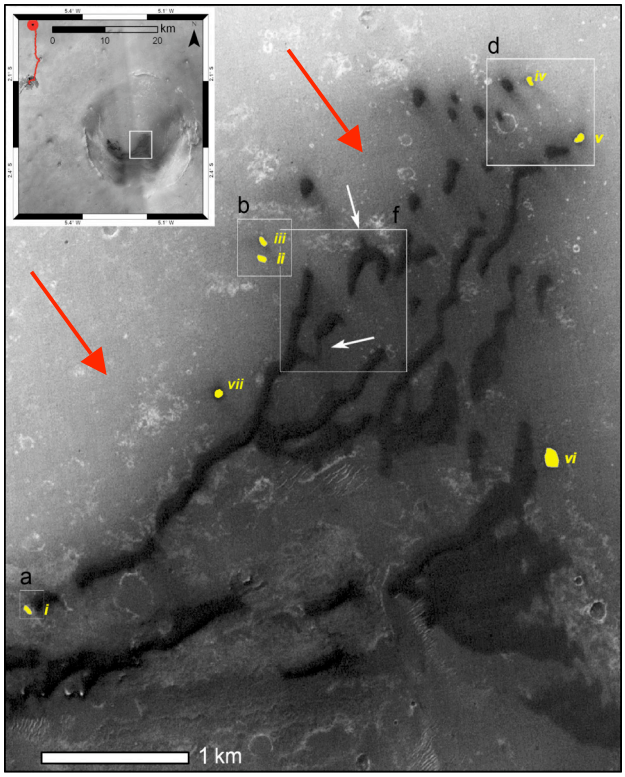

Figure 1. A CTX visible image mosaic showing the location of the Opportunity rover (as of March 2010) on its way to investigate Endeavour crater (inset) and a closer view of the eastern bed forms within the crater. Bed forms i-vii (yellow) show surface change with up to 100% deflation whereas two larger dunes (white arrows) show surface textural modification. Context boxes show locations for Figure 2 and red arrows indicate inferred primary wind direction.

Seven bed forms appear in the 2001 and 2003 MOC images (*e.g.,* Figure 2b & 2d). However, in 2008 CTX and HiRISE images, two of the bed forms (i & ii) had disappeared entirely, while five others (iii-vii) had decreased in area (*e.g.,* Figure 2a, 2c & 2de). Bed forms iv-vi are only covered in the lower resolution MOC+CTX pair of images, making area estimates more difficult than for bed forms i-iii & vii, which are covered in the MOC+HIRSE pair of images. We suggest the most reasonable explanation for the disappearance of these bed forms is aeolian removal and/or deflation. Preferential dust deposition (with consequent increase of albedo) seems less likely because the locations where the dark-toned features have disappeared lack the ripple-like texture seen in

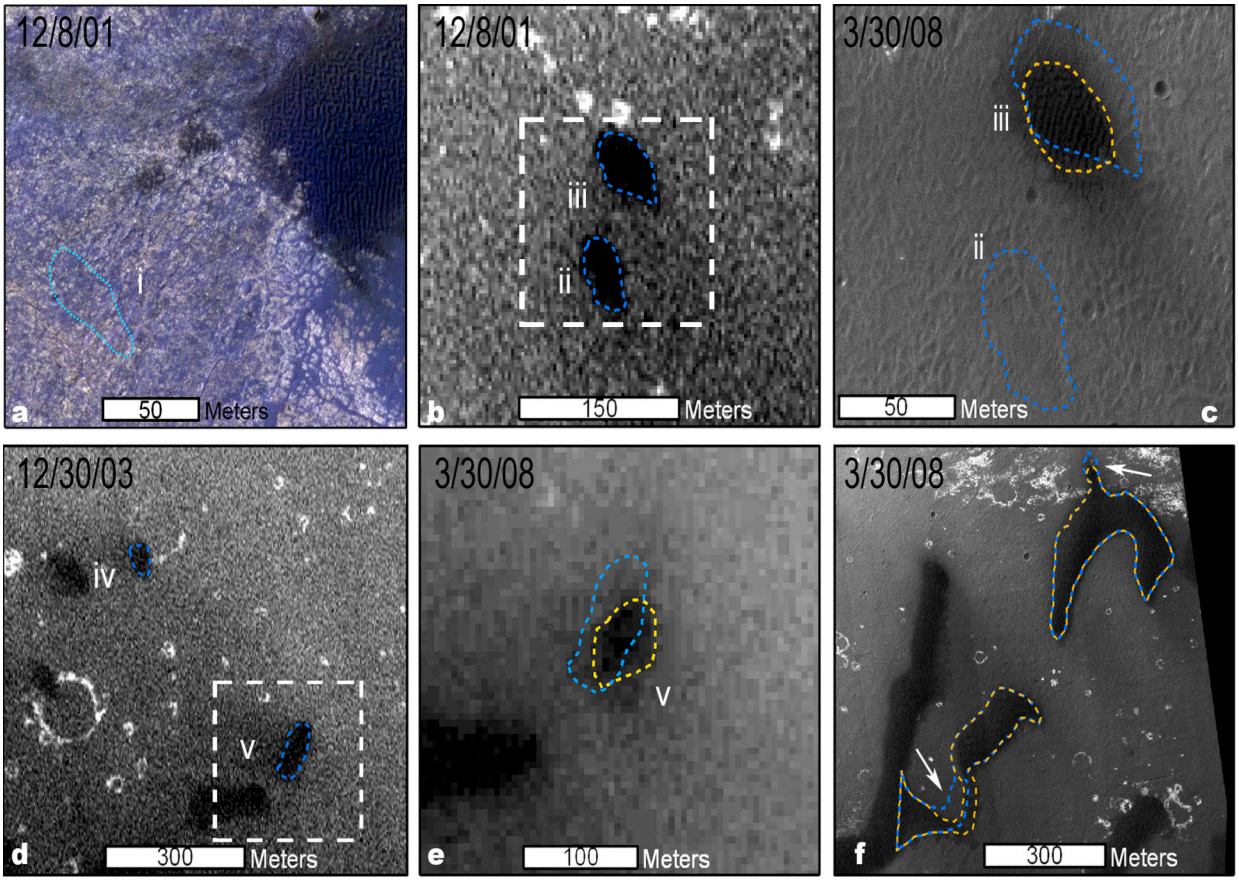

Figure 2. Visible wavelength images showing surface change in Endeavour crater. Blue polygons represent the extent of bed forms in 2001 or 2004 and yellow the extent of bed forms in 2008. (a) False-color HiRISE image PSP_007849_1775 (H1) taken in 2008 shows the prior location of bed form i. (b) MOC image E1101328 taken in 2001 shows bed forms ii-iii. (c) H1 taken 3.4 Mars years later suggests the disappearance of bed form ii and a ~45% reduction in size of bed form iii. (d) MOC image R1203949 taken in 2003 shows the eastern most dunes iv-v. (e) CTX P17_007849_1793_XN_00S005W shows the subsequent ~40% deflation and possible transport of bed from v over 2.3 Mars years. (f) Modifications (white arrows) of larger dunes in H1. North is up in all images.

the dark-toned features that remain (*e.g.,* 1, Figure 2a and 2c). Although the MOC images from 2001 are of insufficient resolution to distinguish this texture, it is reasonable to assume that all the dark-toned features in this vicinity originally had the same rippled surface texture. Bed form v, in addition to losing ~40% of its area, shows a ~20 m southeastward shift of its centroid (Figure 2d and 2e). This evidence is interpreted as southeastward bed form migration. Larger dunes show minor edge and dune shape modification where sand has presumably been redistributed (Figure 2f white arrows).

Discussion: All bed forms (except vi) that show removal or reduction in size are located at the inferred up-wind perimeter of the dune field, making them most exposed to atmospheric flow and deflation. The sand from these bed forms is likely dissipated and/or incorporated into larger dunes ~100s of meters downwind. Greater temporal resolution of this dune field may better document this surface evolution and sand transport.

The deflation, modification and translational migration of Endeavour crater dune sediment and associated estimated removal rates [1] over the course of ~4-6 Earth years may suggest Martian bed form activity is more frequent than previously thought. This result confirms that local winds are sufficient to initiate entrainment (possibly saltation), as observed elsewhere on Mars [2-5]. This result suggests these modest dunes are not in equilibrium with their environment, nor are they stabilized due to induration.

References: [1] Chojnacki et al. (2010a) LPSC, abstract #2326. [2] Geissler et al. (2008) JGR, 113, E12S31. [3] Bourke et al. (2008) Geomorphology, 94, 247–255. [4] Silvestro et al. (2010) LPSC, abstract #1820. [5] Greeley et al. (2006) JGR, 111, E02S09. [6] Malin et al. (1992) JGR, 97, 7699–7718. [7] Malin et al. (2007) JGR, 112, E05S04. [8] McEwen et al. (2007) JGR, 112, E05S02. [9] Rafkin and Michaels (2003) JGR, 108(E12), 8091. [10] Chojnacki et al. (2010b) LPSC, abstract #2175. [11] Christensen et al. (2004) Space Sci. Rev., 110, 85–130. [12] Putzig and Mellon (2007) Icarus, 191, 68-94. [13] Greeley et al. (1980) GRL, 7, 121–124.

COMPOSITIONAL ANALYSIS OF 21 MARTIAN EQUATORIAL DUNE FIELDS AND POSSIBLE SAND SOURCES. C. Cornwall[1,2] and T. N. Titus[2], [1]Northern Arizona University, Flagstaff, AZ 86001 (cc269@nau.edu), [2]U.S.G.S., 2255 N. Gemini Dr., Flagstaff, AZ 86001 (ttitus@usgs.gov)

Introduction: There are a total of 547 moderate to large-sized dune fields located within the equatorial region of Mars [1] but only about 60 of those dune fields have adequate data coverage for a study of provenance. Martian dunes are typically isolated and do not have any obvious transport pathways to sand accumulations. Pre-existing pathways may have been erased or wind energy on Mars today may be too weak to sustain transport pathways [2]. It is also possible that sand sources are local and originate from crater or chasma walls. This study focuses on the mineral composition of 21 equatorial dune fields and their surroundings to determine a possible sediment source for each dune field.

Data: A total of 21 dune fields were selected among the 547 equatorial dune fields (latitudes between 65°N and 65°S) from the Mars Global Digital Dune Database [1] based on their size (a sinusoidal area greater than ~300) and the amount of Compact Reconnaissance Imaging Spectrometer for Mars (CRISM) coverage. Mineral distributions and relative concentrations inside dune fields as well as outside dune fields were gathered primarily using CRISM data and compared to Thermal Emission Spectrometer (TES) data.

Analysis: On average, 50 CRISM footprints were analyzed for each dune field and the surrounding area. CRISM images with small portions of the dune field area were not analyzed to ensure that the spectral index values were from the dune material and not the surrounding area. Footprints outside the dune field included those within a maximum of 850 km radius from the dune field. These footprints also included coverage of the crater wall and floor if the dune field was located inside a crater and that of smaller, neighboring dune fields. Minerals were identified using the indices discussed by Pelkey et al. [3] and the relative concentration of the minerals was determined by threshold values provided by the CRISM team. Hematite index values were treated with caution and compared to TES mineral maps [4], where TES detection of hematite is more reliable. A principle component analysis (PCA) was performed on CRISM index values for each mineral in all 21 dune fields to identify patterns in mineral distributions and concentrations.

Results: PCA analysis of the 21 dune field compositions indicates that olivine and monohydrated sulfate minerals have the greatest variance in abundance. Three compositional end members were determined according to this variance. The first end member corresponded to dune fields poor in olivine and monohydrated sulfates, the second end member consisted of dune fields rich in monohydrated sulfate but poor in olivine, and lastly, the third end member represented dune fields rich in olivine but poor in monohydrated sulfate.

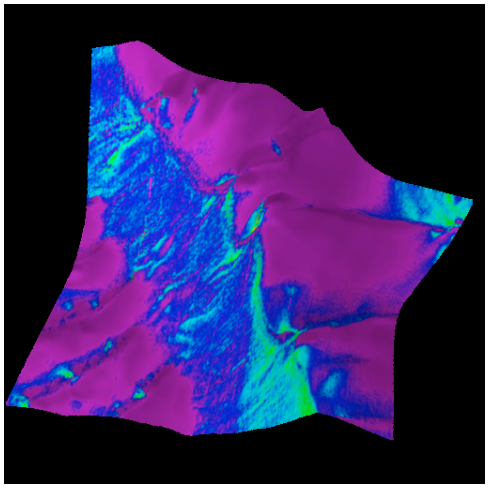

Figure 1. CRISM observation FRT 39DF showing the Russell crater mega dune and the presence of olivine on the crest and slope of the dune. Warmer colors indicate a higher olivine concentration.

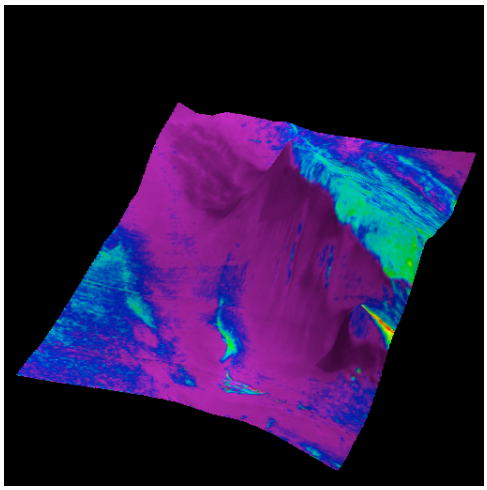

Figure 2. CRISM observation FRT 9271 showing the crater wall and floor west of the dune field shown in Figure 1. Warm colors indicate a higher concentration of olivine. The crater floor or rim might be the source of olivine in the dune field 0126-545 (Russell crater).

Many of the dune fields have similar compositions and their differences can be attributed to variations in

mineral concentrations (Table 1). However, a few dune fields had distinct compositions from neighboring dune fields. These dune fields are located in Nili Patera, Juventae and Ganges Chasmata, Meridiani Planum, Proctor crater, Lomonosov crater, and Gale crater. Differences in some of these dune compositions correlate with crater depth. Other compositional differences could be caused by the introduction of wind blown sediments or possible aqueous alterations. In general the composition of dune fields within craters or chasmata were similar to the composition of the walls or floor of the crater or chasma (Fig. 1 and 2).

However, there were four dune fields (Table 1) with a unique composition that did not match the composition of the crater walls or floor, neighboring dune fields, neighboring craters, or the surface mineralogy outside of the craters. These were labeled as "exotic" and presumed to have a distant wind-blown source.

Summary: CRISM data and PCA analysis of spectral index threshold values of 21 equatorial dunes indicates that dune sediment compositions have three distinct end members relating to the abundance of olivine and monohydrated sulfate minerals. Further analysis of dune field compositions suggests that the majority of source material is most likely local, coming from the crater or chasma walls but there are a few dune fields that have a potentially distant wind-blown source.

References: [1] Hayward et al., (2007), U.S.G.S. Open File Report 2007-1158 [http://pubs.usgs.gov/of/2007/1158]. [2] Fenton, L. K. and M. I. Richardson, (2001), *J. Geophys. Res.*, 106(E12) 32,885-32,902. [3] Pelkey et al., (2007), *J. Geophys. Res.*, 112, E08S14, doi: 10.1029/2006JE002831. [4] Bandfield, J. L., (2002), *J. Geophys. Res.*, 107(E6), 5042, doi: 10.1029/2001JE001510.

Table 1. Summary of minerals present and their relative abundances in the 21 equatorial dune fields from this study. Abundance is based on threshold values for each index. N/A represents lack of data and a single dash signifies the absence of that particular mineral or index inside the dune field. The presence of hematite was often greater in areas of shadow and high albedo. Thus, hematite values shown are typically higher than indicated by TES data. Dune fields labeled as "exotic" are shown in red.

Dune ID	H2O	Olivine	High Ca Pyrox	Low Ca Pyrox	Sindex	Mono-Hyd Sulf	Fe/Mg	Al	Hematite
2332-530	-	Low	Low	-	Low	-	-	-	-
2404-535	-	-	-	-	Low	Low	Low	Low	Low
2461-581	-	-	-	-	Low	-	-	Low	-
2971-046	-	Low	-	-	Low	Moderate	Low	Low	-
3124-080	-	Low	Low	-	Low	Low	-	Low	-
3352-407	-	Low	Low	-	Low	-	-	Low	-
3403-572	-	-	Low	-	-	Low	Low	Low	Low
3515-596	-	-	-	-	Low	-	-	-	-
3553-642	-	Low	Low	-	-	-	-	Low	-
0126-545	-	Low	Low	-	-	Low	Low	Low	Moderate
0194-468	-	-	Low	-	Low	Low	Low	Low	Moderate
0304-475	-	Low	-	Low	Low	Low	-	Low	Moderate
0347-437	-	-	-	-	Low	Low	-	Low	Low
0045+031	Low	Moderate	Low	-	Low	-	Low	Moderate	-
3513+648	-	-	-	-	-	-	Low	Moderate	-
0443+417	-	Low	Low	-	-	-	-	Low	-
0628+266	-	-	-	-	Low	-	-	Low	-
0671+088	-	Moderate	-	Low	Low	-	Low	Low	-
1249-136	-	Low	Low	-	Low	Low	-	Low	Low
1370-050	-	Low	Low	-	Low	-	-	-	-
1640-615	-	-	-	-	Low	Low	Low	Moderate	N/A

CONNECTING AEOLIAN AND NIVEAN PROCESSES WITH MARTIAN POLAR DUNE MORPHOLOGY.

S. Diniega[1,*], S. Byrne[2], K. Glasner[1], [*]Program in Applied Mathematics, The University of Arizona, 617 N. Santa Rita Ave., P.O. Box 210089, Tucson, AZ 85721-0089 (serina@math.arizona.edu), [2]Program in Applied Mathematics, The University of Arizona, [2]Dept. of Planetary Sciences, The University of Arizona.

We investigate the influence of reversing wind directions, diffusion, and ice cementation on dune slope evolution. The aim of this study is to quantitatively connect specific morphologies to processes and related parameters, which will aid in decoupling the effects of these processes in the interpretation of actual dune forms.

Martian dune morphology

Seasonally reversing wind directions will slow dune migration and create more symmetric dunes [1, 2]. Within polar regions, interbedded snow layers and ice cementation will perturb dune morphology and behavior [3, 4]. Such processes may be especially important in martian dune fields, as current dune evolution may occur over 10 000's of years [5], a timescale comparable to estimates for climate shifts and polar processes. Recent studies have shown that martian polar and mid-latitude dunes contain geomorphic markers of wind reversals (Fig. 1; [6]) and nivean processes [7].

Quantitative connections

This study utilized a standard two-dimensional continuum dune evolution model [8] to evaluate dune slope evolution. Parameters used for wind speeds and sand flux were taken from [5], with windspeed held constant (so results will need to be scaled relative to actual saltation rates). Simulations were initiated with a dune form with slipface to the left.

As observed within terrestrial dunes (e.g., [2]), a reversing wind slows dune migration and steepens the dune's slopes (Fig. 2). Simulations showed that the amount of steepening depends primarily on the frequency of wind reversal (Fig. 3), and only weakly on the period of wind cycling and the dune size.

Simulated dune mean slope values also depend on assumptions made about diffusion, as the dune shape results from a competion between saltation (which piles sand and increases slope) and diffusion (which decreases slope). In terrestrial desert dune systems, it generally can be assumed that diffusion is comparable in strength to saltation only within avalanches (when the slope exceeds the angle of repose). However, the effective diffusion on the dune can be increased through processes that preferentially transport material downslope, such as atmospheric turbulence, creep, freeze-thaw cycles, seismic shaking, or micro-meteorite impacts.

Figure 1: An example of the break in slipface seen in many martian polar dunes. The $\sim$10m wide "bright ribbon" that runs along the crest-line is due to a lack of ripples and increased slope relative to the lower portion of the slipface. This type of slipface morphology forms on terrestrial dunes due to wind reversals [2]. On Mars it is found only in the mid-latitudes and polar regions, implying possible formation due to a niveo-aeolian process interaction. To see the full image (81.7N,133.6E) - http://hirise.lpl.arizona.edu/PSP_010269_2620.

Additionally, if saltation does not occur for a large fraction of time (due to sediment or wind limits), then simulation results and model time need to be scaled via this fraction to yield real-time results. As the diffusion coefficient is inversely related to time ($\sim$ length^2/time), this coefficient needs to be increased by the same multiplicative scale as time, to accurately reflect the effect of diffusion operating over the longer real-time period.

Certain measurables, such as the ratio of the length of the slipface to the total lee slope length (Fig. 4), may relate strongly to the relative rates of saltation vs. diffusion.

Preliminary results indicate that analysis of simulation results and comparison with observable dune morphologies will provide ways of decoupling the effects of

2

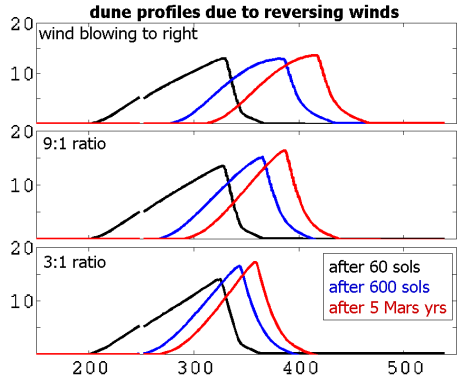

Figure 2: Under unidirectional winds, the dune migrates 97m; under 9:1 (9/10 of time wind blows to left, 1/10 to right) winds, 63m; and under 3:1 winds, 35m. The dune also grows in height, as its slopes steepen.

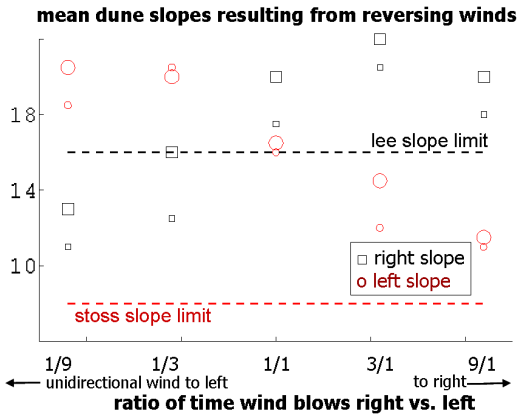

Figure 3: Both slopes adjust to a mean value that depends on the frequency of wind reversals, but is nearly independent of the period length (not shown) and dune size (indicated by marker size). Dashed lines show effect of unidirectional wind, which is consistent in stoss values with observations [2, 9]. The mean lee slope is lower than the angle or repose as calculations include smoothing at the top and bottom of the slope.

interacting contemporaneous processes. Future studies will also be aided by connection with climate, polar process, and sediment cementation studies, which can provide independent constraints of some process parameters. Additionally, we will compare dune morphologies located within the mid-latitudes vs. the polar regions to isolate the effects of polar processes.

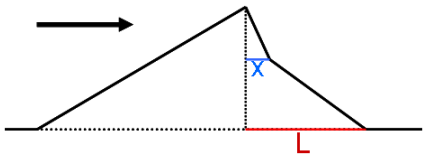

Figure 4: The ratio of the slipface length (x; the portion of the lee slope at the angle of repose) to lee slope (L) may be related to the relative rates of diffusion and saltation. Wind direction is indicated by the arrow.

Creating flat-topped dunes

Currently, simulation results have been used to replicate the general features of most martian dune forms. However, we have not yet created the flat-topped dunes found in Antartica (Fig. 5) and on Mars. We are exploring the effects of a location-dependent diffusion and/or cementation depth in creating this shape.

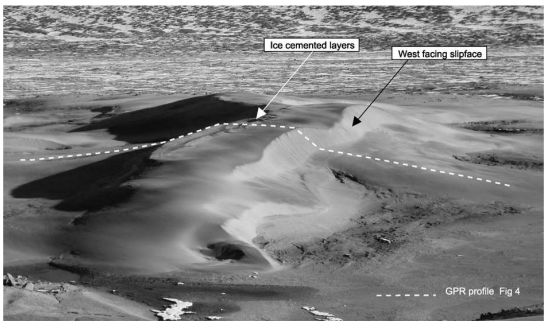

Figure 5: A flat topped Antarctic dune, similar in shape to some martian dunes. In Antarctica, these dunes appear to form due to ice cementation and reversing winds. Image is from [1].

References

[1] Bristow C. S. *et al. Earth Planet. Sci. Lett.*, 289:30–42, 2010.
[2] Burkinshaw J. R. *et al. Geological Soc.*, 72:25–36, 1993.
[3] Calkin P. E. & Rutford R. H. *Geograph. Rev.*, 64:189–216, 1974.
[4] Bourke M. C. *et al. Geomorph.*, 109:148–160, 2009.
[5] Parteli E. J. R. & Herrmann H. J. *Phys. Rev. E*, 76:041307, 2007.
[6] Fenton L. K. *et al. J. Geophys. Res.*, 110:E06005, 2005.
[7] Horgan B. *et al. LPSC* **41**, Abs. 1325, 2010.
[8] Kroy K. *et al. Phys. Rev. E*, 66:031302, September 2002.
[9] Parteli E. J. R. *et al. Internat. J. Mod. Phys. C*, 16:1879–1892, 2005.

SAND, WIND, AND ICE: MARS ANALOG AEOLIAN STUDIES AT THE GREAT KOBUK SAND DUNES, ALASKA. C. L. Dinwiddie[1] (cdinwiddie@swri.org), R. N. McGinnis[1], D. E. Stillman[2], D. M. Hooper[1], T. I. Michaels[2], K. L. Bjella[3], R. E. Grimm[2], and M. Necsoiu[1]. [1]Geosciences and Engineering Division, Southwest Research Institute®, 6220 Culebra Road, San Antonio, TX 78238, [2]Space Science and Engineering Division, Southwest Research Institute®, 1050 Walnut Street, Suite 300, Boulder, CO 80302, [3]Cold Regions Research and Engineering Laboratory, U. S. Army Corps of Engineers, Ft. Wainwright, Alaska 99703.

Introduction: High-latitude Martian dunes may have reduced mobility due to seasonal, surficial volatile cycles of H_2O and CO_2 ice/frost and the presence of deeper interior reservoirs of permafrost. This hypothesis is generally consistent with multiple unsuccessful searches of spacecraft imagery {e.g., [1,2]} for robust signs of high-latitude dune activity {an exception is [3]}. During Martian summer, solar heating may remove volatiles from a thin surficial layer of aeolian particles, thereby increasing particle mobility, but their transport may not result in bedform changes significant enough to detect {although an intriguing finding of Martian ripple migration at low latitudes is noted [4]}.

Sparse Martian data forces aeolian scientists to use the theory and lessons from terrestrial dunes to interpret and predict the evolution of Martian dune morphologies. Terrestrial dunes studied as planetary analogs are often warm-climate dunes without perennially frozen volatiles, but cold-climate dunes with perennially frozen volatiles may be significantly more analogous to Martian dunes. There is little detailed knowledge of such terrestrial systems, however, due to their remote locales and demanding logistical efforts required for their study. To begin understanding cold-climate sand mobility and transport, we are undertaking a site characterization and meteorological modeling study of cryospheric, geomorphologic and atmospheric processes active in the 67°N latitude Great Kobuk Sand Dunes (GKSD), Kobuk Valley National Park, Alaska (Fig. 1), as a terrestrial analog for high-latitude Martian dunes.

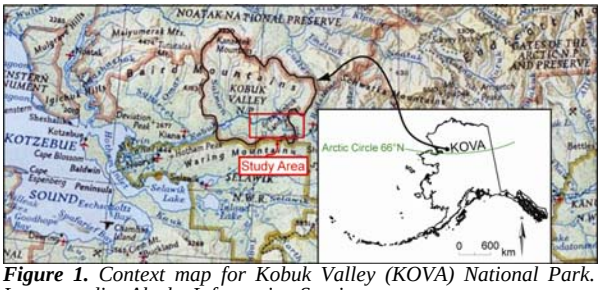

Figure 1. *Context map for Kobuk Valley (KOVA) National Park. Image credit: Alaska Information Services.*

Using this high-latitude, slowly migrating [5] terrestrial aeolian analog to Mars, we will study interactions between the atmosphere above, the cryosphere below, and the geomorphology at the land surface from March 15 until April 2, 2010. We will collect near-surface geophysical, geomorphological, and meteorological data and employ numerical mesoscale (km) to microscale (10–100 m) meteorological modeling capabilities to meet the objectives specified below.

Setting: The GKSD are a result of Pleistocene glaciation in the Brooks Range that produced glacial drift reworked by subsequent meltwater streams. The streams deposited quartzose sand and silt along the Kobuk River valley concurrent with the last glacial advance {24 ka; [6]} and created loess deposits and dune fields. The valley lies ~65 km north of the Arctic Circle and ~160 km inland to the east from Kotzebue Sound within an east–west-oriented hydrologic basin on the Kobuk R. lying between the Baird and Waring mountains to the north and south. The GKSD are subject to an opposite, bimodal wind regime at the macroscale, where the dominant winds are strong polar easterlies from September to May, with a brief wind reversal each summer [6]. The climate is subarctic and semiarid (average annual temperature: –6°C; average precipitation: 400 mm) with long, cold winters (January average: –27°C) and brief warm summers (July average: 15°C).

The 62-km^2 [7] active GKSD are characterized by a variety of dune forms, including transverse, barchanoid, star, and coppice (nebkha) dunes and sand sheets [6,7,8]. The dunes range from 33 to 170 m amsl and occur within a plateaus/highlands physiographic region with a 10° slope; this system mainly lies within the Kavet Creek watershed [9]. Several tributaries to the Kobuk R. (Fig. 2) offer cutbank exposures. Kavet Cr. is diverted to the dune field margin at the downwind side of the GKSD (Fig. 2). Alcove-shaped springs drain the base of the dune field to Kavet Cr. and Ahnewetut Cr. [6,7]. Ahnewetut Cr. dissects the GKSD (Fig. 2), exposing inactive precipitation ridges in cross-section and separating the larger northwesterly lobe of the GKSD from the smaller southeasterly lobe; in the region surrounding this divide, barchanoid climbing dunes move upslope and encroach on the base of the Waring Mountains [6]. Like Kavet Cr., Niaktuvik Cr. is diverted to the dune field margin on the southeast edge of the smaller lobe (Fig. 2). The downwind side of GKSD is characterized by a main body of large transverse to barchanoid dune ridges and flat, locally ponded interdune areas [6]. The brief westerly summer winds form secondary lee slipfaces on dune crests [7]. The main body of sand is dry with a large sand supply, whereas the upwind, older portion

of the system is moister and vegetated [6,10]. Several thermokarst lakes abut the dune boundary of an upwind sand sheet on the north side of the northwest GKSD lobe (Fig. 2).

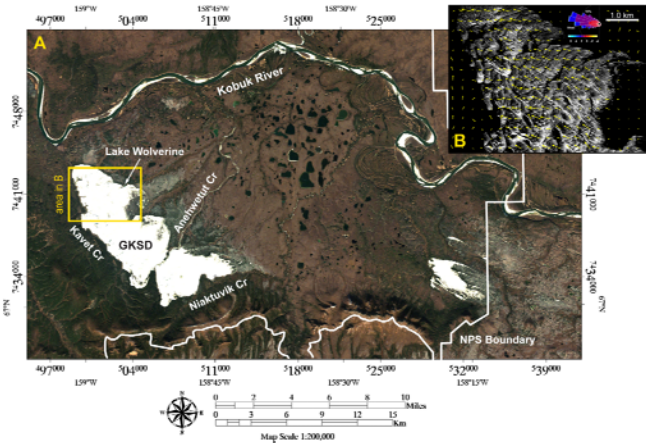

Figure 2. A. *AVNIR-2 contrast-enhanced context image (bands 3, 2, 1) of KOVA and the GKSD.* ***B.*** *Migration vectors calculated by [5] superimposed on a SPOT panchromatic image.*

Niveo-aeolian sedimentation of wind-blown snow and sand occurs at the GKSD [7]. Annual denivation forms include snow ramparts, sinkholes, hummocks, microridges, meltwater fans, contorted bedding, open and sand-filled tensional cracks of varying geometries, and dimpled/pelleted/spongy/air-bubbly wet sand covers [7]. The role of sublimation in the dissipation of snow during the early spring is uncertain because research here has typically been undertaken during clement months and detailed information on winter niveo-aeolian transportation and deposition processes is limited. Our planned observations during March 2010 will augment this knowledge base.

The presence of permafrost within the GKSD combined with the opposite, bimodal wind regime of Kobuk Valley is thought to lead to a lower than average dune migration rate [7,10], and SwRI's multispectral data displacement analysis quantitatively supports this hypothesis, yielding an average GKSD migration rate of only ~1 m/yr over a recent 5-year period [5].

Objectives: Through this late-winter field campaign and atmospheric modeling study we will begin to provide answers to the following science questions:

- What factors (e.g., sediment source, wind regime, grain size, water content, basinal topographic confinement) are relevant (at this site) to the control of dune size, spacing, orientation, and form?
- What is the late-winter reversing dune signature, given the bimodal wind regime?
- Given the apparently very slow migration rate of the dunes, what is the relative importance of permafrost, a seasonally frozen active layer, and niveo-aeolian deposits on mechanical arrest of dune movement?
- Is mechanical arrest of the dunes a more important factor to migration rate than bimodal wind regime and topographic confinement?
- What are the microscale circulation dynamics of the atmospheric boundary layer of this aeolian system, and how do they interact with local topography and aeolian geomorphology?

Methodology: NASA Mars Fundamental Research grant NNX08AN65G, "Ground-Penetrating Radar Investigations of Mars Analog Permafrost Sites in Alaska," has funded our late-winter, March 2010 geophysical characterization of the cryosphere of the GKSD. This study will provide ground truth for interpretation of depth to potentially recoverable massive water ice and other cryospheric signatures in radar data, and a foundation upon which to assess broadband radar performance in a cold, volatile-rich environment.

Because we are convinced of the broader value of the GKSD as a cold-climate terrestrial analog to Martian aeolian systems, SwRI's IR&D program is augmenting the March 2010 field study by funding a study to simultaneously collect hydrometeorological and geomorphological data.

Together, these two projects will enable us to begin construction of a season-specific library of Mars-relevant meteorologic, geomorphic, and cryospheric modeling parameters.

References: [1] Zimbelman J. R. (2000) *GRL, 27,* 1069–1072. [2] Schatz V. et al. (2006) *JGR–Planets, 111,* doi:10.1029/2005JE002514. [3] Bourke M. C. et al. (2008) *Geomorphology, 94,* 247–255. [4] Silvestro S. et al. (2010) *LPS XXXXI,* Abstract #1820. [5] Necsoiu, M. et al. (2009) *Remote Sensing of Environment, 113,* 2441–2447. [6] Dijkmans J. W. A. and Koster E. A. (1990) *Geografiska Annaler, 72A,* 93–109. [7] Koster E. A. and Dijkmans J. W. A. (1988) *Earth Surface Processes and Landforms, 13,* 153–170. [8] Fernald A. T. (1964) *U.S. Geological Survey Bulletin 1181–K,* k1–k31. [9] Brabets, T. P. (2001) U. S. Geological Survey Water-Resources Investigations Report 01–4141. [10] Mann, D. H. et al. (2002) *Quaternary Science Reviews, 21,* 709–731.

Acknowledgements: This work was supported by NASA Mars Fundamental Research Program grant NNX08AN65G from 2008 to present and SwRI IR&D Project 20.R8136. Any opinions, findings, and conclusions or recommendations expressed in this paper are those of the authors and do not necessarily reflect the views of NASA.

The authors thank Seth Kantner for his invaluable field knowledge and field support, David Hamilton for keeping our team warm and fed, Clarence Wood for the use of his private allotment, Jim Kincaid and Alvin Williams for their logistical support, and the National Park Service for research permit KOVA-2010-SCI-0001.

MODELING AEOLIAN EROSION POTENTIAL ON MARS WITH THE MRAMS LES. Michaels[1], T. I. and Fenton[1], L. K. and Michaels[2], T. I. [1]Carl Sagan Center, SETI Institute; NASA Ames Research Center, lfenton@carlsagancenter.org, [2]Department of Space Studies, Southwest Research Institute, 1050 Walnut St., Suite 400, Boulder, CO 80302, tmichael@boulder.swri.edu.

Introduction: A significant goal of Mars science is to understand the present-day interaction between the atmospheric environment and the planet's surface that ultimately results in climatically- and geologically-important aeolian phenomena (*e.g.*, dust storms, dust devils, albedo changes, dune migration, and surface erosion). Although the potential impact of larger atmospheric flows on surface-atmosphere interactions has been studied at length with regional and global climate models (GCMs) [*e.g.*, 1-3], studies of simulations resolving the complex, highly three-dimensional dry convective circulations that produce dust-lifting events are still uncommon [*e.g.*, 4,5].

We present preliminary results of large eddy simulations (LES) on Mars. In order to produce results that are directly comparable from one region or season of Mars to another, we have used idealized wind profiles as initial conditions to the simulations, rather than those derived from a coarser (but perhaps more locally realistic) regional climate model domain. We demonstrate that wind "gustiness" (*i.e.*, the stronger intermittent winds produced by daytime convective turbulence) is dependent on both the time variation of insolation and the initial wind profile.

MRAMS Large Eddy Simulations (LES): The Mars Regional Atmospheric Modeling System (MRAMS) is a non-hydrostatic, finite-difference, limited domain mesoscale model [6,7]. It can perform LES when the subgrid scale turbulence is modified to explicitly model eddies down to the domain resolution, based on the method of [8]. The simulations were run under idealized conditions, such that the LES setup did not include topography and the domain had periodic boundary conditions to effectively simulate the atmosphere over a vast plain.

We have run several large eddy simulations at two locations on Mars: the approximate Viking Lander 1 (VL1) site (22.28˚ N, 312.05˚ E, elevation ≈ -3640 m) and Phoenix Lander site (68.21˚ N, 234.26˚ E, elevation ≈ -4130 m). Other than location and initial conditions inherited from mesoscale simulations, each LES was run with the same characteristics. The horizontal domain grid spacing was 100 m, spanning 24 km in each direction (240 x 240 grid points). The 99 vertical layers in the domain stretched in thickness from 4 m at the surface to 150 m near the top (at ~12 km). The dynamical time step was 1 s. Each simulation was run at L_s = 120˚ (northern hemisphere summer), with a duration from approximately sunrise to sunset of a single day. In order to isolate the effects on the boundary layer convection due to differing wind profiles, we used three idealized wind profiles chosen for their relative simplicity. The three initial wind profiles were defined as follows:

Case 1: No initial wind, $u(z,t=0) = 0$, $v(z,t=0) = 0$

Case 2: Uniform wind, $u(z,t=0) = 5$ m/s, $v(z,t=0) = 0$

Case 3: Wind speed shear, $u(z,t=0) \approx 1.46z+2$, $v(z,t=0) = 0$, (such that $u(z=0) \approx 2$ m/s and $u(z=12\text{ km}) \approx 20$ m/s).

Results: In the Case 1, there is no mean wind, so that all wind gusts (measured here at the surface as high values of friction velocity) are produced solely by the development of buoyantly-induced turbulence within the convective boundary layer. One measure of insolation-driven buoyancy is the vertical potential temperature gradient at the surface ($d\theta/dz$, the surface static (in)stability): values less than zero indicate static instability, where the solar forcing has heated the surface more than the near-surface atmosphere, triggering dry convective turbulence that tries to equalize the energetic disparity between the two.

Figure 1 shows the distribution of surface static instability and friction velocity at ten local times across the VL1 domain. The surface air is statically unstable by midmorning, reaches a maximum level of static instability around local noon, and gradually grows less statically unstable as the afternoon progresses. By late afternoon (17.63h LMST), the sun is low in the sky and can no longer heat the surface enough to produce a negative vertical potential temperature gradient; at this point the convective boundary layer begins to collapse. Friction velocity distributions broaden throughout the morning and early afternoon, reflecting increased gustiness produced by buoyantly-driven turbulence within the boundary layer. The peak gustiness occurs in the early afternoon (12.63h – 14.63h LMST), shortly after the surface static instability has reached a maximum and the boundary layer has had time to react to this strong gradient with vigorous circulations. According to Mars lander observations, dust devil activity peaks in the early afternoon, consistent with our LES results [*e.g.*, 9,10].

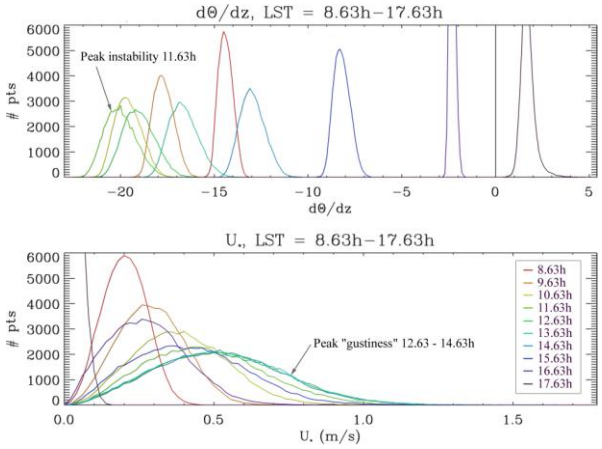

Figure 1. VL1 site, Case 1 domain distributions of surface instability and friction velocity in the morning and afternoon.

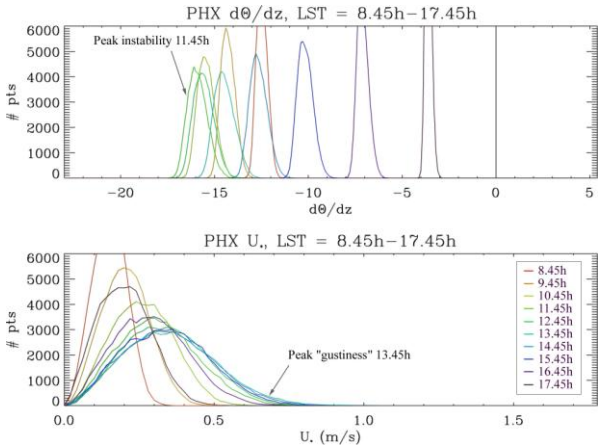

Figure 2. Phoenix site, Case 1 domain distributions of surface instability and friction velocity in the morning and afternoon.

Figure 2 shows similar plots of surface static stability and friction velocity at the Phoenix site. As at the VL1 site, instability at the Phoenix site reaches a maximum around local noon, although at such northern latitudes insolation is not direct enough to produce as strong a vertical potential temperature gradient. As the insolation decreases during the afternoon, the static instability decreases but much more slowly than at the VL1 site, since during the arctic summer the sun is above the horizon at all times. Thus the convective boundary layer at the Phoenix site may not produce such vigorous turbulence as that at the VL1 site, but buoyantly-driven turbulence takes longer to subside in the evening. This result is reflected in the distribution of friction velocities in Fig. 2, which never reach the same maxima as those at the VL1 site, but which take longer to weaken in the afternoon.

Results from Cases 2 and 3 indicate that the initial wind profile has a profound effect on wind distributions several hours later in the day. At both the VL1 and Phoenix sites, higher velocity initial winds lead to stronger peak winds relative to Case 1. At the VL1 site, buoyantly-driven turbulence dominates over wind-shear-driven turbulence from the initial wind structure during the hours of peak insolation. However, at the Phoenix site, convective activity is weaker, allowing the initial wind structure at the Phoenix site to more prominently influence the turbulence.

Conclusions: Large eddy simulations, using idealized initial wind profiles at two lander locations, have demonstrated that daytime convective turbulence can significantly increase the likelihood of particle entrainment on Mars, and that the degree of this enhancement is dependent on several factors. Wind gustiness generally increases with insolation, such that the strongest winds produced by convective turbulence would occur when the sun is highest in the sky, as dictated by local time and latitude.

The distribution of friction velocities is also dependent on the initial wind profile, which influences wind gustiness throughout the day and varies in impact with insolation and local time. Such imposed "mean wind" structures generally elevate peak friction velocities, increasing the likelihood that particle entrainment will occur. When the sun is high in the sky, convective activity reaches its peak and, if vigorous enough, can nearly override the initial wind structure.

The general nature of these relationships is not surprising, since conceptually, the nature of turbulence is determined by the relative strengths of two competing production terms: buoyant processes (tied to surface insolation) and mechanical processes (tied to wind shear). We intend to continue our study of simulated wind distributions and their effect on particle entrainment. Large eddy simulations at other locations (with varying elevation, albedo, and thermal inertia) and seasons will help to establish how these factors influence wind gustiness. Ultimately our goal is to develop a parameterization of the high tail of friction velocities for researchers to use as "perturbation" winds that can be superimposed on "mean" winds from mesoscale models, leading to estimates of particle entrainment on Mars that are more realistic.

References: [1] Toigo A.D. et al. (2002) *JGR, 107*(E7), doi:10.1029/2001JE001592. [2] Haberle R.M. et al. (2003) *Ic., 161,* 66-89. [3] Armstrong J.C. and Leovy C.B. (2005) *Ic., 176*(1), 57-74. [4] Toigo A.D. et al. (2003) *JGR, 108*(E6), doi:10.1029/2002JE002002. [5] Michaels T.I. (2006) *GRL, 33,* doi:10.1029/2006GL026268. [6] Rafkin S.C.R. et al. (2001) *Ic., 151,* 228-256. [7] Michaels T.I. (2002) MSc thesis, San Jose St. Univ. [8] Deardorff J.W. (1980) *Bound.-Layer Meteorol., 18,* 495-527. [9] Ellehøj et al. (2009) *LPS XL,* Abstract #1558. [10] Greeley, R. et al. (2006) *JGR, 111,* E12S09, doi:10.1029/2006JE002743.

BRIGHT FOOTPRINTS SUGGEST POSSIBLE DUNE MIGRATION ON MARS E. Gardin[1,2], M.C. Bourke[3,4], P. Allemand[1] and C. Quantin[1], [1] Laboratoire des Sciences de la Terre, Université de Lyon, Ecole Normale Supérieure de Lyon, Université Lyon 1, CNRS UMR 5570, France, Bat Géode, 43 bd du 11 Novembre, 69622 Villeurbanne cedex, France, [2] Laboratoire de Planétologie et Géodynamique de Nantes, CNRS UMR 6112, 2 rue de la Houssinière, 44322 Nantes cedex 3, emilie.gardin@univ-nantes.fr, [3] Planetary Science Institute, Tucson, Arizona, [4] OUCE, University of Oxford, UK.

Abstract: *High albedo arcuate features have been observed in one dune field, located in the Martian equatorial region. We have measured morphological and morphometric characteristics of the dune field to understand the origin of these features [1]. A comparison with a terrestrial analog at White Sand National Monument suggests that the high albedo features are formed by geochemical cementation. This implies that moisture was present in the dunes at the shallow sub-surface in the (recent) past.*

Introduction: Dunes are one of the youngest surface landforms on Mars. Despite their pristine appearance, there has been no evidence of the migration of large dark dunes during recent mission timeframes. Interestingly, surface modification of dune avalanche faces by fluid flow has been observed suggesting the presence of liquid water in a relative recent time [2, 3].

On Earth, liquid water from fluvial, lacustrine groundwater and precipitation sources can play an important role in aeolian sediment systems. Evidence of this is preserved in dune stratigraphy as soil horizons, cemented layers, vegetation and geochemical alteration [4]. Here we report on a study of a dune field located in an equatorial crater on Mars where we have observed a series of high albedo features in association with barchan dunes. We suggest that these features were formed in a period where liquid water was available in the close sub-surface [1].

Context setting: The intercrater dunefield is located at 11.89°N and 185.87°E. The dune field is composed of barchans, barchanoid and dome dunes. The presence of asymmetric barchans suggests that the dunefield is mainly influenced by a bimodal wind regime from west and north [5]. Towards the center of the dunefield the barchans are symmetrical with slipfaces orientated towards the south-east suggesting that they formed by resultant winds from the west to west-north-west (fig 3).

Geological study: High albedo features have been observed in the interdune and through the thin sediment cover of the dune windward slope. The HiRISE images show that the planform of the high albedo features is mainly arcuate (fig 1).

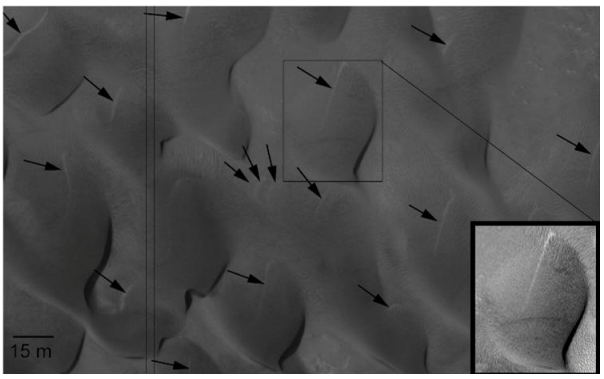

Figure 1: Close-up of the Martian dune field. Black arrows show the location of the high albedo features in the interdune and also near the foot of the windward slope of the barchans. Background is HiRiSE image: (PSP_001882_1920) at 25cm/pixel of resolution.

The morphometric study of the high albedo features (HAF) (Table 1) suggests that they have similar dimensions throughout the dune field. Moreover, all dark dunes have a low albedo with mean Digital Number (DN) values of 16 whereas HAF have mean DN values of 75.

Measurements of high albedo features	High albedo features
Distance to foot of the windward slope of the dune	5.6 m ± 0.6 m
Distance between brink of the measured barchan and HAF	16.0 m±0.2 m
Distance between two consecutive HAF	4.4 m±0.3 m
Width	0.6 m± 0.1 m
Length	9.3 m ± 0.3 m
Mean DN	75

Table 1: Reported average values and standard deviation of high albedo features. DN is the Digital Number.

Terrestrial Analog: There are similar features preserved in the interdunes at the White Sands National Monument, in south-central New Mexico [6, 7, 8 and 9].

Two types of facies were preserved in the interdune. First, there is an avalanche face strata, where ripple and grain flow features are preserved [4]. Second there is preservation of the basal portion of the dune. Note that these features have an arcuate shape that is similar to the planform of the base of the dune footslope.

At White Sand National Monument the dunes are barchans composed of soluble gypsum grains (fig 2). The briny water can accumulate inside the dunes. In the evaporation condition, the soluble grains produce the induration of the low dune (fig 2). Therefore, an induration crust is observed at the bottom of the avalanche slipface of the dunes.

Figure 2: photos taken at White Sand National Desert Monument Left: Photo of a barchan slipface. Right: Close-up of the foot of the barchan slipface acquired on photo left. A cemented crust is formed by reprecipitation of gypsum.

Comparison between Martian and terrestrial dunes: On Mars, the dunes are likely composed of basaltic sand except in the Olympiae Undae where a gypsum signature has been detected [10, 11]. In comparison on Earth, dunes at White Sand National Desert Monument are composed of gypsum grains whereas on Mars, no spectral signature of hydrated minerals is detected inside the dune field observed in our study.

At White Sand National Desert Monument, planforms are arcuate and features are approximately 20 cm height. On Mars, no visible topography on HiRISE images suggests the height of the high albedo features is less than 1 m.

Discussion: First, the Martian high albedo features have similar Digital Number values, dimensions and planforms. This suggests that the high albedo features observed in our study are formed by a similar process.

Unfortunately, spatial resolutions of OMEGA and CRISM data are insufficient to determine the mineralogy of the Martian high albedo features.

Arcuate features have also been reported in the interdune areas of Olympiae Undae [10] and in Chasma Boreale [11]. The Chasma Boreale arcurate features have morphological differences to those reported in this study and are proposed to result from ground ice cementation of dune sediments [1].

There are three implications of our findings. First, we assume that moisture was close to the surface at this low latitude on Mars in recent times. We suggest that it is recent because of the young age of the dunes relative to other surface features on Mars. Secondly, the high albedo features mark the former positions of the slipface, and thus represent a former location of the dune. The identification of arcuate features upwind of barchans dunes suggests that dune migration has occurred at this low latitude location in recent times on Mars.

Finally, the observations regarding the alignment of the arcuate features with the current dune position suggest that the formative winds have remained essential the same with change only from NW/NNW to predominantly NW.

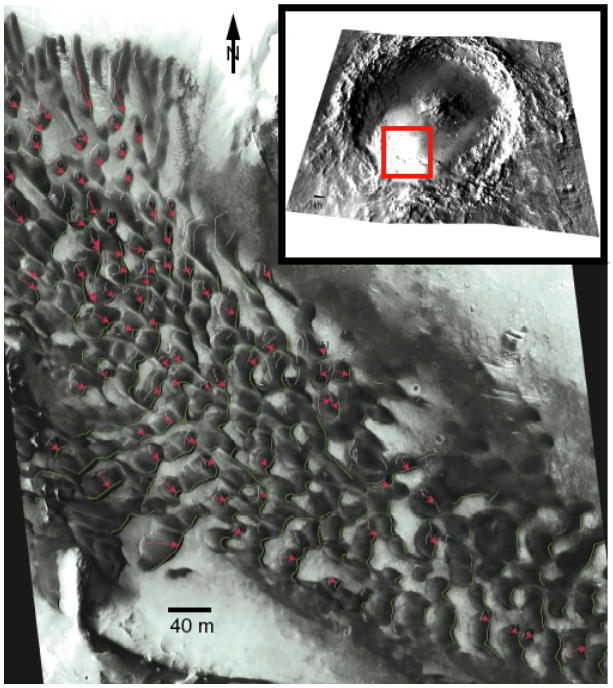

Figure 3: Dune field located inside a crater (11.89°N; 185.87°E) box right. Background is a HiRISE image. Green lines represent the brink of the barchans. White lines represent the high albedo features. Red arrows represent the distance between high albedo features and brink of the nearest dune.

Conclusion: High albedo features appear mainly in the interdune area and do not have significant relief. On Mars, surface liquid water is unstable under current atmospheric pressures and temperatures; however, briny water may have played a role both in supplying the water and the salts to cement the sediments [1].

This data can be used to reconstruct the resultant wind direction at this location and test the output from meso-scale climate models.

References: [1]: Gardin et al. (2010), *Icarus* in press. [2]: Gardin et al. (2010), *Journal of Geophysical Research* in press. [3]: Mangold et al. (2003), *Journal of Geophysical Research* ***108***. [4]: Schenk and Fryberger (1988), *Sedimentary Geology*, **55**. [5]: Bourke M.C. (2010), *Icarus* **205**. [6]: McKee E.D. (1966), *Sedimentology*, **7**. [7]: Simpson and Loope (1985), *Journal of Space Science*, **55**. [8]: Kocurek et al. (2007), *Sedimentary Geology*, **197**. [9]: Langford et al. (2009), *Geomorphology*, **105**. [10]: Szynkiewicz et al. (2009), *LPSC* 40th. [11]: Bourke et al. (2008), *Geomorphology*, **94**.

Acknowledgements: Funding for this work came in part from NASA MDAP grant NNG05GQ60G. We also thank the region Rhône Alpes of France for the financial support project CIBLE 2006. We also thank the HiRISE team for the public availability of images.

MARS ANALOG: GRAND FALLS DUNE FIELD, ARIZONA R. K. Hayward[1], J. R. Zimbelman[2], L. K. Fenton[3], T. N. Titus[1], G. E. Cushing[1], [1]USGS, Astrogeology Science Center, 2255 N. Gemini Dr., Flagstaff, AZ 86001, rhayward@usgs.gov; [2]CEPS/NASM MRC 315, Smithsonian Institution, Washington, DC 20013-7012; [3]Carl Sagan Center/Ames Research Center, Moffett Field, CA.

Introduction: The history of the formation, growth and migration of dune fields on Mars can reveal much about Martian climatic history, but large features change so slowly on Mars [1, 2] that we may need hundreds to thousands of years of repeat imagery to calculate the flux rates needed to use dunes for climate reconstruction. The Grand Falls dune field, analogous in many ways to Martian dune fields, formed about 60 years ago and remains mobile today. It provides the opportunity to examine sediment mobility and meteorological data (historical records and *in situ* measurements) to determine how terrestrial dune field formation and mobility is affected by environmental/climatic conditions. We can use terrestrial-based relationships to help us interpret what the dune fields on Mars have to say about that planet's climate history. Here we introduce the Grand Falls dune field and examine it as a Mars analog. Analogous features include dune field size, topographic setting, sand composition, periodic source availability, and dune morphology.

Grand Falls, Arizona: *Overview*. The Grand Falls dune field is located ~ 70 km NE of Flagstaff, AZ, 2 km east of Grand Falls, and just north of the Little Colorado River (LCR). Vegetation is minimal. The dune field consists of barchans, smaller dunes/ripples, and bare interdunes with indurated surfaces, all features that commonly comingle on the Martian surface. Figure 1 highlights the visual similarity between rippled sand surfaces on Mars and the Grand Falls dune field.

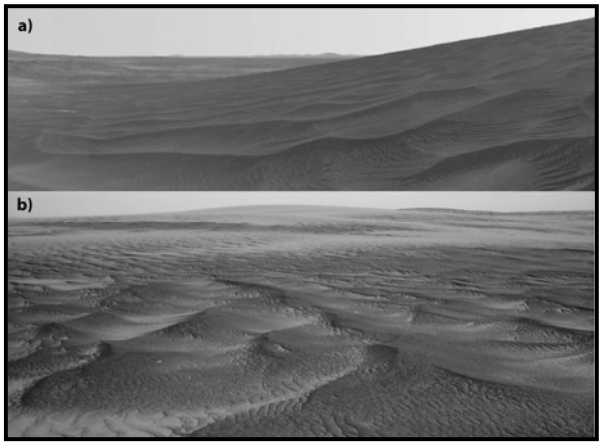

Figure 1. Which is Mars and which is Grand Falls, AZ? The top image, PIA03274, taken by Mars Exploration Rover *Spirit*, shows an example of a rippled sand deposit in Gusev crater on Mars. The bottom image shows a rippled surface in the Grand Falls dune field. Dark areas in 1.b are basalt grains, concentrated on ripple crests.

In 1935, aerial photos of the Grand Falls area showed no evidence of a dune field, but by 1954, a small dune field (~500 m by 750 m) had formed. Figure 2 documents the dune field's growth and rapid migration (averaging ~30 m/year), from 1954 to 2007.

Figure 2. Migration of Grand Falls dune field based on 1954 (red) aerial photo, 1997 (orange) and 2005 (gold) DOQQs and 2007 (yellow) NAPP. Between 1954 and 2007, the dune field moved ~1.6 km. Figure back-ground is 2007 NAPP.

Dune Field Size and Setting. The size of the dune field today (~1.5 km by 1 km) and its location within a topographic trap make it similar to small intracrater dune fields on Mars. The dunes at Grand Falls are in a relative topographic low, migrating toward topographic highs that will impede their progress. This setting is analogous to the setting of an estimated 1500 dune fields on Mars that occur within craters and valleys [e.g. 3, 4].

The composition and grain size of Grand Falls dunes contribute to its value as a Mars analog. Most of the dune sand on Mars is composed of basalt, but gypsum in dunes is also present [5]. At the Grand Falls dune field, composition is also bimodal. Dunes are composed of light-toned, fine-grained quartz sand and dark-toned medium- to coarse-grained basalt sand (Figure 3). The difference in composition results in contrasting albedo as shown in Figure 1.b. The basalt

sand component may have originated as local ash and lapilli-fall from volcanic eruptions in the region. Flash floods from local tributaries may have washed additional ash and lapilli-fall deposits into the LCR, making more basalt available to the dune field. The source of the quartz sand, the major component of the dunes, is likely the LCR. Changes in the river flow and sediment load control the availability of quartz sand. A sudden influx from the LCR probably triggered dune formation in the first half of the 20th century. Aerial photographs show that the LCR had a well defined channel in 1935, but in 1954 the river channel was less well defined and loaded with sediment. This sudden availability of a local source of sand could be analogous to Mars, where a local source of unconsolidated sand may become available (e.g., through excavation by erosion or impact) and begin dune formation.

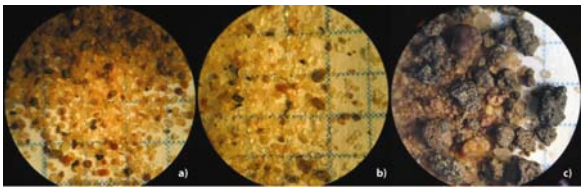

Figure 3. Microphotographs (1 mm grid) of samples taken from a) barchan slip face, b) adjacent LCR bed, and c) ripple crest in Grand Falls dune field. Grains are bimodal in composition and size. The river bed sample is similar to the slipface sample, but is not consistent with the coarse basalt found on the ripple crest.

Dune Morphology. The Grand Falls dune field consists of ~65 barchans/modified barchans that range from ~20 m to ~70 m in width. The tallest are an estimated 5 m to 8 m in height. Interspersed among the barchans are smaller dunes/ripples, and bare interdune areas with indurated surfaces. Figures 4 and 5 show examples of the similarity of dune morphology at the Grand Falls dune field and on Mars. Figure 4 shows classic barchan dunes and modified barchans with tails. Figure 5 shows barchans that have been modified to have one kinked limb [6].

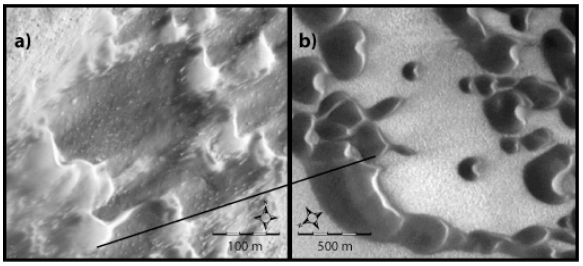

Figure 4. Comparison of dunes at Grand Falls (a) and on Mars (b). Martian dunes shown are ~ 5 times larger than terrestrial dunes shown. Note similarity in morphology, relative spacing, shape of modified barchans with tails (connected by line), and relative size of tails. Figure (a) NW tip of Grand Falls dune field, centered at 35.438° N, 111.167° W (2007 NAPP digital image, 1 m res). Figure (b) is centered at 83.57° N, 119.94° E, (CTX image P01_ 1593_ 2635_XI_83 N241W, 6m/pixel res).

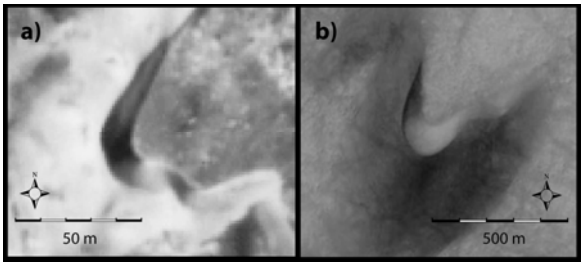

Figure 5. Comparison of dunes at Grand Falls (a) and on Mars (b). Dunes have a similar morphology, a modified barchan shape with a kinked limb. Here, as in Figure 4, the Martian dune shown is ~ 5 times larger than the terrestrial dune shown. Figure (a) Eastern portion of Grand Falls dune field, centered at 35.427° N, 111.163° W (2007 NAPP digital image, 1 m res). Figure (b) is cropped from MOC NA image R1401899, (image is centered at 41.38° S, 334.81° E, 3.5 m/pixel res).

Summary: Many of the aeolian questions on Mars are difficult to address, given the time required to detect change in Martian dunes. An active analog dune field on Earth, where environmental changes can be documented since the inception of the dune field and linked to dune migration rates, will help us understand environmental changes on Mars. Dune field size, topographic setting, sand composition, periodic source availability, and dune morphology are among the features that qualify the Grand Falls dune field as a Mars analog. Its value is enhanced because the dune field's history can be documented since it first appeared about 60 years ago.

References: [1] Bourke, M.C., Edgett, K.S., Cantor, B. A. (2008) *Geomorph. 94*, 247-255, doi:10.1016/j.geomorph. 2007.05.012. [2] Zimbelman, J. R. et al. (2009) *Icarus*, doi: 10.1016/j.icarus.2009.03.033 [3] Hayward, R. K., et al. (2007), *JGR, 112*, E11007, doi:10.1029/2007JE002943 [4] Fenton, L. K. and Hayward, R. K., *Geomorph.* (2009), doi: 10.1016/j.geomorph.2009.11.006. [5] Langevin, Y., F. Poulet, J.-P. Bibring, and B. Gondet (2005) *Science*, *307*, 1584-1586. [6] Bourke, M. C. (2009), *Icarus*, doi:10.1016/j.icarus.2009.08.023.

Volcaniclastic Aeolian Deposits at Sunset Crater Volcano, Arizona: Applications for Martian Analogs.

Donald M. Hooper, Ronald N. McGinnis, Marius Necsoiu, Cynthia L. Dinwiddie, and Debashis Basu
Geosciences and Engineering Division, Southwest Research Institute®, San Antonio, TX 78238-5166.

Introduction: Volcaniclastic aeolian deposits at Sunset Crater volcano serve as a compositional analog to dunes on Mars. Most aeolian dune systems on Earth are dominated by quartz grains; however, the current understanding is that many dunes on Mars are composed of basaltic (mafic) particles. Sunset Crater in north-central Arizona (USA) is a 900-year-old [1] scoria-cone volcano composed of alkali olivine basalt. Wind action has subsequently redistributed its widespread tephra (ash and lapilli) deposit into a variety of aeolian landforms. We have collected geomorphological and sedimentological data to help establish a baseline for the type and morphometry of dunes, physical properties (e.g., grain size and composition), saltation pathways, and interactions with topography.

Coppice dunes: Coppice dunes (also known as nebkhas) form where sand-sized particles are trapped by clumps of vegetation and create small sand mounds or hummocks (Fig. 1). While there are no coppice dunes on Mars, shadow dunes on Mars have similar characteristics. Dune height was measured for 15 coppice dunes and ranged from 0.3 to 3.3 m with a mean of 1 m. Nine of these dunes comprised a subset located 10 km northeast of Sunset Crater near Black Bottom Crater that was mapped using kinematic differential GPS as part of a detailed dune domain. Coppice dunes are typically elliptical to nearly circular in plan view, and field measurements determined a mean length of 6.7 m and a mean width of 4.8 m. The major axis for many of the dunes trends in the direction of the prevailing wind, but this tendency is mitigated by patchy vegetation that creates an irregularly shaped mound.

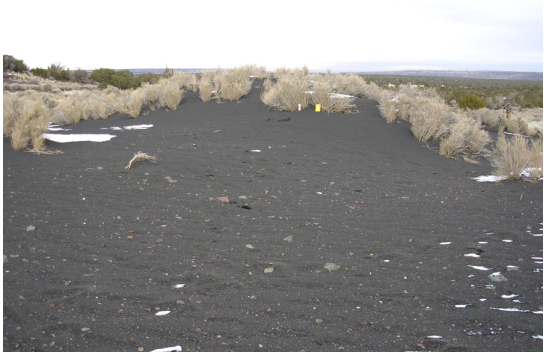

Fig. 1. Large coppice dune (sample 008a). Note wind ripples in foreground and patches of snow. Sagebrush (Artemisia tridentate) is the major plant type entrapping sand particles.

The mean grain size for 18 sedimentological samples from coppice dunes was 0.70 mm (0.50 phi), which is a coarse sand (Fig. 2). However, for 13 samples located approximately 10 km from Sunset Crater and 5 samples located approximately 20 km from the volcano, the grain size decreases from 0.83 mm (0.27 phi) to 0.36 mm (1.5 phi), respectively. Although there is an overall decrease in pyroclastic grain size as distance increases from a volcano during an eruption, the observed trend indicates sorting and winnowing by aeolian processes.

Wind ripples: Ripples are not widespread but were found on sandy, vegetation-free surfaces and on the flanks of some large coppice dunes. They are valuable because they provide an almost instantaneous indication of local sediment transport and wind direction. Wavelengths were measured over representative lengths for three ripple sets, and the mean wavelengths were 36, 22, and 29 cm. Amplitude was estimated to be approximately 0.5 cm. Typical wind ripples have a wavelength of 5–20 cm and an amplitude of 0.5–1.0 cm [2,3,4]. The longer wavelengths of these ripples are most likely due to the grain size of the sediment, which is a coarse sand with an abundance of granules (1–4 mm median grain-size particles). The mean size of sand comprising ripples was coarser than that of the underlying sandy sediment, but grain-size variation from trough to crest was visually indistinguishable. These observed wind ripples in basaltic sediments may serve as valuable analogs for similar features on Mars, including "transverse aeolian ridges" (TARs) [5,6].

Other aeolian features: Sand streaks (also known as sand stringers) at Sunset Crater taper to the northeast according to the prevailing wind direction. They are linear surficial deposits (≤25 cm in thickness), but retain a relatively constant width in the downwind direction. Some sand streaks extend downwind for more than a kilometer and may be 200 m in width. Both light- and dark-colored sand streaks have been observed on Mars. To the northeast and east of Sunset Crater, falling dunes occur in the lee of Woodhouse Mesa and along other escarpments. These dunes are accumulations of sand on the downwind side of topographic highs. The falling dunes observed in this study are poorly developed and thin, lacking a prominent ramplike structure. In some locations they can be considered simple cliff-top dunes or sand streaks. Similar topographic obstructions are abundant on Mars and may serve as a sediment sink [5].

Discussion: For all collected samples (ripple, coppice, and interdune corridor), the percentage of nonbasaltic particles ranged from 2 to 6%, meaning the sam-

ples are overwhelmingly composed of basalt fragments and related mineral grains. Quartz-rich dust forms the majority of the fraction in the pan and is most likely accretionary aeolian silt. For medium-sand-to silt-size fractions, the percentage of nonbasaltic particles generally increases as grain size decreases.

Grain-size analysis also provides a method to separate each sample into gravel, sand, and silt fractions. As anticipated for volcaniclastic aeolian deposits, the samples are dominated by the sand-size fraction, ranging from almost 100% sand to 74.6% sand for one interdune corridor sample (009). No sample had more than 1.6% silt. While other authors report silt-rich coppice dunes [7], the coppice dunes at Sunset Crater are primarily formed of sand-size grains.

Finally, there is a coarse sand/granule surface lag found primarily across the lower elevations of the study site as the geographic setting transitions to the adjacent Painted Desert. This armoring consists of a thin (approximately 5 mm or one or two particles in thickness), surface layer above a fine-grained substrate. Well-developed desert or stone pavements are found on abandoned alluvial surfaces, stabilized sand sheets and sand ramps, and aeolian mantles on lava flows [8]. The surface veneer at the study site, which is influenced by the initial tephra-fall deposit, is volcaniclastic and acts as a coarse sand sheet. Aeolian aggradation—rather than deflation—is proposed to be the major formative mechanism as particles undergo syndepositional lifting with an accreting soil layer [9,10]. In the Sunset Crater region, the upward migration of coarse particles is most likely aided by alternating wetting and drying as well as freezing and thawing. Because of the recent age (<1 ka) of the Sunset Crater eruption, infiltration of quartz-rich silts transported largely as windblown suspended load is minimal—as demonstrated by our analyses—and is still in the initial stages. Instead, volcaniclastic aeolian particles comprise the fine-grained component and may facilitate aggradation.

Conclusion: There are numerous questions regarding dunes on Mars that could be answered by thoroughly studying analogous dune environments like the Sunset Crater region and by analyzing and comparing satellite data of Martian dune fields and the Sunset Crater dune field. Field work and laboratory analyses have helped describe the morphology, morphometry, and granulometry of several coppice dunes as well as other aeolian features across a study site dominated by volcaniclastic sediments. This baseline of information is helping to focus a potential Martian analog study and increase our understanding of the role of topographic obstacles in dune formation, physical properties of dune sands, sand/saltation transport, and the sediment history in regions dominated by aeolian processes.

Acknowledgments: Project funding was through SwRI®'s IR&D Program, Quick-Look Project R8110. The authors appreciate lab support provided by J. Frels, D. Waiting, and D. Sims; technical reviews by P. Dubreuilh and E. Pearcy; and editorial assistance by S. Odam and L. Mulverhill.

References: [1] Ort M.H. et al. (2002) Tech. Report No. 2002-16, Desert Archaeology, Inc., Tucson, AZ. [2] Bagnold R. A. (1941) The physics of blown sand and desert dunes, Methuen, London (reprinted 1954; 1960; 2005, by Dover, Mineola, NY). [3] Sharp R. P. (1963) J. Geol. 71(5):617-636. [4] Lancaster N. (1995) Geomorphology of desert dunes, Routledge, London, UK, and New York City, NY. [5] Bourke M. C. et al. (2003) LPS XXXIV, Abs. 2090. [6] Wilson S. A. and Zimbelman J. R. (2004) JGR-Planets, 109, E10003, doi:10.1029/2004JE002247. [7] Nickling W. G. and Wolfe S. A. (1994) J. Arid Env. 28, 13-30. [8] Laity J. (2008) Deserts and desert environments, Wiley-Blackwell, West Sussex, UK. [9] Wells S. G. et al. (1985) GSA Bull. 96(12):1518-1529. [10] McFadden L. D. et al. (1987) Geol. 15(6):504-508.

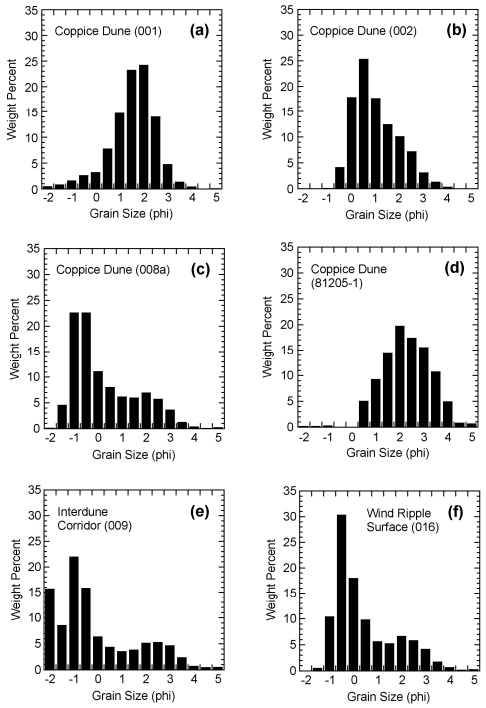

Fig. 2. Histograms for six sieved samples: (a) Coppice dune sample 002, D (distance from Sunset Crater) = 17.5 km, x (mean) = 1.29 phi (0.409 mm), σ (standard deviation or sorting) = 0.98 phi; (b) Coppice dune sample 001, D = 13.6 km, x = 0.762 phi (0.590 mm), σ = 0.94 phi; (c) Coppice dune sample 008a, D = 10.4 km, x = 0.00588 phi (0.996 mm), σ = 1.4 phi; (d) Coppice dune sample 81205-1, D = 19.8 km, x = 2.03 phi (0.245 mm), σ = 1.0 phi; (e) Interdune corridor sample 009, D = 10.4 km, x = −0.332 phi (1.26 mm), σ = 1.7 phi; and (f) Wind ripple (1 cm surface) sample 016, D = 10.8 km, x = 0.196 phi (0.873 mm), σ = 1.3 phi.

ICE AND SULFATE INDURATION IN THE MARTIAN NORTH POLAR SAND SEA. B. Horgan[1], J. F. Bell III[1], and M. C. Bourke[2], [1]Cornell University (briony@astro.cornell.edu), [2]Planetary Science Institute.

Introduction: Saltation has been a major erosional and depositional force on the surface of Mars, but the dynamics and timescales that govern the movement of martian sand dunes are poorly understood. In particular, major insights are needed into the mechanisms that cause induration of sand dunes and how these mechanisms affect dune migration rates. Possible modes of induration include chemical (cementation by salts, ferricrete, etc.), physical (settling and compaction of sand and/or dust), and niveo-aeolian (cementation by pore or interbedded ice) [1-3]. This study aims to search for evdience of each of these processes and evaluate their relative influence by examining dunes within the north polar sand sea, which encircles and is sourced from within the north polar plateau (Planum Boreum) [4]. The north polar sand sea offers a unique opportunity to study all of the above processes in one location, as both ice and soluble sulfates are present in the dune fields.

Evidence for dune interior ice:. Analysis of Neutron Spectrometer and thermal-infrared data indicate that dunes in the north polar erg are best modeled as ice-rich cores covered by several cm of loose sand [2]. Studies of ice-rich duneforms in the Antarctic Dry Valleys have shown that ice can substantially slow the movement of dunes [3], so subsurface ice could explain why dunes in the north polar erg look fresh but have shown no observable migration (at a ~tens of meters scale) in 30 years of observations [5,6].

Evidence for soluble sulfates: The most extensive sulfate deposit on Mars is located within Olympia Undae (OU), the largest dune field within the north polar sand sea. Near-infrared (NIR) spectra of OU from the Mars Express OMEGA imaging spectrometer are consistent with the hydrated calcium sulfate gypsum [7,8]. Although the highest gypsum concentrations (up to 40 wt.%) are limited in extent, gypsum is likely present at low levels throughout the the entire sand sea [8].

Methods In this study, we use high-resolution images (HiRISE) to identify and map decameter-scale features on sand dunes in the north polar erg. Ice melting or sublimation (denivation) has been postulated as the cause of some of these features, while others may be caused by dry granular flow or surface induration due to compaction or cementation [2,9]. However, further evidence is needed to confirm these hypotheses. By mapping the distribution of dune surface features in key locations in the north polar region and comparing the distribution to geographic context, dune morphology, thermophysical properties (THEMIS),

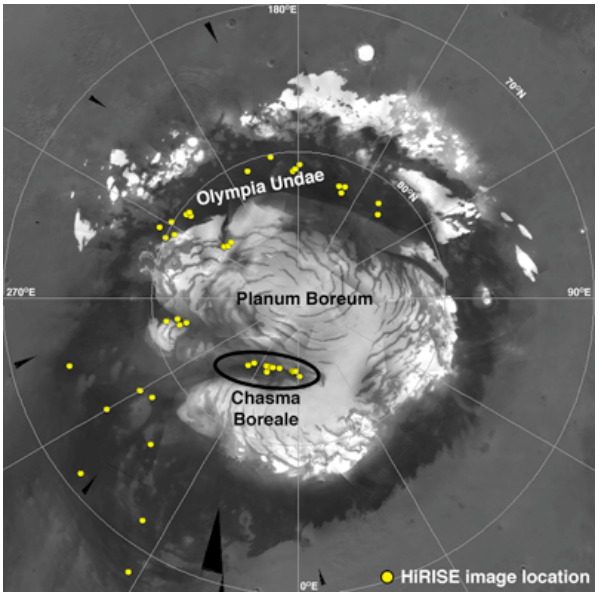

Fig. 1: North polar region and locations of HiRISE images examined in this study (Basemap: MOC-WA). Sand sea encompasses all low-albedo terrains.

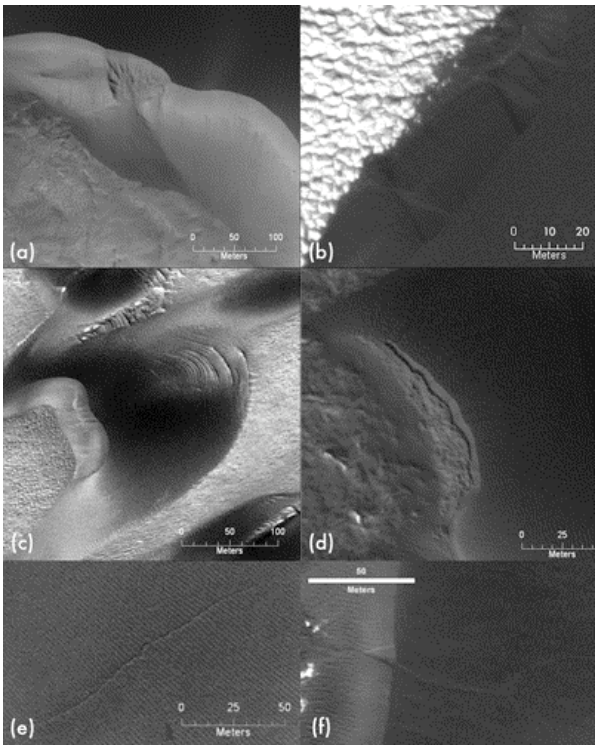

Fig. 2: (a) Complex fan, (b) simple fans, (c) protruding layers, (d) pitted slump, (e-f) surface cracks.

and spectral properties (OMEGA), we can place constraints on the processes responsible for each class of features, and therefore on the structure and mobility of the dunes. In particular, we have targeted the highest latitude dune fields within Chasma Boreale, where we expect to observe ice-related dune features, and the OU dune field, where we may observe correlations with sulfate abundance (Fig. 1). We have divided observed dune surface features into five classes (Fig 2), based on morphology and association [10].

Fans (dry granular flow features): Fans are features with wedge-shaped alcoves above fan-shaped deposits, likely the result of dry granular flow during failure of an over-steepened slipface (Fig. 2). The steep sides of the alcoves may imply that the surrounding material is indurated [9]. Fan morphologies range from simple (single failure, 1-20m) to complex (multiple failures, up to 150m). Co-located HiRISE images taken over consecutive summers and within the same season show fans appearing and fading, indicating that fans are common features that are actively forming and eroding. Fans are more common near scarps, where katabatic winds are strong, and seem to occur less often in areas with OMEGA water ice detections [10]. These observations suggest that fans are good markers for the most active regions of dune fields, and could be used to target dune change detection efforts.

Surface cracks (sulfate cementation features): Surface cracks have linear, branching morphologies and generally run away from the dune crest on the stoss slope [9]. Linear cracks suggest a thin (several cm) surficial crust under tension due to thermal expansion or structural changes within the dune. Cracks are often observed emanating from fan alcoves, possibly indicating a genetic relationship (Fig. 2).

Across OU, the distribution of surface cracks is not uniform (Fig. 3), and appears to correlate with hydration band depth, which linearly tracks gypsum abundance [8]. This implies that gypsum is cementing the dunes. Chemical cementation by salts occurs when the salts are dissolved in water and reprecipitated at contacts between sand grains [*e.g.* 11]. This process requires liquid water, at least in the form of thin films, thus implying that brines have been present in these dunes since they last moved. Such brines could be sourced from interior ice, and may be similar to the putative brines observed on the Phoenix lander [12].

Remnant layers (sulfate or ice cementation features): Remnant layers are indurated layers exposed on, protruding from, or preserved behind the stoss slope of a dune [9]. Both ice- and salt-cemented layers can exhibit this behavior. Remnant layers occur in two common locations: (1) on dunes near scarps with abundant fans, and (2) on small isolated barchans

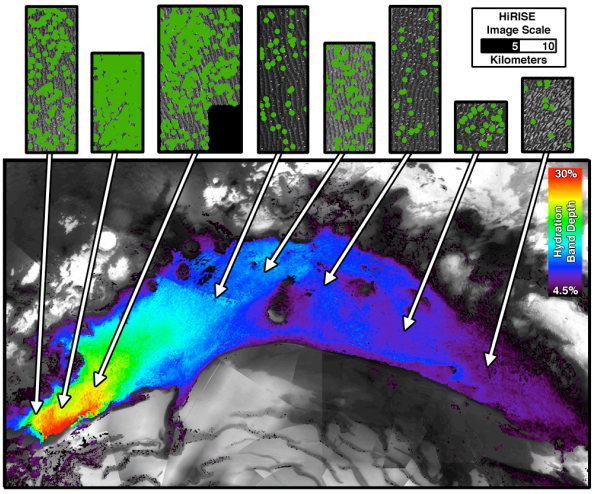

Fig. 3: Surface cracks (green dots) on dunes compared to OU hydration band depth (gypsum abundance).

farthest from scarps. These features suggest that these dunes have migrated, although in the latter case, the lack of dry granular flow features suggests that they may not have migrated recently.

Pits and slumps (ice cementation features): Pits occur as singular, chains, or coalesced chains of collapse features usually found along dune crests. Slumps are collapse features on slipfaces, with the collapse occurring along a portion or the entire length of the slipface. These features are difficult to distinguish, as slumps are often pitted. These collapses are likely a result of denivation [9]. Pits may be caused by localized denivation and the associated loss of material, while slumps may occur when catastrophic denivation destabilizes a slipface layer. Both pits and slumps occur much more often on dunes at the highest latitudes.

Ongoing work: We are currently: (1) analyzing the distribution of features other than surface cracks in OU; (2) searching for correlations with dune morphology; (3) incorporating high-resolution CRISM spectral maps to analyze the ice content of dunes; and (4) investigating relationships with dune daytime temperature and thermal inertia (THEMIS).

References: [1] Sullivan, R. *et al.* (2008) *JGR*, *113*, doi:10.1029/2008JE003101. [2] Feldman, W. *et al.* (2008) *Icarus*, *196*, 422-432. [3] Bourke, M.C. *et al.* (2009) *Geomorphology*, *109*, 148-160. [4] Tanaka, K. *et al.* (2008) *Icarus*, *196*, 318. [5] Schatz, V. *et al.* (2006) *JGR*, *111*, doi:10.1029/2005JE002514. [6] Bourke, M.C. *et al.* (2008) *Geomorphology*, *94*, 247-255. [7] Langevin, Y. *et al.* (2005) *Science*, *307*, 1584. [8] Horgan, B. *et al.* (2009) *JGR*, *114*, doi: 10.1029/2008JE003187. [9] Bourke, M. *in prep.* [10] Horgan, B. *et al.* (2010) *LPSC XLI*, #1325. [11] Schenk, C. and S. Fryberger (1988) *Sed. Geol.*, *55*, 109. [12] Renno, N. *et al.* (2009) *LPSC XL*, #1440.

A PROGRESSION OF INDURATION IN MEDUSAE FOSSAE FORMATION DUNES. L. Kerber[1] and J. W. Head[1], [1] Brown University Department of Geological Sciences. 324 Brook Street, Box 1846, Providence, RI 02912, Laura_Kerber@brown.edu

Introduction: Aeolian erosion and transport is hypothesized to be an important geomorphological process on Mars. Recent work has shown that some dune fields on Mars are active today [1, 2]. However, the majority of martian dunes that have been observed over time have shown no evidence of growth or translation [3, 4]. Some of these dunes with low levels of activity may be indurated [5]. Despite this apparent lack of movement, however, only a few martian dune fields appear to be old enough to have accumulated craters or other indications of degradation and erosion [6].

Dunes located within the Medusae Fossae Formation (MFF), a fine-grained unit of unknown origin located near the equator [e.g. 7, 8], display a range of morphologies, from very fresh-looking dune-forms to cratered and eroding remnant dunes. Yardangs and other wind-related features dominate the surface of the MFF, and there is evidence from morphology and stratigraphic relationships that the unit has been fairly mobile in the past [9]. While the details of the particle-size distribution of the MFF are unknown, the presence of dunes suggests that there are particles or particle-aggregates that are of the appropriate size for saltation. The variety in degradational states observed in MFF dunes suggests that dune formation, induration, and degradation is a significant and ongoing process within the formation.

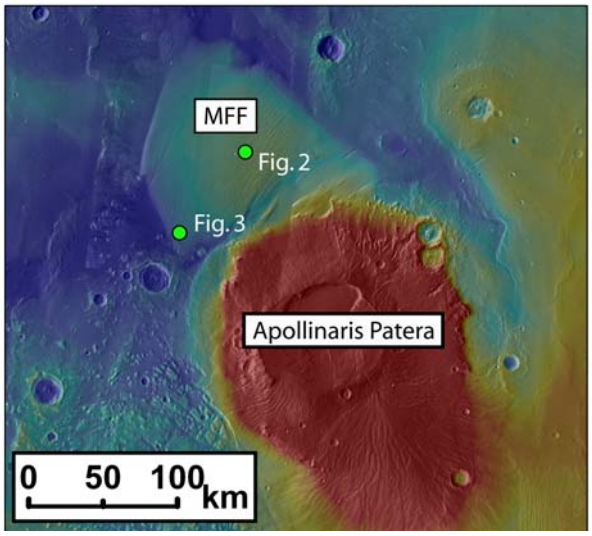

Figure 1. A regional view of Apollinaris Patera and an adjacent MFF deposit. Global MOLA data overlain on a global THEMIS mosaic.

Observations: The MFF is composed of massive deposits, erosional yardang-dominated terrain, etched terrain, and sand dunes [10, 11]. A deposit of the MFF northeast of Apollinaris Patera (Fig. 1) provides a type locality for some of the many degradational states of sand dunes that are found in the Medusae Fossae Formation.

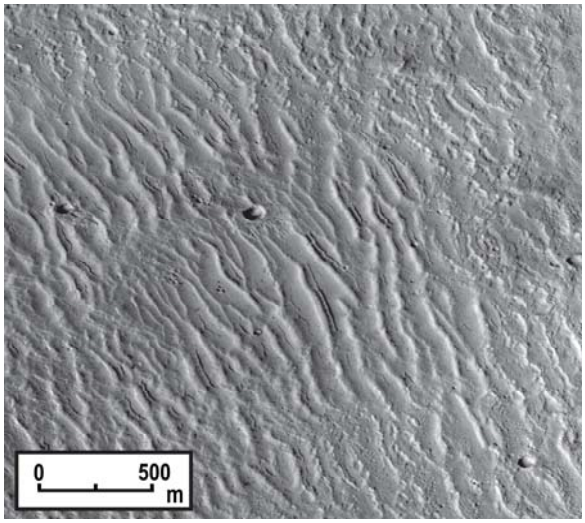

Figure 2. Heavily eroded, etched and cratered dune-forms in the Medusae Fossae Formation, indicating a high level of induration. MOC image M1301069.

While the eastern part of this outcrop of the MFF is dominated by smooth deposits and yardangs, the central part of the outcrop is characterized by a rough, indurated terrain with degraded and cratered dune-forms (Fig 2.). The western section of the outcrop is composed of a fairly smooth surface marked by numerous secondaries from a nearby 22-km impact crater to the southwest. At high resolution it can be seen that there are sand dunes on the surface, many of which are highly eroded (Fig. 3). Fresher-looking sand dunes can be observed in the deeper craters, where they were either more recently active or better sheltered from erosion. Moderately degraded dune-forms can be seen in slightly shallower craters, and very degraded sand dunes are present on the upper flat surface of the deposit. In Figure 3 there is a fresh primary crater whose rays covered and preserved some of the original dune textures, providing evidence that the sparse dunes that cover the surface were once more continuous.

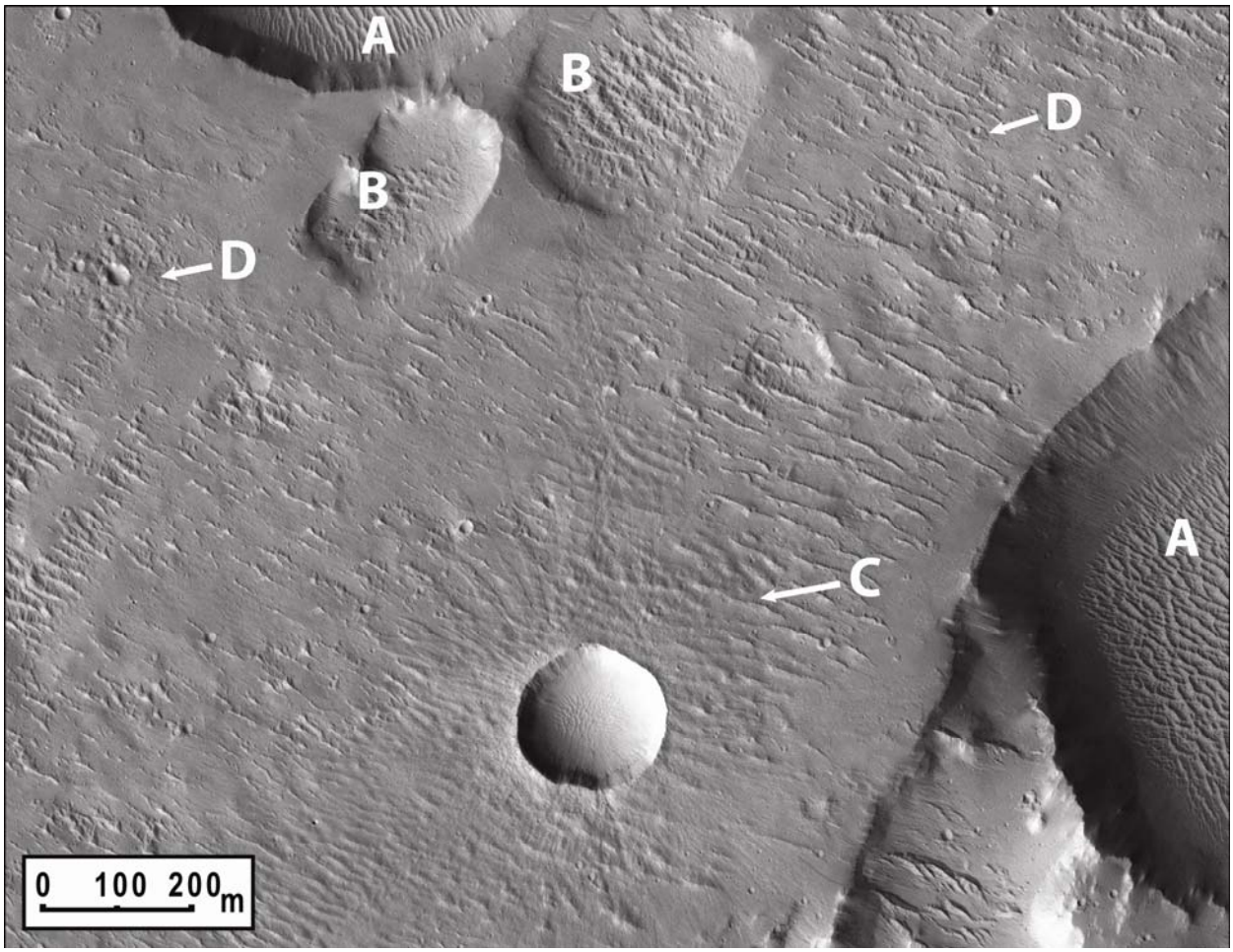

Figure 3. A region of the Medusae Fossae Formation northeast of Apollinaris Patera with secondary craters (A and B) from a nearby 22 km impact crater. A) Relatively fresh-looking dunes have collected in the large secondary craters. B) Slightly more indurated dunes fill the shallower craters. C) The rays from a fresh primary crater have preserved the morphology of pre-existing dunes; elsewhere on the surface the dune-forms have been eroded. D) Small impact craters are superposed on the remnant dunes. HiRise image PSP_003966_1725.

Conclusions: In order for dunes to be preserved in the eroded state seen in the MFF, they must have been subject to some kind of induration process which was able to strengthen them against moderate wind. Unlike most terrestrial sandstones, there is no visible evidence that these dune fields were exhumed from depth, though this possibility cannot be eliminated.

The induration process taking place in the MFF has allowed dunefields to survive long enough to become degraded and cratered, a somewhat rare occurrence on Mars. This suggests that either the mode of induration taking place in the MFF yields more robust surfaces than elsewhere on Mars, or that the dunes formed and became indurated at an earlier time than dunes elsewhere on Mars.

References: [1] Fenton, L.K. (2006) *GRL, 33,* L20201. [2] Bourke M. C. et al. (2008) *Geomorphology, 94,* 247-255. [3] Edgett, K., Malin, M.C. (2000) *JGR, 105* E1. [4] Edgett, K. (2002) *JGR,107* E6. [5] Schatz, V. et al. (2006) *JGR, 111,* E04006. [6] Edgett, K.S., Malin, M.C. (2000) *LPSC XXXI*, Abs. 1071. [7] Scott, D.H. and Tanaka, K.L. (1986) *USGS Misc. Invest. Ser.* Map I-1802-A [8] Bradley, B.A. and Sakimoto, S.E.H. (2002) *JGR, 107,* E8 [9] Kerber, L., Head, J.W. (2010) *Icarus, 206,* 669-684. [10] Zimbelman, J.R., Griffin, L.J. (2010) *Icarus, 205,* 198-210. [11] Mandt, K.E. et al. (2008) *JGR, 113,* E12011.

Eolian features on Mars and Titan: resemblance and difference; G.G. Kochemasov, IGEM of the Russian Academy of Sciences, 35 Staromonetny, 119017 Moscow, Russia, (kochem.36@mail.ru).

Two large planetary bodies –a planet (Mars) and a satellite (Titan) – both keep significant atmospheres and show traces of eolian action on their surfaces. In the martian case widespread classical dunes can be discovered in many areas at various latitudes. Fig. 1 demonstrates as the younger dunes "eats' the older ones that is normal for winds changing directions. On Titan ripples prefer dark methane lowlands at the equatorial belt (tropics) (Fig. 2) and bear some peculiar characteristics.

A persistent ripple pattern covers mostly dark smooth plains. This pattern consists of very regular often cross-cutting (Fig. 3) wavy forms hundred and thousand kilometers long with spacing between ridges or grooves about 1-2 km (PIA03555, PIA03566, PIA03567, PIA03568) or 10-20 km (PIA08454) -so called "cat scratches". Some important characteristics of this pattern usually considered as a result of eolian action still have to be explained. **1)** The pattern consists of intersecting (cross-cutting) ridge-groove structures not destroying each other under intersection; radar can fix at least two structure directions (Fig. 3); normal eolian forms tied to winds of changing directions show earlier dunes wiped out by the later ones (Fig. 1). **2)** Ridges (dunes) are radar-brighter, grooves are darker normally at the equatorial belt (Fig. 3-4), but the opposite is observed (ridges are darker, grooves lighter) in the image PIA11802 at the southern edge (19.2 degrees south) of the wide equatorial dune field (Fig.5 to 7). **3)** Symmetric shape of tight and straight dunes (Fig. 5); a perfect symmetry is not typical for Earth and Mars (Fig. 1). **4)** Width of ridges and grooves is nearly equal with variations to both sides (Fig. 3-4); at the southern end of the equatorial "dune" belt spacing between dunes increases and can reach 10 km, the ripple pattern becomes less regular (PIA 11802, the southern part) (Fig. 7). **5)** Meeting an obstacle (high standing light icy blocks) dunes are abruptly cut keeping their shape and width (Fig. 5-6); one would expect some radical changes in dune appearance under an action of a wind turbulence caused by a barrier. **6)** Morphologically resembling dunes groove-ridge systems on sectors of a tectonic grain (Fig. 8) have different strikes. Uplifted sectors (radar-lighter) have nearly E-W strike, separating them subsided ones (especially the upper one) show N-S strike. Such pattern of the groove-ridge system can be better interpreted as a tectonic pattern.

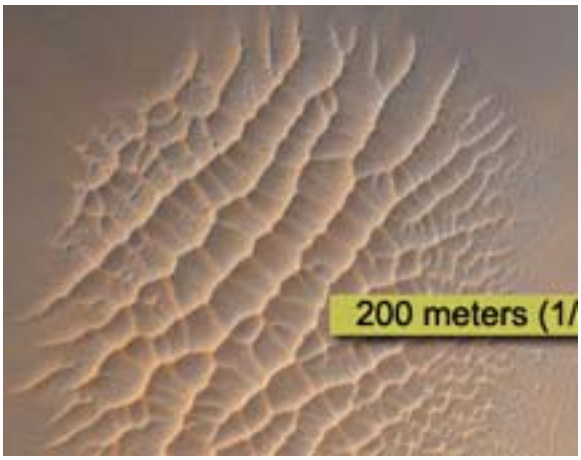

Fig. 1.

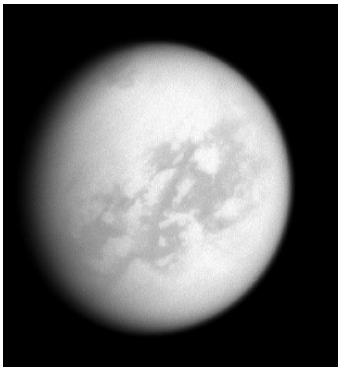
Fig. 2.

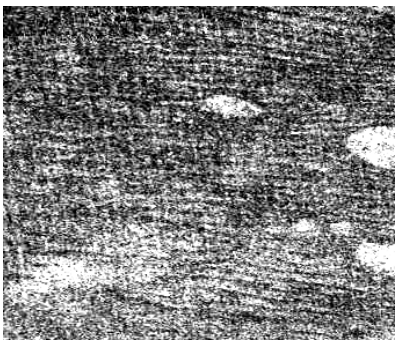
Fig. 3.

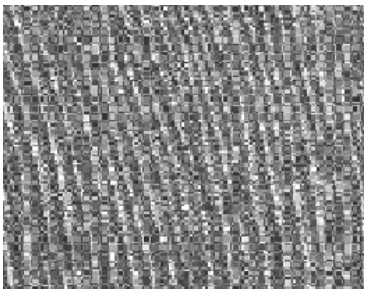
Fig.4.

Fig. 5.

Fig. 6.

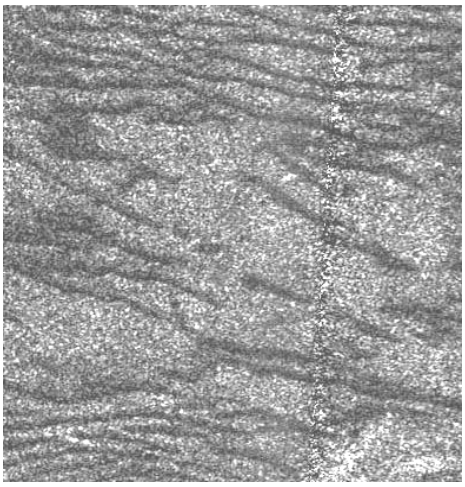

Fig. 7.

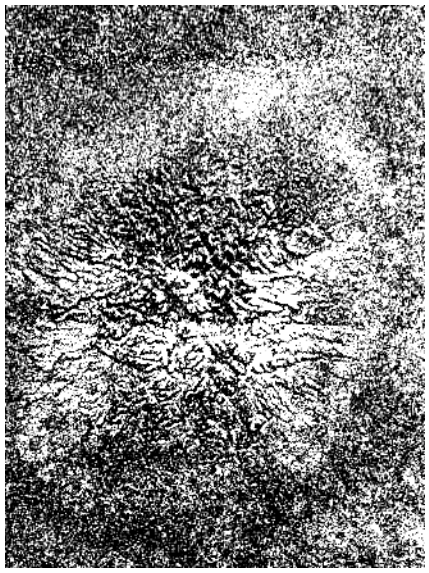

Fig. 8.

Fig. 1. Dunes on the Victiria Crater bottom, Mars (TRA_000873_1780). Two dunes directions. The later direction (to the left) wipes the earlier one (to the right) what is a necessary characteristics of eolian (wind) formations.

Fig. 2. Titan, PIA10594. Destruction of the light icy crust in the equatorial belt and appearance of cementing dark wavy methane plains (lowlands).

Fig. 3. Titan's surface, radar image, a portion of PIA03567 (13˚ south lat., 300˚ west long.), grid spacing 1-2 km.

Fig. 4. Titan, radar image, a portion of PIA08454, grid (ridge-to-ridge) spacing ~12 km.

Fig. 5. Titan's dunes. A portion of PIA11802 (19.2˚ south lat., 257.4˚ west long.). the frame width is ~31 km.

Fig. 6. Titan's dunes. A portion of PIA11802, the frame width is ~ 30 km.

Fig. 7. Titan's dunes. A portion of PIA11802, the frame width is ~53 km.

Fig. 8. Titan. A portion of PIA12496 (41˚ north latitude, 213˚ west longitude). Tectonic granule has characteristic size $\pi R/91$ (~88 km) and sectored structure. Two uplifted sectors (radar-light) are separated by two subsided sectors (dark). Groove-ridge systems are roughly oriented W-E on the light sectors and N-S on the dark ones.

CHARACTERISTIC TIME SCALES OF DUNE-RELATED PROCESSES IN POLAR REGIONS OF MARS. ***M. A. Kreslavsky***[1], [1]Earth and Planetary Sciences, University of California - Santa Cruz, 1156 High Street, Santa Cruz, CA, 95064, USA, mkreslav@ucsc.edu

Introduction: Dark sand dunes are abundant in high-latitude areas of Mars [e.g., 1, 2]. They are indicators of surface-atmosphere interaction and potentially record details of the recent climate changes on Mars. Recent studies of dune morphology and observations of actual changes [e.g., 3, 4] indicate that sand movement does occur in the present epoch, but the overall rate of sand migration is significantly lower than for active dune fields on the Earth.

One of the recognized factors potentially responsible for the low activity levels is induration of the sand by ground ice [e.g., 4]: at high latitudes on Mars, H_2O ice is known to be stable against diffusive exchange of H_2O vapor with the atmosphere [e.g., 5, 6], which means that H_2O vapor would diffusively migrate from the atmosphere into sand and condense as ice at some depth.

Here I consider an independent observational constraint on dune activity time scales from the population of small impact craters in Olympia Undae, the largest sand sea on Mars located at high northern latitudes. Then I analyze characteristic time scales related to diffusive H_2O exchange between sand, the atmosphere and the substrate and use these considerations to explain some observed phenomena.

Impact crater population in Olympia Undae: I visually searched HiRISE images of Olympia Undae dunes for small impact craters superposed over the dark sand. I surveyed all full-resolution summer-time (no seasonal frost) images released by March 2010, totally 24 images. Their total area was 1640 km^2, and the area covered with dark sand was estimated to be 1340 km^2. My experience with searches of this kind shows that craters larger than ~5 m can be reliably identified. Only one crater was found (Fig. 1); its diameter is about 7 m. The formal error bar for statistics of one crater is wide: at 90% confidence level, the expected number of craters (related to the crater retention age) is bracketed within 0.1 - 3.9 interval.

I use the accumulation population of small craters on ejecta of a young 10-km crater Zunil as a proxy for production function of small craters [7]. Found single crater means that the crater retention age on Olympia Undae is bracketed between $2.7\times10^{-5}\ T_Z$ and $1.0\times10^{-3}\ T_Z$, where T_Z is the age of Zunil. This estimate is biased on two reasons. (1) Thicker atmosphere (due to lower elevation in comparison to Zunil) and seasonal frost (especially because it is present during the aphelion season, when impact rate is higher [8, 9]) make crater production rate in Olympia Undae lower than for Zunil. (2) All other condition being the same, an impact into loose or slightly indurated sand produces a larger crater than the same impact into rocky Zunil ejecta. These two biases partly compensate each other.

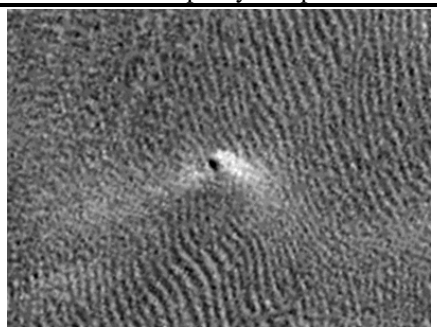

Fig. 1. Impact crater in Olympia Undae. Portion of HiRISE image PSP_009728_2620. The scene is 100 m wide, north is on the top, solar illumination is from lower left.

The absolute calibration of ages obtained from small craters is also highly uncertain. The observed present-day cratering rate of 5.3×10^{-7} km^{-2} a^{-1} has been reported in [9], and 5 m is close to the observed diameter cut-off of the new craters. Two observations indicate that the true rate is probably a factor of a few higher. (1) New impacts are unevenly distributed in the dusty region of Mars, which indicates that impacts in some places in these region do not produce large dark halos and hence cannot be spotted [10]. (2) The size-frequency distribution of the new craters is shallower than that of the production population on Zunil ejecta.

Taking in account all uncertainties, the age constraints from the impact crater population can be summarized in the following statements:

- During a thousand of martian summers (or quicker), any 5-10-m size crater would be completely obliterated.
- Crater in Fig. 1 certainly survived at least a few martian summers.

This is consistent with the following:

- ➢ Migration of Dunes in Olympia Undae does occur under the present-day climate conditions
- ➢ Characteristic sand migration rates are significantly lower than for terrestrial active dunes

Water vapor and ice in sand dunes on Mars: The diffusion coefficients of water vapor in soils under martian conditions has been measured in [11]. For sand (unless its pore space is saturated with ice), the highest measured diffusion coefficient of 5 cm^2s^{-1} is appropri-

ate. This high value looks perfectly plausible given high porosity, large pores and low tortuosity of the pore space in sands, as well as low gas pressure. High diffusion coefficient of water vapor in martian soil is consistent with the diurnal atmospheric humidity cycle observed by Phoenix lander [12]. The diffusion coefficient of water vapor can be directly compared with thermal diffusivity of sand. Thermophysical parameters adopted in [4] and consistent with TES temperature observations of Olympia Undae dunes give thermal diffusivity 4×10^{-4} cm^2s^{-1} for ice-free sand and 1×10^{-2} cm^2s^{-1} for ice-saturated sand. Thus, the diffusion coefficient is much higher than the thermal diffusivity. This means that the stable diffusive flux is established instantly in response to temperature changes.

Exchange with the atmosphere. Detailed calculations of ground ice stability against vapor diffusion under the present-day climate conditions [6] show that ice is unstable in the uppermost decimeter(s)-thick layer of the soil and is stable beneath it. For Olympia Undae the model calculations [6] predict the ice table at ~30 cm, deeper than for other surfaces at the same latitude due to lower albedo and higher thermal inertia of the dark sand. This is consistent with neutron flux observations [4]. In the upper secularly dry soil layer, minor amounts of ice can come and go seasonally and diurnally due to vapor exchange with the atmosphere [6]. Typical concentrations of this seasonal ice in models of [6] were on the order of 10^{-6} by weight. These calculations were done for diffusion coefficient on the order of 0.1 cm^2s^{-1}. Significantly higher actual diffusion coefficient would lead to higher ice abundance. In addition to diffusive transport, vapor can be advectively transported into sand due to forced ventilation caused by daily pressure cycle and wind turbulence. Thus, seasonally varying ice amount of 10^{-4} to 10^{-3} of the pore volume can be expected. Laboratory experiments under martian conditions [13] have shown preferential early deposition of ice at grain contact points. This means that sand can get and lose at least some cohesion very quickly, at seasonal or diurnal time scale, due to tiny amount of ice coming and going in response to temperature and humidity changes.

Sand can potentially be mobilized by winds only during certain season and certain hours of a day, when the uppermost millimeters of sand are free of ice. Dunes are "frozen" all other time due to small amounts of ice in sand. This effect contributes to the observed low rate of sand transport. This also explain the puzzling coexistence of apparently fresh slip faces of dunes in Olympia Undae (that are formed by loose non-cohesive sand) and gully-like avalanche scars and other landslide-like features (that need depth-dependent cohesion for their formation).

Insolation conditions and temperature regimes depend on slope orientation, hence the seasonal and diurnal "unfrozen windows" may be different for different slopes. Some slopes can be source of saltating sand, while other slopes can be slightly cohesive and develop small-scale morphology of eolian erosion, which is also observed in Olympia Undae.

Exchange with the substrate. Analysis of images indicates that the dark sand in northern circumpolar areas of Mars and perhaps in other high-latitude locations is deposited over ice-rich substrate. If sand rests on such a substrate for a long time, a vertical temperature gradient due to the geothermal heat flux will be established in the deposit, and water vapor diffusion will cause slow migration of H_2O from the warmer substrate into colder sand. A very rough order of magnitude estimate is 1 Ma time scales for complete filling pore space in 10-m thick sand layer by this process.

The situation is very different for migrating sand masses. Dark sand has lower albedo and hence higher year-average temperature than neighboring exposed surfaces. Thus, in freshly deposited sand beds the temperature gradient will be opposite (until the geothermal flux is reestablished at 100s- and 1000s-year time scales): the substrate will be colder than sand, hence the diffusive water vapor flux will go from sand into the substrate, thus drying the sand. This effect prevents filling the main mass of dunes with ice and helps keeping them dry and mobile. This effect may explain, why in the martian polar areas dunes are made of dark sand.

A similar effect occurs when dark sand beds are exhumed from polar ice deposits (images show numerous cases of this kind). When high-albedo ice cover goes away, the year-average surface temperature dramatically increases, which causes downward diffusive flux of water vapor and removal of ice from upper sand layers. This effect probably contributes to mobilization of freshly exposed sand at high latitudes.

References: [1] Tsoar H. R. et al. (1979) *JGR, 84,* 8167–8180. [2] Hayward R. K. et al. (2007) *JGR, 112,* E11007. [3] Bourke M. C. et al. (2008) *Geomorphology, 94*, 247-255. [4] Feldman W. C. et al. (2008) *Icarus 196*, 422-432. [5] Farmer C. B. and Doms P. E. (1979) *JGR 84*, 2881-2888. [6] Schorghofer N. and Aharonson O. (2005) *JGR 110*, E05003. [7] Kreslavsky M. A. (2008) *AGU Fall Meeting*, #P41B-1361. [8] Ivanov B. A. (2001) *Space Sci. Rev. 91*, 87-104. [9] Daubar, I. J. et al. (2010) *LPS XLI*, 1978. [10] Kreslavsky M. A. (2007) *7th Mars Conf.*, #33325. [11] Hudson, T. et al. (2007) *JGR 112*, E05016. [12] Hecht, M. (2010) *LPS XLI*, #1481. [13] Hudson, T. et al. (2009) *JGR 114*, E01002.

ASSESSING DUNE-FORMING WINDS ON PLANETARY SURFACES – APPLICATION OF THE GROSS BEDFORM NORMAL CONCEPT

Nicholas Lancaster, Desert Research Institute, 2215 Raggio Parkway, Reno, NV 89512, USA..

Introduction: Understanding the relationships between dune trend or alignment with respect to the wind is essential for reconstruction of planetary wind regimes, past and present, as well as for verification of circulation patterns predicted by global and regional climate models. Many workers have concluded that dunes are oriented relative to the resultant or vector sum of sand transport [1]. Thus dunes can be classified as transverse (strike of crestline approximately normal to resultant), longitudinal (crest parallel to resultant), or oblique (15-75° to resultant direction) [2-5]. Field and laboratory experiments with wind ripples and sub-aqueous dunes [6, 7] suggest, however, that all bedforms are oriented in the direction subject to the maximum gross bedform-normal transport across the crest, so that sand transport from all directions contributes to bedform development. By comparison, use of the resultant direction of transport as a control of bedform orientation implies that transport vectors from opposing directions cancel out each other and thus do not contribute to bedform growth. These experiments and subsequent numerical simulations [8] show that the type of dune that forms is determined by the divergence angle between the dominant and subordinate transport vectors and the ratio between the two primary transport directions (Transport ratio). A trend parallel to or normal to the resultant direction of sand transport is purely coincidental. Applications of this concept to modern and paleo-dune patterns are, however, limited [9-11].

In this study, the trend or alignment of a global sample of major dune types is compared to gross bedform normal potential sand transport calculated from observations of wind speed and direction at nearby weather stations to verify the application of this concept to terrestrial dunefields.

Methods and data sources: Data on wind speed and direction were extracted from a single and consistent observational dataset, the International Station Meteorological Climate Summary (ISMCS) [http://www.ncdc.noaa.gov/oa/mpp/cdroms.html], supplemented by additional datasets for certain areas as available. From these data, the sand transport potential for each wind direction as well was calculated using the approach of [1]. The calculated sand transport potential data were then used as input for calculation of the gross bedform normals and resultant sand transport direction and magnitude using a JAVA version of the program Trend [6]. Data on dune trends were measured on satellite images in the area adjacent to the weather stations using Google Earth, which also provided information on dune type (classified using [12]).

Results: Data on dune trends and gross bedform normal (GBN) were derived for a sample of 24 localities worldwide. The relationships between measured dune trend and calculated GBN trend is shown in Figure 1. There is a generally close relationship between dune orientation and GBN for barchans and crescentic dunes (average difference – 9°); the relationships for linear dunes and some star dunes are less close (average difference – 44 and 26° respectively]. In general, a mismatch results from variations in wind regime between the observation site and the dunes. In some cases, however, there is a clear mismatch between linear dune trend and GBN. This appears to indicate that these dunes are not in equilibrium with modern wind regimes.

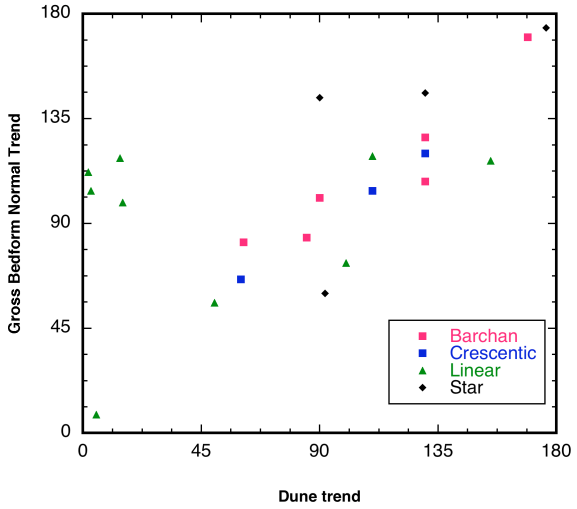

Fig. 1: Relationships between observed dune trends and gross bedform normal trends calculated from wind data.

Conclusions: Comparisons between the observed and predicted gross bedform-normal orientations of dunes classified as barchan, crescentic, linear, and star in different sand seas and dunefields confirms that all major dune types are oriented to maximize gross bedform-normal sediment transport. Thus all dune types are dynamically similar. Differences between the form of dunes therefore result from variations in the directional characteristics of the flow, especially the

angle(s) between the major transport directions and the ratio(s) between the magnitude of flows from different directions. The good predictive ability of the gross bedform-normal rule suggests that it is possible to distinguish clearly between dunes that are in equilibrium with present wind regimes and those that were formed in past conditions. This facilitates prediction of past wind regime characteristics from dunes.

References: [1] S. G. Fryberger, in *A Study of Global Sand Seas: United States Geological Survey, Professional Paper,* E. D. McKee, Ed. (1979), 1052. [2] M. Mainguet, Y. Callot, *Mémoires et Documents CNRS* **18**, 178 (1978). [3] R. E. Hunter, B. M. Richmond, T. R. Alpha, *Geological Society of America Bulletin* **94**, 1450 (1983). [4] K. W. Glennie, *Desert Sedimentary Environments*. [5] R. A. Bagnold, in *Desert Research, Proceedings of the International Symposium*. (Research Council of Israel, Jerusalem, 1953), 89. [6.] D. M. Rubin, H. Ikeda, *Sedimentology* **37**, 673 (1990). [7] D. M. Rubin, R. E. Hunter, *Science* **237**, 276 (1987). [8] E. Reffet, S. C. Du Pont, P. Hersen, S. Douady, M. Fulchignoni, paper presented at the Planetary Dunes Workshop, Alamogordo, NM, 2008. [9] N. Lancaster *et al.*, *Geology* **30**, 991 (2002). [10] N. Lancaster, in *NATO Advanced Research Workshop on sand, dust, and soil in their relation to aeolian and littoral processes*. (University of Aarhus, Sandbjerg, Denmark, 1991], 47. [11] V. Sridhar *et al.*, *Science* **313**, 345. [12] E. D. McKee, in *A Study of Global Sand Seas,* E. D. McKee, Ed. (United States Geological Survey, 1979), 1052, pp. 3-19.

DUNES AS STREAMLINES : MODELING TOPOGRAPHIC DIVERSION AND BLOCKING OF LINEAR DUNES WITH POTENTIAL FLOW THEORY R. Lorenz, JHU Applied Physics Laboratory, Laurel, MD 20723 (Ralph.lorenz@jhuapl.edu).

Abstract: Potential flow theory is used to generate 2-dimensional streamlines which compare favorably with the observed patterns of linear dunes on Earth and Titan. The blocking of dunes by topographic obstacles, and their diversion around topography, is modeled by the superposition of source (and possibly sink) terms onto a uniform flow. This formalism provides a means of quantifying the effect of obstacles on the dune field and opens the way to correlating this effect with the scale and height of the obstacles.

1. Introduction

One of the most striking aspects of the appearance of dunes on Titan[1,2,3] in Cassini Radar images was how they resembled streamlines, parting around bright topographic obstacles (e.g. figure 1). Such diversion of linear dunes around obstacles is also evident on Earth (e.g. figure 2). Yet how can we quantitatively describe this diversion? Topography on Titan is not well known, although an initial assessment with some of the sparse data available[3] suggests a steepness threshold of about 1/100 determines whether dunes are blocked or diverted. Perhaps dune arrangements can be used to estimate the topography.

Figure 1. Example of dark organic sand dunes on Titan parting around a bright, presumably elevated, obstacle.

2. Potential Flow Theory

The morphological resemblance of the dune arrangement with streamlines suggests that perhaps a fluid dynamical description may be effective. One of the simplest of these is the 2-dimensional description of an incompressible and inviscid flow by potential flow theory. Here one defines a velocity potential (whose derivative yields the velocity). A corresponding potential, termed the stream function, can also be defined, and streamlines are contours of constant stream function (the flow never crosses the streamlines). Analytic expressions exist for uniform flow, and for sources and sinks. An example is shown in figure 3, wherein a set of sources, arranged like the ridge in the Australian desert, diverts a uniform flow.

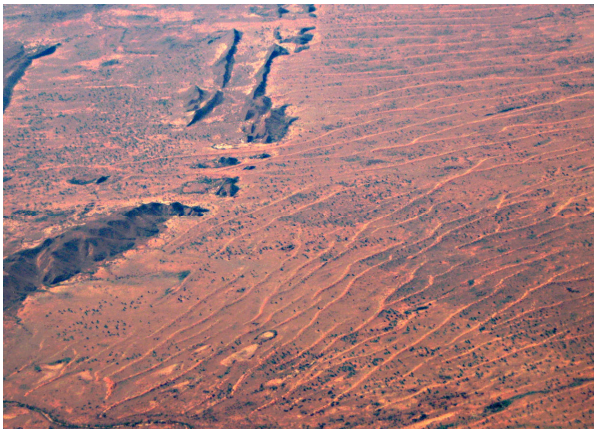

Figure 2. An photograph (from a commercial airliner Melbourne-Alice Springs) of linear dunes in the northwestern Simpson Desert in Australia. The dunes are diverted by a broken ridge of hills.

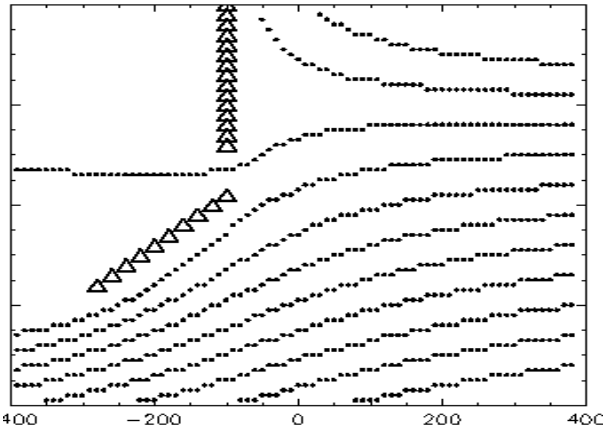

Figure 3. Dunes (dots) plotted to follow constant values of the streamfunction. Streamfunction is modeled for a uniform flow right to left, wth a set of sources indicated by triangles.The morphology compares favorably with figure 2.

3. Discussion

Figure 3 shows that at least part of a dunefield can be described to a degree by a uniform flow plus source terms. However, there are some deficiencies in the description. Around the edge of the obstacle, the streamlines are compressed, which does not happen for dunes (where the spacing[4] is likely controlled by the height of the atmospheric boundary layer).

Potential flow theory requires that the equation of continuity be satisfied, so streamlines cannot simply terminate, yet of course that is observed in dunefields. In future work we will examine whether sink terms may be used to force such effects.

The quantitative meaning of the size of the source terms defining the obstacle, as compared with the value of stream function defining the background flow (i.e. the assumed uniform velocity) remains to be determined. Presumably it can be related to the streamline curvature (i.e. degrees of deviation per kilometer, or a radius of curvature).

.

4. Conclusions

Potential flow theory shows some promise as an analytic means of describing linear dune arrangements on Earth and Titan. The source terms used to cause the deviation of model dunes can be used as quantitative metrics of the effect of topographic obstacles, and can be correlated with the height of such obstacles.

References: [1] R. Lorenz et al., Science, 312, 724-727, 2006 [2] J. Radebaugh, et al., Geomorphology, 2010 [3] R. Lorenz and J. Radebaugh, Geophysical Research Letters, 36, L03202, 2009. [4] Lorenz et al., Icarus, in press, 2010.

Acknowledgements. This work was supported by the Cassini project.

ELEVATION DEPENDENCE OF BEDFORM WAVELENGTH ON THARSIS MONTES, MARS

R. D. Lorenz[1], N. T. Bridges[1], A. A. Rosenthal[2]. [1]Space Department, JHU Applied Physics Laboratory, Laurel, MD 20723, USA. (Ralph.lorenz@jhuapl.edu) [2]Earth and Planetary Science Department, UC Santa Cruz, Santa Cruz, CA 95064, USA.

Abstract

We measure the wavelength of aeolian bedforms on the surface of Martian volcanos, spanning a 23km range in elevation, or nearly an order of magnitude in atmospheric pressure and density. We find that the bedform wavelength varies as the reciprocal of density. We discuss theoretical models that predict such a dependence.

1. Introduction

The unprecedented high resolution of the HiRISE experiment on Mars Reconnaissance Orbiter allows new insights into aeolian features and processes on Mars. HiRISE images of Mars with ground sampling down to 25 cm/pixel show that the dust-rich mantle covering the surfaces of the Tharsis Montes is organized into reticulate ridges whose form and distribution are consistent with formation by aeolian processes. Previous analysis[1] has indicated that dust aggregates are the most likely material composing these bedforms, since the area has low thermal inertia, and the low atmospheric density at these high elevation sites would make difficult the transport of solid materials.

It might be expected (see later) that certain characteristics of aeolian bedforms might have a dependence on atmospheric density. The high imaging resolution, and the range of elevations spanned by the slopes of Martian volcanos, allow us to investigate this question.

2. Observations

We measured the wavelength of reticulate bedforms in 13 HiRISE images on or near the Tharsis Montes over an elevation range of -0.8 to 22.8 km, the largest elevation range readily available on Mars with what can be assumed to be a relatively uniform bedform composition. This exposes elevation (and thus pressure or density - we assume an isothermal atmosphere and thus density is proportional to pressure) as the likely only variable and thus allows us to critically examine any wavelength dependence on pressure.

Within each image, 4 sub-regions were selected. In each of these sub-regions, 10 traverses were made in which the wavelengths of 4-7 ripple sets were measured, each along a parallel line. This resulted in 200-234 'ripple' wavelength measurements per image.

Example images are shown in figure 1 – the difference in wavelength at different elevations is striking.

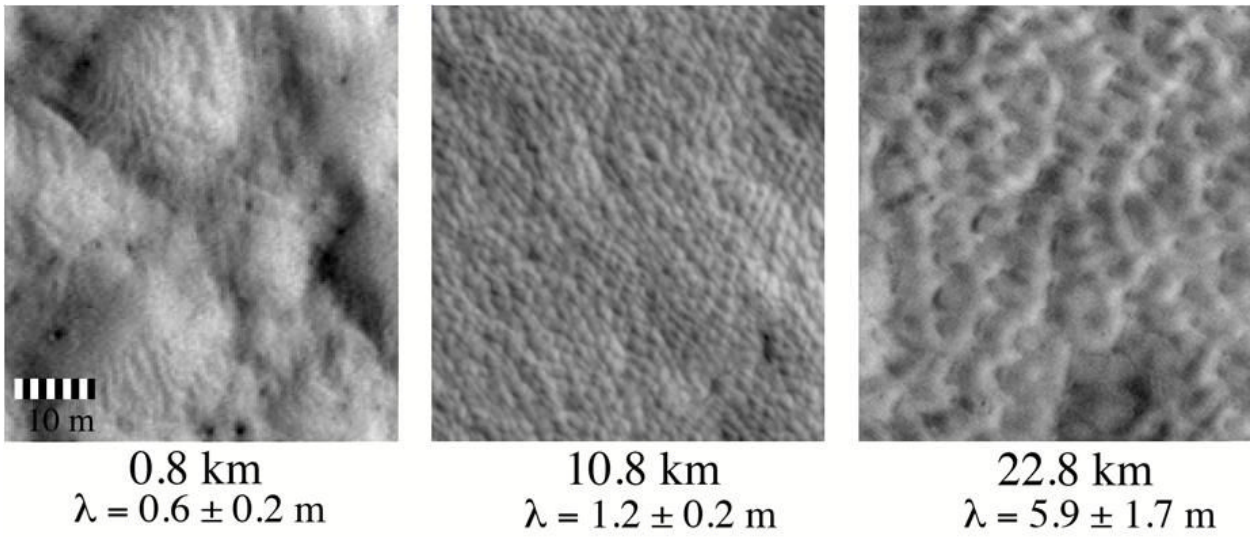

Figure 1. HiRISE imagery of Tharis bedforms. Even with the high resolution, the smallest bedforms (at lowest elevation) are barely resolved. The dependence at higher elevations is very clear, however.

3. Results

Converting elevation to pressure using a scale height of 11.2km, we display the relationship of wavelength with pressure and 1/density in figures 2 and 3.

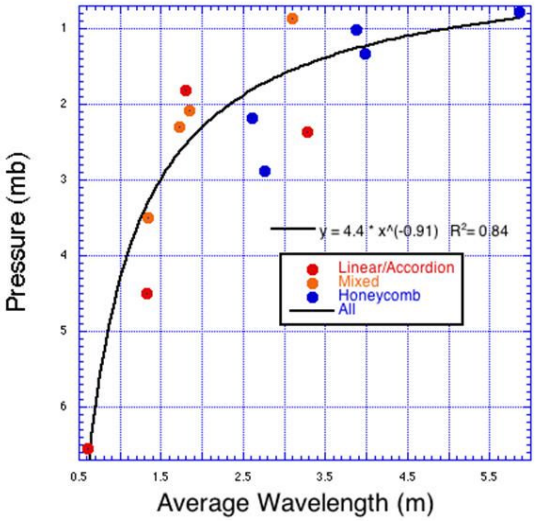

Figure 2. Wavelength variation with pressure. Although a best-fit power law is shown, the fit is statistically indistinguishable from an exponent of (-1).

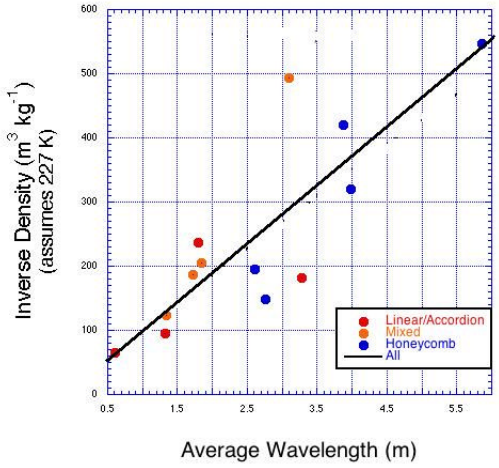

Figure 3. The data of figure 2 replotted as $1/\rho_f$ - a linear fit describes the data well.

4. Theoretical Considerations

We show here that whether these bedforms are considered to be dunes or ripples, the wavelength may be expected to vary as the reciprocal of density in each case.

First, we consider dunes. Recent work[2] suggests that a flat sediment bed will destabilize under shear flow to form 'elemental' dunes with a spacing (the wavelength of the fastest-growing bedform) that relates to the saturation length, or in turn with the 'drag length', the distance scale over which a particle will be accelerated to a large fraction of the freestream speed. The resultant expression is $\sim 53(\rho_s/\rho_f)d$ where d is the particle size and ρ_s is the (solid) particle density and ρ_f the fluid density.

Second, if we consider these bedforms as ripples, we note the assertion of Bagnold[3] that ripples are defined by the saltation length. This perspective, while no longer seen as accurate, does contain a grain of truth. More recent work[4] much more successfully reproduces the phenomenology of real bedforms, and relates to the aerodynamic shear stress variations over a perturbed surface. We mirror Pelletier's analysis as follows.

1)The friction speed (u*) is defined as: $u^* = (\tau/\rho_f)^{0.5}$, where τ is the shear stress and ρ_f is the atmospheric density as before.

2) In order for particles to get raised from the surface by the wind, the friction speed must exceed a threshold value (u_{*t}). The amount of shear stress needed should be constant for a given material and particle size. Therefore, the threshold friction speed should be inversely proportional to the square root of ρ_f .

3) Numerical modeling[4] of ripple wavelength (l) shows that: $l = \sim 3000 z_0$, where z_0 is the aerodynamic roughness height.

4) On an active, flat surface, the heuristic correlation exists that $z_0 \sim d/15 + C_m(u_* - u_{*t})^2/g$, where C_m is a constant.

Now, it is easy to show by numerical experiment that the average value of a windspeed (or friction speed) that follows a statistical distribution (such as the Weibull distribution, which is widely used in terrestrial wind energy work, and provides a satisfactory fit to Viking windspeed data[5]), for those values in the distribution above some threshold, is proportional to that threshold by a factor of order 1~2. It therefore follows that the excess shear velocity ($u_* - u_{*t}$), is proportional to u_{*t}, and squaring, that $l \sim 1/\rho_f$

5. Conclusions

We have measured a strong elevation dependence of bedform wavelength on Martian volcanos, that corresponds to proportionality to the reciprocal of atmospheric density. This relationship agrees with two independent perspectives on theoretical bedform scale length.

References: [1] N. T. Bridges et al., Geophysical Research Letters, 34, L23205, 2007, [2] P. Claudin, and B. Andreotti.. Earth and Planetary Science Letters, 252, 30–44, 2006 [3] Bagnold, R. A., Physics of Blown Sand and Desert Dunes, Methuen, 1941. [4] J. D. Pelletier, Geomorphology, 105, 322–333, 2009 [5] R. D. Lorenz, Journal of Spacecraft and Rockets, 33, 754-756, 1996

HUYGENS BOUNDARY LAYER DATA EXPLAIN THE ~3KM SPACING OF TITAN'S DUNES

R. D. Lorenz[1], J. Radebaugh[2], P. Claudin[3], B. Andreotti[3], T. Tokano[4]. [1]JHU Applied Physics Laboratory, Laurel, MD 20723 (Ralph.lorenz@jhuapl.edu) [2]Brigham Young University, Provo, UT 84602. [3]Laboratoire de Physique et Mécanique des Milieux Hétérogènes (PMMH UMR 7636 CNRS-ESPCI-UPMC-UPD), ESPCI, 10 rue Vauquelin, 75231 Paris, France. [4]Institut für Geophysik und Meteorologie, Universität zu Köln, 50923 Köln, Germany.

Abstract: Titan's linear dunes[1] resemble in morphology, size and spacing (1-3km) those seen on Earth. Although gravity, atmospheric density and sand composition are very different on these two worlds, this coincident size scale suggests that the controlling parameter limiting the growth of giant dunes, namely the boundary layer thickness, is similar. We show[2] that a ~3km boundary layer thickness is supported by Huygens descent data and is consistent with results from Global Circulation Models.

1. Introduction : About 20% of Saturn's moon Titan is covered by giant organic sand dunes, found almost exclusively in a band at the equator bounded by +/-30° latitude[3]. The dunes were discovered in Cassini Radar images, and appear morphologically identical[4], and indeed rather similar in size, to large linear dunes on Earth, such as those in the Namib or Arabian deserts. An initial survey[2] suggested typical lengths of 30-50km and a width of about 1km and spacing of 1-3km: radarclinometry indicates their height to be about 150m.

Recent work[5,6] has shown that there are two fundamental scaling parameters that control the sizeof dunes. The first is the so-called saturation length, i.e. the length over which the sediment flux relaxes towards its equilibrium value. This defines a scale of 'elementary dunes', of size ~53(ρ_s/ρ_f)d can grow and coalesce to form progressively larger dunes, but the growth rate asymptotically declines as the dune length scale approaches the second scale, the thickness of the atmospheric boundary layer. The static stability at the top of this layer provides a 'capping' function, much as does the free surface of the water for subaqueous dunes, and limits the dune growth. On Earth, elementary dunes have a scale of ~20m, whereas on Titan (ρ_f ~5.4kg/m^3) the corresponding size (assuming organic 'sand' with ρ_s ~800kg/m^3, d~200μm is ~1.5m, far below the resolution of Cassini instrumentation. The dunes observed by Cassini are therefore 'giant' dunes, formed by the growth or aggregation of elementary bedforms.

In the absence of direct measurement of the boundary layer , an effective proxy is ~$\delta\Theta/\gamma$, where $\delta\Theta$ is the characteristic (seasonal) variation in potential temperature near the ground, and γ is the potential temperature lapse rate $d\Theta/dz$. This correlation appears to hold for over an order of magnitude of terrestrial dune sizes from coastal dunes of ~300m to giant continental dunes of ~3.5km, and the arguments are based on completely general fluid dynamics considerations. Note that while the boundary layer thickness controls the limiting size of giant dunes, and also controls the size of helical roll vortices sometimes rendered visible by condensation forming long roll clouds, it should not be inferred that roll vortices necessarily form the dunes[7]. The two observable effects represent a common cause, not cause and effect.

2. Observations of Dune Spacing We measured[1] dune spacing in Cassini RADAR images such as figure 1 and found spacing spacing to be rather uniform 2.7-3.2km. Other studies have found spacings of 2.1km[8], and in one case[9] 1-2km.

There is no large-scale regional trend, nor an obvious variation with latitude. Since dune growth is limited by the thickness of the boundary layer[5], this suggests that the Titan layer must have been 3km or more when the dunes were formed.

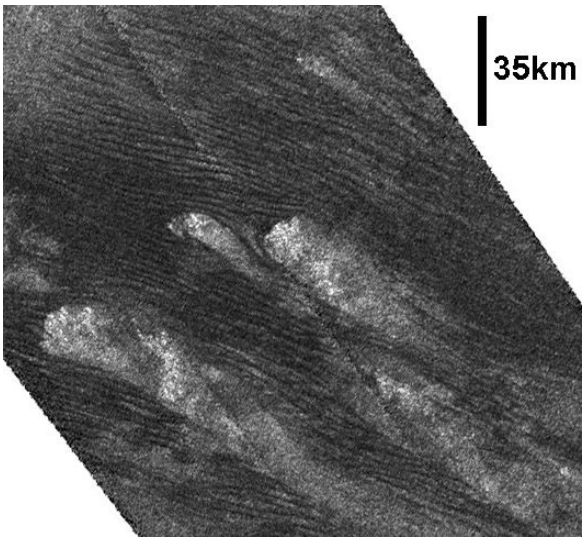

Figure 1. A section of the T41 SAR swath, south of the Huygens landing site, showing typical dune spacing. Although bright topographic obstacles can interrupt the dunefield, the characteristic ~3km spacing is evident.

3. Huygens Probe Boundary Layer Profile A single detailed profile of Titan's atmosphere was obtained by Huygens[10]. This profile occurred at around 9am local

solar time, near 10°S, 192°W. A uniform region of potential temperature Θ between the surface and 300m altitude was initially interpreted[11] as the thickness of a weakly convecting planetary boundary layer. However, Θ is also near-constant[12] over the regions 0.5-0.7 km and 1-2 km, suggesting that an original 2km boundary layer may have been modified by subsequent surface evaporation or morning heating[2] to produce the lower steps in Θ. These, and the 3km inflection in the potential temperature profile show in figure 2 are likely remnants of the boundary layer formed in previous days, the so-called 'residual layer', while the convective boundary layer developing on landing day defines the most obvious 300m layer.

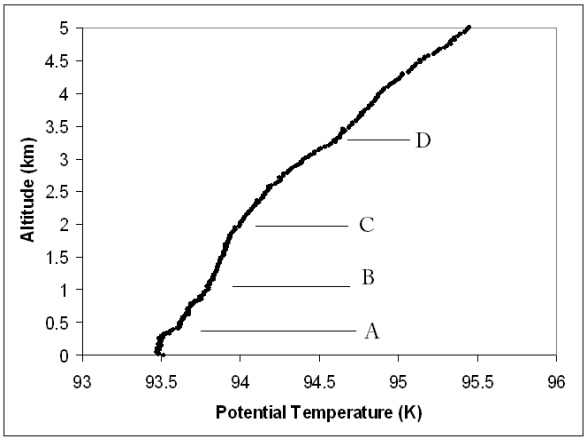

Figure 2. The near-surface potential temperature profile derived from Huygens data (Tokano et al., 2006) The constant Θ region 0-300m identified in that paper as the boundary layer is clearly seen (A); two additional steps in the profile at ~0.9km and ~2km (B,C) were suggested by Griffith et al. (2008) as suggesting a rather thicker, older boundary layer (C) had been modified subsequently (A,B). An additional inflection is seen at ~3.3km (D).

4. Global Circulation Model Predictions and Implications for Titan The boundary layer was estimated[13] pre-Cassini at ~700m. We can also use the heuristic $H \sim \Delta\Theta/\gamma$ as a proxy for the boundary layer thickness and dune spacing. Further, in the absence of additional data, we must assume that the potential temperature variation can be equated to the thermodynamic temperature variation (i.e. $\delta\Theta \sim \delta T$, which appears[5] correct to within ~20% for all the locations studied on Earth. For the relevant γ, we adopt the ~0.5 K/km seen in the lowermost few km of the Huygens profile (figure 2).

As discussed elsewhere[2] we may estimate the low-latitude surface temperature variation[14] at 2-4K with the boundary layer temperatures having δT at 1~2K. The hydrocarbon lake scenario, with an appropriately low albedo but higher thermal inertia than dune sands has similarly a surface low-latitude temperature swing of ~3K (note that latent heat effects of lake evaporation were not modeled, so in fact this scenario is a reasonable approximation of a sand sea, although it has a drag coefficient that may be small compared with that appropriate for a dune-covered terrain).

Taking these results together, it seems that δT of the order of 1-2K is not unreasonable, and thus $\delta T/\gamma$ of ~2-4km would be predicted, which is in encouraging agreement with the observed dune spacing, and the boundary layer thickness suggested by Huygens.

5. Conclusions Titan's dunes prove to be an important diagnostic of that world's atmosphere. It has already been shown[15,16] that the latitudinal extent of the dunes seems to be consistent with the transport of methane humidity away from low latitudes, and the prograde (West to East) sand transport implied by the dune morphology[1,3,4] poses some interesting challenges to circulation models, which expect low-latitude near-surface winds to be generally E-W.

We note in closing that there is much to be learned by studying Titan's landscape and atmosphere : the complexity of the Huygens profile suggests that meteorological characterization of the boundary layer and its variations will be important and interesting. Further, the small drag length in Titan's thick atmosphere and resultant elementary dune size of ~1.5m suggests that imaging of resolution ~0.1m will be needed on future missions to adequately characterize the aeolian geomorphology on Titan.

References: [1] R. Lorenz et al., Science, 312, 724-727, 2006 [2] R. Lorenz et al, Icarus, 2010 [3] R. Lorenz and J. Radebaugh, 2009. Geophysical Research Letters, 36, L03202, 2009 [4] J. Radebaugh, et al. 2009, Geomorphology, 2010 [5] B. Andreotti, et al., Nature, 457, 1120-1123, 2009. [6] P. Claudin, and B. Andreotti.. Earth and Planetary Science Letters, 252, 30–44, 2006 [7] S. Hanna, Journal of Applied Meteorology, 8, 874-883, 1969 [8] J. Barnes et al., Icarus 195, 400-414, 2008. [9] J. Radebaugh et al. Icarus 194, 690-703, 2008. [10] M. Fulchignoni et al., Nature, 438, 785–791, 2005 [11] T. Tokano et al., Journal of Geophysical Research, 111, E08007 [12] C. Griffith, et al., Astrophysical Journal, 687, L41-L44, 2008. [13] M. Allison, ESA SP-338, pp.113-118, Symposium on Titan, ESA SP-338, 1992 [14] T. Tokano, Icarus, 173, 222-242, 2005 [15] J. Mitchell, J. Geophys. Res., Vol. 113, E08015, 2008. [16] P. Rannou et al., Science, 311, 201-205, 2006.

Acknowledgements. This work was supported by the Cassini project, the NASA OPR program, CNRS and DFG.

SEGREGATION OF OLIVINE GRAINS IN VOLCANIC SANDS IN ICELAND - IMPLICATIONS FOR MARS. N. Mangold[1], D. Baratoux[2], O. Arnalds[3], J.-M. Bardintzeff[4], B. Platevoët[4], M. Grégoire[2], P. Pinet[2], [1]LPGN, CNRS Université de Nantes, Nantes, France, [2] DTP/OMP Toulouse, CNRS, France, [3] RALA, Reykjavik, Iceland, [4] IDES, Université Paris Sud, CNRS, Orsay, France.

Introduction: Dark sand is widespread on the planet Mars especially in the north polar region and in the floor of several craters. On Earth, volcanic sands are present in desertic areas like volcanic islands such as Canaria Islands, Iceland, Réunion, or Hawaii, and arid to semi-arid volcanic provinces such as Washington plateau, New Zealand, Andes plateaus [1]. Their composition displays a large variety including basaltic minerals, volcanic glasses, cinders, and lithic fragments derived from explosions. These sands have been poorly studied, mainly because of the predominance of quartz-bearing sand and the lack of large deserts dominated volcanic sands. The primary goal of this study is to better understand the composition and sorting of volcanic sands in a context where basaltic minerals are predominant. In Iceland, many sand plains are composed of volcanic glass grains formed in subglacial context [2]. Nevertheless, one plain located in the Lambahraun plain, in the southwest of the country, is composed of basaltic minerals eroded from two shield volcanoes. In this plain it is possible to analyze variations in composition from eolian sorting. This location has been used as a natural laboratory to test wind effects on volcanic grains.

Observations: The Lambahraun lava field is blanketed by a mantle of eolian sands, especially to the western part where the terrain is relatively flat. Eolian ripples are frequent, but no true eolian dune exists. During field campaigns katabatic winds were observed coming down from the Langjökull glaciers producing a strong northern wind. Drifting of sand was visible on the ground raising up in the air a large amount of dust through saltation of sand particles. The corridor defined by the sand movement is visible on the Landsat image where the smoothest part of the lava field is elongated from north to south at the western edge of the field (Fig. 1).

Composition of sand and source rocks were achieved with fluorescence X. Most major and minor elements have a weight oxides proportion in between the two source rocks. However, an enrichment in Mg, Fe and Ni is observed for most sand samples compared to source rocks. This enrichment can be explained by a significant increase in the proportion of olivine. Indeed, this mineral is dominated by Mg and Fe. In Eldborgir lavas, the predominant metal present is Mg, as established from ion microprobe. The olivine measured are indeed forsterite (Fo64-Fo82). Ion microprobe results also indicates that the olivine grains contain strong proportion of Ni (0.16% in average), whereas other grains are devoid of Ni. Thus, Nickel corresponds to a good chemical indicator of variations of olivine proportion in the different samples. As these three elements (Mg, Fe, Ni) are enriched simultaneously in sand, they may indicate a higher proportion of olivine in sand.

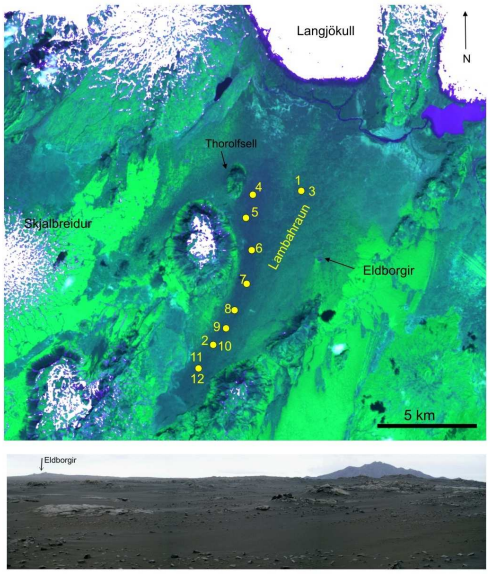

Fig. 1: SPOT image of the Lambahraun plain with samples collected along the main wind direction (north to south). Bottom: Image of the Lambahraun plain.

To analyze this hypothesis more in-depth a plot displaying Ni versus Mg abundance has been derived for all sands and rocks (Fig. 2). The plot of the ELD rock composition is normalized by a mean of six samples of the Eldborgir lava flows. It is visible that the other sand source, the basalts from the Skersli volcano, has a proportion in Ni and Mg almost similar to Eldborgir lavas. All sand compositions are significantly enriched in Ni and Mg with regards to the source rocks. Moreover, they all plot on a straight line which demonstrate that the trend observed results of a conjugated enrichment in Mg and Ni. Only samples ELD4S and ELD5S are poorly enriched. They are located close to the source region. The point ELD3G indicates gravels taken on a glacial moraine in the source area with a slightly higher abundance in Mg and Ni. These moraines already contain sand size grains, probably explaining this slightly higher ratio. Thin sections were used to derive relative proportions of olivine in sand

and rocks. It has been observed that olivine consitute typically 5 to 10% of rock mineralogy, whereas it constitute about 20% of grains in sands.

At this point it should be demonstrated that the enrichment in olivine in sands is related to eolian processes. Sand sizes for all sand samples were measured from a laser granulometer. Finest sand samples correspond to those showing a predominant grain fraction below 400 μm, thus #ELD3S, ELD8S, ELD11S and ELD12S. The sample ELD12S has been collected from saltating grains during a storm, therefore corresponding a typical eolian sand sorted by wind. It shows a peak in grain size at about 200 μm. Coarser sands correspond to ELD4S and ELD5S that are composed largely by >400 μm grains. They are poorly sorted by wind with only minor fraction of small grains in the 200 μm range. The most sorted sands correspond to those with the highest Ni and Mg fraction, therefore demonstrating that the enrichment in olivine is related to the eolian sorting.

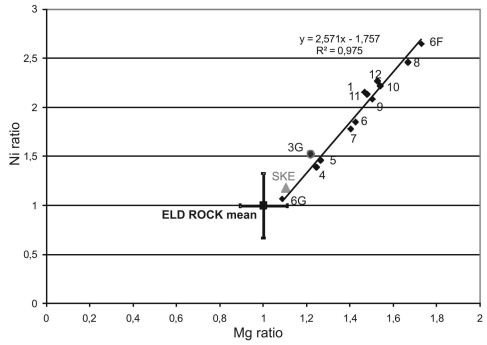

Fig. 2: Proportion of Ni and Mg ratioed over the mean source rock composition. The correlation between Mg and Ni increase in sand demonstrates the increase in olivine proportion in sands number 1, 8, 9, 10, 11, 12. The sample 6F is a fraction of fine grains taken from the sample 6.

Volcanic plains are not predominant on Earth, therefore limiting the consequences of these results to a few regions of the world. In contrast, Mars is a planet widely covered by volcanic plain in a dry climate that creates widespread sand dunes. Infrared hyperspectral imagery taken from orbit has found that the composition of dark dunes is frequently dominated by pyroxenes, with local presence of olivine, plagioclase, volcanic or impact glass, or magnetite depending on locations [e.g. 3, 4]. This is not surprising given the predominance of basaltic plains at the surface of Mars. However, many volcanic regions are covered by sand, and the composition of sand is often taken as a mean for extracting the average composition of the underlying bedrock [5]. Global maps do not care to the detailed morphology for establishing the composition of volcanic regions despite plains can be extensively covered by sand. Yet, sorting effects in sand grains may modify the composition of sand and therefore may change the apparent composition of the underlying bedrock. Despite being small variations, these effects in Iceland occurred over 4000 years, while Martian eolian erosion over million of years enables much longer eolian sorting and related minerals segregation.

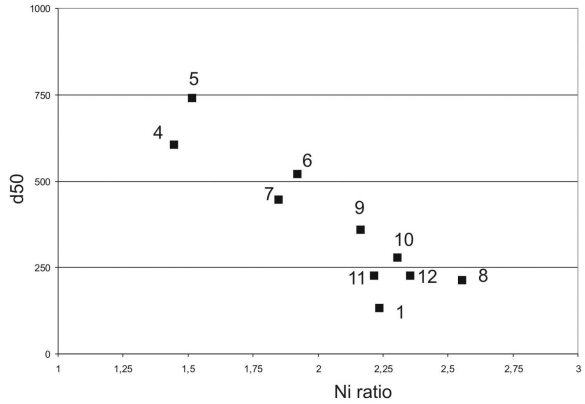

Fig. 3: Median dimater (d50) of each samples versus the Ni proportion, which is a direct mean for olivine proportion increase. The most sorted sands are the most enriched in olivine demonstrating that eolian sorting is responsible of the olivine increase in sand.

Conclusions:

The Lambahraun volcanic plain in Iceland displays widespread sand composed of local basaltic grains. Sands display subtle differences from the source rocks. The chemical and mineralogical analyses demonstrate that a conjugate of Mg and Ni enrichment in sands relative to rocks is due to the higher proportion of olivine grains in sand. This enrichment is correlated to a lower mean grain size of sands, therefore to a higher eolian sorting. Applications of these results to previous studies about volcanic sands on Mars suggest that the physical sorting of olivine grains should be taken into account when extracting composition from orbital data.

References:

[1] Edgett and Lancaster, J. Arid Env., 1993. [2] Arnalds et al., J. Arid Env. 2001 [3] Mustard et al., Science, 2005 [4] Fenton et aL,JGR, 2003 [5] Stockstill-Cahill et al., JGR, 2008.

OBTAINING RELEVANT ATMOSPHERIC CONTEXTS FOR DUNE STUDIES. T. I. Michaels[1], [1]Southwest Research Institute, 1050 Walnut St Suite 300, Boulder, CO 80302, tmichael@boulder.swri.edu.

Introduction: Dunes are known to exist on every solar system body that possesses a robust surface and a thicker atmosphere (surface pressure > 100 Pa; Venus, Earth, Mars, and Titan). From an idealized (simplified) perspective, dunes and related depositional aeolian features are a natural consequence of the interactions between atmospheric fluid dynamics and the physics of granular materials, given a simple driving wind and dry homogeneous particles. Wind-driven particle saltation is the primary mechanism by which such idealized dunes change over time. Substantial progress in the understanding of the evolution of idealized dunes and dune fields has been made in recent years through computer modeling efforts (e.g., [1] and [2]).

However, many (perhaps even most) real dunes experience significant departures from idealized conditions. Such non-idealistic conditions include, but are by no means limited to, precipitation (rain, snow, dust, etcetera), biology (on Earth), atmospheric stability, phase changes of volatile components, and the intricacies of realistic time-dependent wind fields (see [3]). Real dunes are the expression of a complex integration of all relevant environmental factors in time and space. Thus these additional real-world processes can substantially alter the dune morphologies and time evolution that would otherwise exist, and potentially even produce dunes that can be easily misinterpreted when using only the idealized dune framework as a guide.

It is of course currently impractical to include all such variables in dune simulations or theory. However, this does not mean that such conditions should be neglected by those trying to interpret what the dunes record about their formative environment. This document will reflect on what can perhaps be done to mitigate one of these factors, the relatively common neglect of the local atmospheric context.

Dunes' Atmospheric Context: The most primitive form of atmospheric measurements that are in some way relevant to dunes are observations that have a resolution much coarser than the dunes being studied. An example would be global-scale imagery of a dust storm (indicative of some wind event) near the dunes. It is best to think of such observations only as potential proxies for the general type of condition that might be affecting the dunes near the time of the observation. This type of observation is generally only useful when other measurements are not available (such as is most often the case at Mars, Titan, and Venus).

One might think of using the atmospheric conditions recorded at the nearest pre-existing location (even if it is tens of kilometers distant; on Earth this might be a town or forest service station). This method would provide substantially better interpretive guidance than nothing at all, particularly with respect to temporal changes. However, in many locales this would not provide an accurate gauge of the conditions (particularly the winds) relevant to the dunes being studied, due for example to topographic effects and the tendency of deep convective precipitation (e.g., thunderstorms) to be spatially patchy.

One might also deploy (even for a limited time) one or more meteorological stations on or near the dune study site (in addition to obtaining data from surrounding pre-existing weather stations). This strategy enables perhaps the best atmospheric context information for dune interpretation that is practical while in the field. Even so, smaller-scale atmospheric variations are likely near a dune or dunefield, due to variations in surface characteristics (rocks, vegetation, ponds, etcetera) or topography (even that of the dune(s)).

The fact remains that measurements, while invaluable as "ground truth", cannot practically provide a comprehensive, time-varying three-dimensional (or even 2D) atmospheric context over a dune, a dune field, sediment transport pathways, a valley or crater that contains the dune(s), etc. However, for Earth and Mars (currently), higher-resolution atmospheric models can provide such information. Although not perfect by any means, the output from such models can be compared with any *in situ* weather data collected in order to characterize potential biases.

References:

[1] Ortiz P. and Smolarkiewicz P. K. (2009) *Phys. Rev. E, 79*, 041307. [2] Diniega S. et al. (2009) *Geomorphology*, doi:10.1016/j.geomorph.2009.02.010, *in press.* [3] Michaels T. I. (2008) *Planetary Dunes Workshop*, Abstract #7039.

THERMAL ANOMALY IN MARTIAN NORTH POLAR ERG LIKELY DUE TO NEAR-SURFACE ICE.
N. E. Putzig[1], M. T. Mellon[2], K. E. Herkenhoff[3], R. J. Phillips[1], B. J. Davis[1], and K. J. Ewer[4]. [1]Southwest Research Institute, Planetary Science Directorate, Boulder, CO (contact: nathaniel@putzig.com); [2]University of Colorado, Laboratory for Atmospheric and Space Physics, Boulder, CO; [3]United States Geological Survey, Astrogeology Team, Flagstaff, AZ; [4]Embry-Riddle Aeronautical University, Prescott, AZ.

Synopsis: A wider range of thermal observations and forward modeling of heterogeneity are used to show that a long-standing thermal discrepancy in the north polar erg is consistent with normal basaltic sand overlying shallow ground ice, obviating the need to invoke sand-sized agglomerations of dust.

Background: The north polar layered deposits are surrounded by dark dunes known as the circum-polar erg (Fig. 1a) and are likely related to climate variations [1,2]. Neutron data suggest that water ice is present within a meter of the erg's surface [3], additionally constraining climate. Dunes of similar morphology, color, and albedo at lower latitudes [4] have thermal inertia (~250 tiu [J m^{-2} K^{-1} $s^{-1/2}$]) consistent with sand-sized basaltic grains [5,6,7]. In the erg, much lower values (~75 tiu) suggestive of dust-sized grains were reported [8,9]. A widely accepted solution to this discrepancy is bonding of fines into larger, low-density aggregate particles capable of forming dunes [10,11], perhaps as they are weathered out of the layered deposits [1,2,11] or the underlying units [12,13].

Thermal inertia and heterogeneity: Modeling studies show that surface heterogeneity may cause anomalous thermal behavior [14,15], allowing an alternative explanation for the thermal properties of the erg. Counterintuitively, certain configurations of near-surface layering may produce apparent thermal inertia (derived assuming constant properties) that is substantially lower than the intrinsic thermal inertia of both the surface layer and its substrate [15]. Thus, the polar erg may be surfaced by ordinary basaltic sand (with up to 30 wt% gypsum [16]), its low apparent thermal inertia attributable to an effect of surface heterogeneity due to the icy substrate.

Diurnal and seasonal variations in apparent thermal inertia indicate that heterogeneity is widespread globally, consistent in the polar region with layering (Fig. 1b,c) [17]. The use of both nighttime and daytime observations is a key element of this analysis, especially near the poles where seasons free of CO_2 ice largely correspond to those when the Sun is predominantly above the horizon.

Heterogeneity at Phoenix and in the polar erg: At the Phoenix landing site, seasonal and diurnal variations in apparent thermal inertia as derived from Mars Global Surveyor Thermal Emission Spectrometer (TES) data can be modelled well by ~4 cm of sand overlying ground ice (Fig. 2a), consistent with the observations made from the lander [18]. When the model sand thickness approaches or exceeds a diurnal skin depth (1/26 of the seasonal skin depth), the 2AM apparent thermal inertia can be substantially less than that of the sand. Thus, the thermal inertia of surface materials may be underestimated if one uses nighttime only or annual-mean values fit to diurnal temperatures, as was done with Viking data.

At the higher latitudes of the polar erg, seasons of useful TES data are more restricted than at Phoenix, and their variations are larger (Figs. 2b-d). To resolve

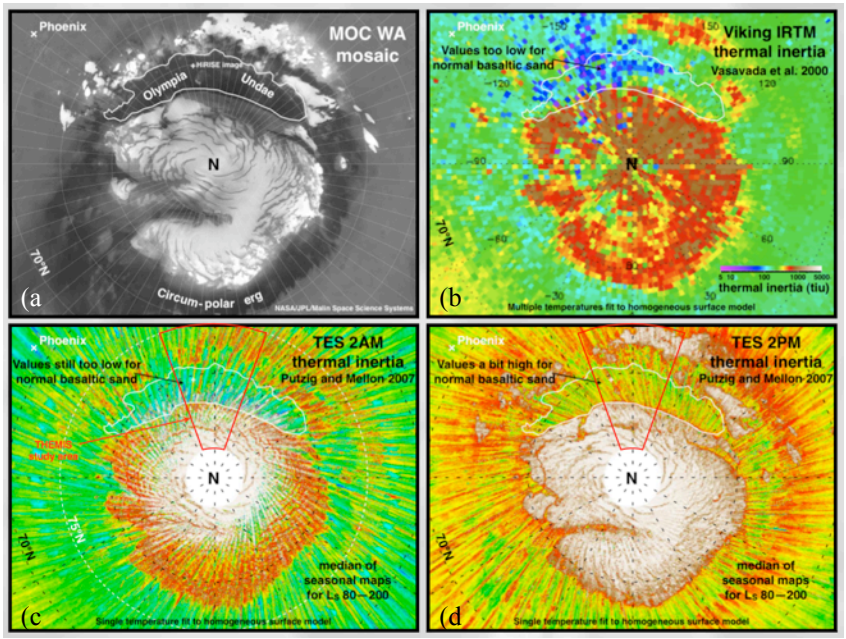

Figure 1. North polar region, 65–90°N, 0°W at bottom. (a) Mosaic of MOC wide-angle images; polar erg is irregular, dark material surrounding bright polar layered deposits. (b) Thermal inertia derived from Viking data [9]. Low values, especially in Olympia Undae, were seen as more consistent with dust than with sand. (c) 2AM and (d) 2PM annual-median apparent thermal inertia derived from TES data [17]. Streaks aligned with orbit tracks are due to seasonal variations. Thermal inertia scale same as in (b).

these short-term, rapid changes, we remapped the north polar region with a finer seasonal increment of 5° L_S (cf. 10° used in Fig. 2a and globally by [17]). This change allows better discrimination between models for matching to the observed thermal behavior. We found the TES results for the erg to be most consistent with a sand layer of ~15-25 cm (Fig. 2b), with dust-layer models yielding poorer fits (Fig 2c). Between dune crests in the erg, HiRISE images show brighter, possibly consolidated materials that may have higher thermal inertia. However, the best-fitting models of this type (70:30 mixture of dust and rock; Fig. 2d) do not capture the observed thermal behavior.

THEMIS thermal inertia: We investigated the derivation of thermal inertia from Thermal Imaging Spectrometer (THEMIS) Band 9 images for the north polar region. At 100 m/pixel (cf. TES at ~3 km/pixel), THEMIS data may allow better discrimination between heterogeneity models. We derived thermal inertia from a selection of THEMIS images of Olympia Undae to produce the maps in Fig. 3. The nighttime results show a pattern of high and low values in the erg and its surroundings that is grossly similar to that of TES 2AM maps, but with lower median values. In contrast, the daytime results show dramatically higher values of thermal inertia. However, these images may have been affected by partial CO_2-frost cover on the ground at these earlier seasons. The lack of coverage for later seasons hampers the incorporation of daytime results into our analysis at this time. Since THEMIS continues to acquire images (now at times of day more favorable for thermal analysis), we hope to eventually obtain broader seasonal coverage.

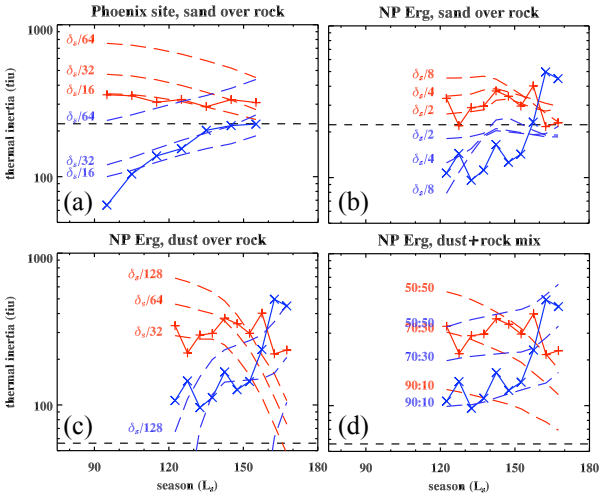

Figure 2. 2AM (blue) and 2PM (red) apparent thermal inertia from TES (×, + symbols) and from various models (dashed curves) of sand or dust and rock (i.e., ground ice) at (a) the Phoenix site (× in Fig. 1) and (b-d) in the polar erg (+ in Fig. 1) during summer seasons. Horizontal dashed lines represent sand (223 tiu) or dust (56 tiu). Labels in (a-c) are upper-layer thickness in fractional seasonal skin depth, δ_S (70 cm for sand, 21 cm for dust). Labels in (d) are dust:rock mixing ratio. Models in (a) and (b) provide the best fits, with ~4 cm and ~20 cm of sand at Phoenix and at the erg site, respectively. Next-best models of dust-rock (c) layering and (d) mixing have larger deviations from the TES results.

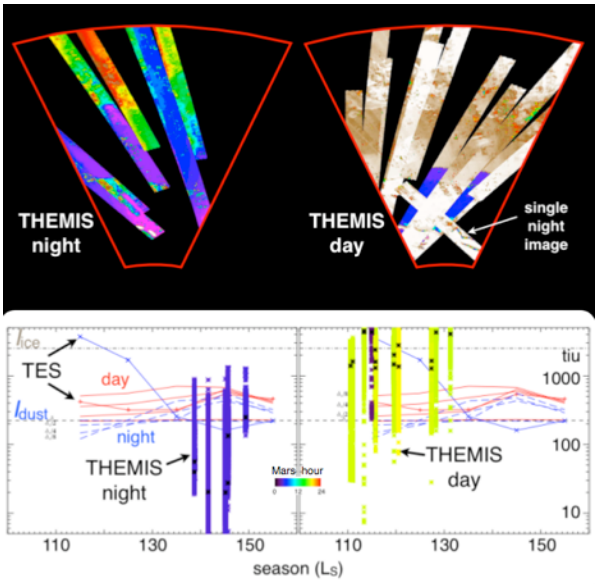

Figure 3. Thermal inertia from THEMIS Band 9 for 160°-200°E, 75°-87°N. Thermal-inertia color scale same as for Fig. 1. Graphs are for Olympia Undae (center of maps, 79-83N) with values extracted from THEMIS images (* symbols, where colors are local time of day and black is median value within each image), median values from TES (x, + symbols), and results from layered models of sand over ice-cemented soil (solid and dashed colored lines). Large THEMIS image-to-image variations and extreme values relative to TES are not fully explained but may be related to suboptimal observing conditions and larger instrument error, particularly for daytime images.

References: [1] Thomas P. et al. (1992) in: *Mars*, Kieffer H.H. et al. (1992) U. AZ Press. [2] Clifford S.M. et al. (2000) *Icarus 144*, 210–242. [3] Feldman W.C. et al. (2008) *Icarus* 196, 422-432. [4] Thomas P. & Weitz C. (1989) *Icarus 81*, 185-215. [5] Sagan C. & Bagnold R.A. (1975) *Icarus 26*, 209-218. [6] El-Baz F. et al. (1979) *JGR 84*, 8205-8221. [7] Breed C.S. et al. (1979) *JGR 84*, 8183-8204. [8] Paige D.A. et al. (1994) *JGR 99*, 25,959–25,991. [9] Vasavada A.R. et al. (2000) *JGR 105*, 6961–6969. [10] Herkenhoff K.E. & Vasavada A.R. (1999) *JGR 104*, 16,487–16,500. [11] Cutts J.A. et al. (1976) *Science 194*, 1329-1337. [12] Byrne S. & Murray B.C. (2002) *JGR 107*, E6, 5044. [13] Fishbaugh K.E. & Head J.W. (2005) *Icarus 174*, 444-474. [14] Putzig N.E. & Mellon M.T. (2007) *Icarus 191*, 52-67. [15] Mellon M.T. & Putzig N.E. (2007) *LPS XXXVIII*, Abstract #2184. [16] Horgan et al. (2009) *JGR* 114, E01005. [17] Putzig N.E. & Mellon M.T. (2007) *Icarus 191*, 68-94. [18] Mellon M.T. et al. (2009), *JGR 114*, E00E07.

DUNES ON TITAN: WIND DIRECTIONS, BEHAVIOR, AND EVOLUTION FROM STATISTICAL AND MORPHOLOGICAL STUDIES. J. Radebaugh[1], C.J. Savage[1], R.D. Lorenz[2], N. Lancaster[3], S.D. Wall[4], E.R. Stofan[5], J.I. Lunine[6], R.L. Kirk[7], A. Le Gall[4], T.G. Farr[4], [1]Brigham Young University, Department of Geological Sciences, Provo, UT 84602, *jani.radebaugh@byu.edu,* [2]JHU Applied Physics Lab, Laurel, MD, [3]Desert Research Institute, Reno, NV, [4]Jet Propulsion Laboratory, Pasadena, CA, [5]Proxemy Research Inc., Laystonsville, MD, [6]Lunar and Planetary Laboratory, Univ. of Arizona, Tucson, AZ, [7]US Geol. Survey Astrobiology Institute, Flagstaff, AZ.

Introduction: The tens of thousands of linear dunes organized into dune fields and sand seas on Titan imaged by the Cassini RADAR are emerging as a dominant landform [1,2] (covering an estimated 15% of the satellite [3]) and an indicator of perhaps active geological processes on this body. Statistical analyses of dune morphologies have proven fruitful in helping determine global and regional wind directions [4] and characterizing the current conditions and history of the dunes [5]. We study terrestrial dune analogues to pursue a solution to the puzzling discord between mean wind directions inferred from sand transport indicated by dune/topography interactions (W to E, or westerly [6]), and winds predicted by Global Circulation Models (GCMs) and from basic physics of angular momentum conservation (easterly [7]).

Wind Directions from Dune Morphologies: We rely on dune morphologies to determine wind directions, since there is only one short-lived set of in situ measurements from the Huygens probe. Linear dune long axes are modeled as aligned with the time-averaged dominant wind direction [2]. Long axes of 16,000 dune segments from the Cassini Prime Mission were mapped globally, with directionality determined from dune interactions with topographic obstacles [6]. The global dune long axis map (Fig. 1) shows most dunes are confined within 30° of the equator, and have orientations dominantly eastwards, with local and regional deviations of up to about 40° [4]. These results are anticorrelated with current GCM model wind directions [7].

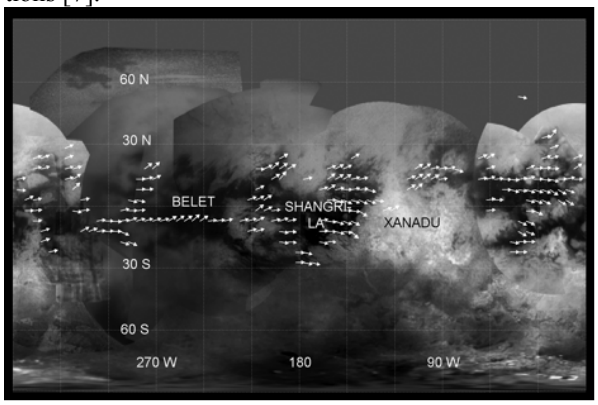

Fig. 1. Dune long axes from >16,000 measurements, binned into 5° intervals. Arrow heads come from analyses of dune interactions with topography. Global winds from these studies are eastwards, with regional deviations, such as that caused by Xanadu. From [4].

Dune Condition and History from Pattern Analysis: Using pattern analysis of dune field parameters, including crest-to-crest spacing and width, as has been done in terrestrial dune studies [8], it is possible to make preliminary inferences about the history of Titan's dunes. Parameter analysis reveals different dune populations, number of dune forming events, relative duration of stable dune building conditions and approximate age [8]. There is a general increasing trend between spacing and width of dunes on Titan from thousands of measurements in the equatorial leading hemisphere (RADAR swaths T21, T23, T25; Fig. 2). This correlates strongly with similar measurements of dunes from around the Earth [e.g., 9], and strengthens the idea that Earth's dunes may be used as a proxy for study of Titan's dunes [5].

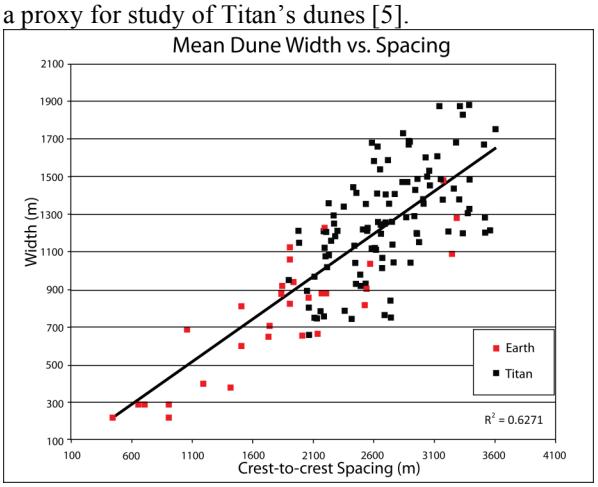

Fig. 2. Width and spacing of dunes from regions on Titan and Earth. Fit to a linear relationship with slope 0.5 for data for Earth and Titan together has an R^2 of 0.63, but is better for Earth alone (R^2 of 0.95) than for Titan (R^2 of 0.4)[5,9].

A study of crest-to-crest spacing of dunes on Earth reveals different populations within some dune regions, such as in the Namib Sand Sea, expressed as changes in slope on cumulative probability curves. These different populations may represent different periods of dune building, changes in wind strength or direction, or variations in sediment supply. No such inflections are observed in similar plots for Titan's dunes, which may indicate there is a single population of linear dunes on the satellite. Perhaps on Titan there are relatively uniform conditions over long time frames, or the most recent episode of dune building has erased evidence of previous conditions [5].

Wind Directions from Terrestrial Analogues: Several terrestrial dune regions with known wind data are robust morphological analogues to features observed on Titan. Studies of these regions should help more clearly determine wind directions on Titan from dune-topography interactions.

Dunes in the Saharan desert have a variety of forms, but are dominantly linear and are parallel to sand transport pathways, which, for the Saharan desert, are controlled by trade winds. Given these are stable over long time scales, dune forms in the Sahara are likely to be in equilibrium with current trade wind patterns [10].

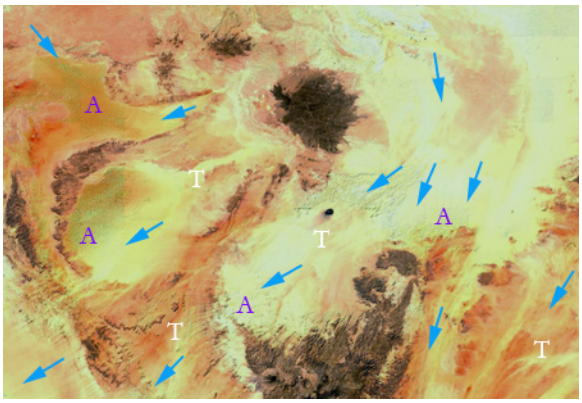

Fig. 3. Sand transport pathways for the Libyan Sahara (from [11]). Sand is yellow. Letters T indicate where transport dominates and A where accumulation is occurring. MODIS image from NASA.

Known current sand transport pathways, correlated with trade wind patterns [10], are shown for the Libyan Sahara in Figure 2. These pathways illustrate the transport of sand from northern mountains and rivers to the central and southern Saharan desert [11]. Here, sediment bypassing occurs over flat regions or through fluvial systems. However, locally, sand collects upwind of topographic obstacles, where winds decrease in strength and saltation is diminished [12]. Once sand begins to collect ahead of obstacles, the process feeds back and leads to upwind migration of the wind velocity minimum [11,12]. Thus, a local sand sink upwind of a topographic obstacle is established. The disruption of wind and collection of sand upwind of obstacles leads to a dearth of sand immediately downwind of obstacles and gradual regeneration of duneforms farther downwind. Results of these processes on landform morphologies – sand-rich vs. sand-sparse areas, obstacle-diverted dunes, and streaks indicating recent sand transport, can be seen clearly in a MODIS regional image (Fig. 3, marked A for accumulation areas) and ASTER close-up image (Fig. 4.a) [6].

These relationships are also seen on Titan, albeit at lower resolutions. In regions away from sand seas, dunes are clearly separated from interdunes, and sands appear to be primarily undergoing transport (Fig. 4b). Morphological comparisons of these dune regions with those in Libya indicate the sand transport direction and related winds are uniformly from the west to the east. These results are correlated with previous studies of wind directions based on dune morphologies [2,6] but are anticorrelated with current GCM model wind directions [7].

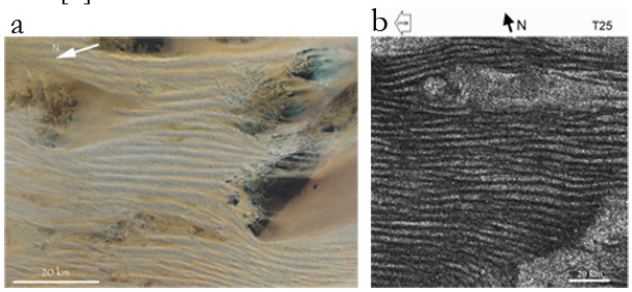

Fig. 4a. Closeup of dune forms in Libya seen in Fig.3. Sand transport is from left to right. 4.b. Similar morphologies in a Cassini radar image of dune forms in T25 region of Titan indicate sand transport direction is to the east (left to right).

Conclusions: The resolution and coverage of Cassini RADAR images have allowed us to pursue detailed pattern analyses of dunes on Titan and morphological comparisions with analogues on Earth. We are finding we can apply many of the methods that have been used for understanding the condition and evolution of dunes on Earth to Titan. It is likely we will find that Titan's dunes will help us approach a better understanding of linear dunes on Earth, their formation, and interaction with other geological features.

References: [1] Lorenz RD e.a. (2006) *Science* 312,724-727. [2] Radebaugh J e.a. (2008) *Icarus* 194, 690-703. [3] LeGall, A e.a. (2009) *AAS DPS 41*, 21.08. [4] Lorenz and Radebaugh (2009) *GRL* 36. [5] Savage C e.a. (2010) *LPSC 41*, 2530. [6] Radebaugh J e.a. (2009) *Geomorphology*. [7] Newman C e.a. (2008) *Fall AGU*. [8] Ewing R C e.a. (2006) *Landforms 31*, 1176-1191. [9] Lancaster N (1995). [10] Mainguet, M and L Canon (1976). *Revue de Geographie Physiqe e de Geologie Dynamique* 18, 241-250. [11] Mainguet (1984) *in* Deserts and Arid Lands. [12] Bowen AJ and Lindley D (1977) *Boundary Layer Meteorology* 12.

Active dune fields of the Navajo Nation, southwestern United States

Redsteer, Margaret H., Bogle, Rian, and Vogel, John;
U.S. Geological Survey, 2255 N. Gemini Dr. Flagstaff, AZ 86001

Dune fields and sheet sands cover approximately one-third of the semi-arid 65,000 km^2 Navajo Nation on the southern Colorado Plateau. This eolian-dominated landscape contains a myriad of dune forms that exist under meteorological conditions promoting the entire spectrum of dune mobility, from mostly stable, mostly active, to fully active during periods of drought. The risk of increased sand dune mobilization within this region is high. A consensus of climate modeling indicates that significant drying in the region throughout the 21st century is expected, and should already be underway. In recent years, the Navajo Nation has been experiencing drought conditions that may surpass the severity of all droughts in the 20th century. Moreover, this region has seen the greatest increase in average annual temperature of all regions in the lower 48 of the U.S., exacerbating arid conditions. Current work indicates that reactivation of stabilized sand is occurring in many areas of the Navajo Nation. Dune mobility is today inundating housing and causing transportation problems. It also may be contributing to a loss of rare and endangered native plants and grazing land. Many of the more recent active dunes may have formed as the region began a long-term drying trend that began in the late 1800's. As a result of increasing aridity, perennial surface water features have become ephemeral. Active dune fields receive new pulses of sediment from periodic flooding of nearby washes and streambeds during high intensity summer monsoons that act to mobilize sediment. The current rate of dune migration in active regions varies from year to year, depending on local meteorological conditions. During recent conditions in 2009, an unusually windy and dry year, we have measured dune migration rates as high as 34 to 48 m/yr.

Planetary Dunes Analogs using laboratory experiments and numerical simulations.

E. Reffet[1,2], M. Fulchignoni[1], [1]LESIA Observatoire de Paris and Université Paris 7-Paris Diderot, France, [2]Laboratoire MSC, Université Paris 7-Paris Diderot, France (erwan.reffet@obspm.fr)

Our work deals with the morphology of solitary dunes under non-unidirectional winds and present experimental and numerical analogs to planetary dunes. We show that barchanoids shapes observed on Mars can be reproduced with bimodal wind regimes and that their morphology depends on the angular separation of the 2 directions of wind. Thus, the observation of these morphologies can indicate the mean direction of sand transport but can also give an idea of the variability in wind direction of the wind regimes responsible for their formation. This study can be extended to more complex wind regimes like the ones required for the formation of star dunes. Our approach could help to create, and complete, a *database* of analogs of prime interests in the interpretation of dune observations.

Introduction

In the aeolian case, dunes are large structures with long time-scales of formation and evolution. When the access to the sedimentary structure of the dune help to retrieve information on dunes history, it remains difficult to achieve,from fields study only, a global understanding of the physical processes involved in the selection of the various morphologies documented. Furthermore, the conditions are complex in the field and it can be difficult to discriminate between the various factors affecting the morphology. Therefore it appears interesting to reproduce dunes under controlled conditions using laboratory experiments and numerical simulations. These tools provide well-known analogs that can then be compared to real dunes observed in the field. We can then assume that similar morphologies can be linked to comparable conditions of formation and evolution which lead to the determination of constraints on the wind regimes. This reverse analysis is especially interesting in planetary sciences where *in situ* measurements are not always available and remote sensing is the only way to study these aeolian features.

Methods

We use underwater laboratory experiments in order to decrease the length- and time-scales involved in dunes formation and evolution. When we observe a typical wavelength of instability of about $10\,m$ for the aeolian case on Earth, a wavelength smaller than $1\,cm$ is observed with such an approach. Our experimental setup comprises a moving baseplate immersed in a water tank. The translation of this baseplate is tuned to reproduce a unidirectional wind regime. The sand is placed on a central disk which orientation can be modified allowing to change the relative direction of the strokes of wind. Therefore, we are able to simulate various wind regimes and study their influence on dunes morphology. We complete these laboratory experiments with numerical simulation based on a continuous dunes model [1].

Results

In a previous work [2], we have shown that the study of dunes fields can provide global constraints on wind regimes. For instance, the observation of longitudinal dunes on Titan's surface implies, if *sand* transport is still active, that variations in the wind direction of more than 90^o occur in its lower atmosphere. Looking at smaller scale features and isolated dunes, we can infer local constraints. In particular, we studied the evolution of the morphology of the barchanoids formed under bimodal wind regimes (FIG.1). When the barchan shape is observed for unidirectional wind, this morphology is modified for various angular separations, θ, between the 2 wind directions. For low values of θ, barchanoids dunes are modelled with progressively smaller horns and slip face and a predominant back for increasing angular separation. Around 90^o, the 2 horns join in a central tip aligned with the mean wind direction creating a *chestnut*-like shape. For larger θ, the central tip develops downwind and a longitudinal dune is formed. These 3 kinds of morphologies are observed on Mars respectively in Hellespontus, Wirtz crater and Noachis Terra indicating that the winds blowing over these aeolian structures are likely to verify these 3 domains of angular separation.

Going a bit further in wind regimes complexity, we can complete the list of analogs to compare to field observations. For instance, star dunes analogs to the ones observed in the field are obtained under winds changing between 3 directions (FIG.2). Both our laboratory experiments and numerical model allow to produce a great variety of dunes which can therefore be studied in details [3] and compared to planetary dunes.

2

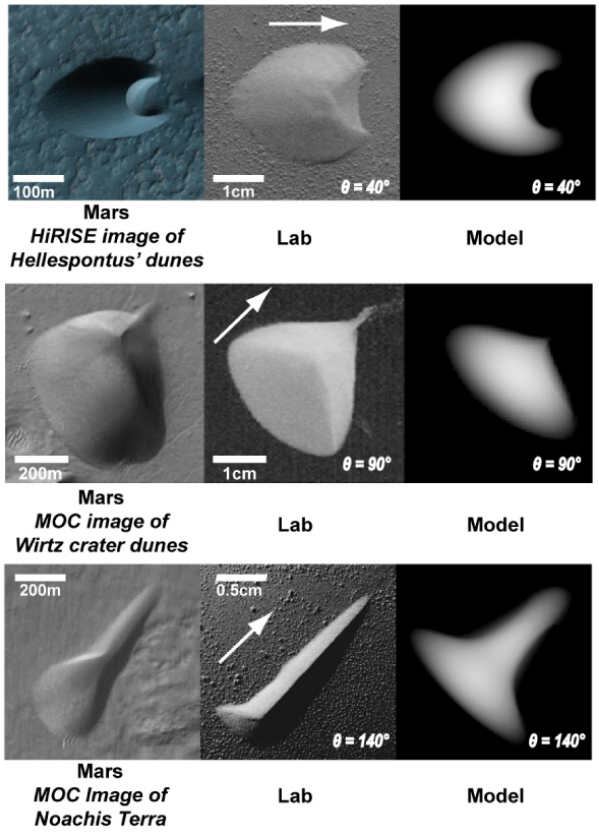

Figure 1: Barchanoids observed on Mars and proposed analogs obtained in the lab and using numerical simulations under bimodal wind regimes. The white arrows indicate the mean wind direction and θ corresponds to the angular separation between the 2 wind directions.

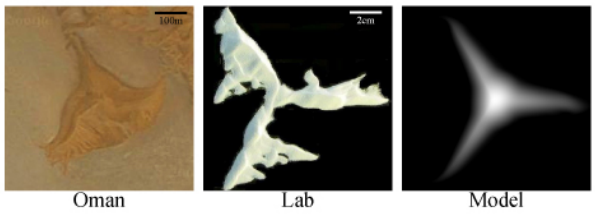

Figure 2: Star dunes in Oman. Laboratory (provided by Raphaël Clément) and numerical analogs formed under winds alternating between 3 directions. These directions are aligned with each of the arms of the star dune for our lab experiment and numerical simulations.

Discussion

Looking at dunes formed for various wind regimes under controlled conditions help understanding the physical processes involved in the selection of morphology. It could be used to determine constraints on the wind regimes from dunes observation. As dunes of different sizes integrate the wind regimes on different time-scales, the characteristic time of adaptation of the smaller ones being shorter, they could be use to retrieve information about the wind regimes on these different time-scales. In the meantime, looking at dunes fields or solitary dunes provides constraints on different spatial scales.
Finally, the morphology of dunes also depends on the supply of sand, their interactions within the dunes field (sand exchange, collision) or with the topography, even if the wind regimes appear to be the motor of their formation. It would be interesting to test our laboratory and numerical models in these more realistic conditions.

References

[1] P. Hersen. On the crescentic shape of barchan dunes. *European Physical Journal B*, 2004.
[2] E. Reffet, S. Courrech du Pont, P. Hersen, S. Douady, and M. Fulchignoni. Longitudinal dunes on titan: A laboratory approach. *Planetary Dunes Workshop*, 2008.
[3] E. Reffet, S. Courrech du Pont, P. Hersen, and S. Douady. Formation and stability of transverse and longitudinal sand dunes. *Geology (accepted)*, 2010.

GIANT CURRENT RIPPLE MARKS: REMOTE SENSING OF NEW LOCATIONS ON THE EARTH. A.N. Rudoy[1] and S.S. Chernomorets[2] , [1]Faculty of Geology and Geography, Tomsk State University, Russia, rudoy@tspu.edu.ru, [2]Faculty of Geography, Lomonosov Moscow State University, Russia, devdorak@gmail.com.

Introduction: Giant current ripple marks usually emerge following rapid outbursts of large proglacial and rock-dammed lakes given extremely high intensity of flow. They represent morphological and genetic macro-analog of sand current ripples. We have produced analysis of known locations of giant current ripples and geographic conditions in which emergence of current ripples is possible at today's stage of active degradation of glaciers and mass formation of large proglacial lakes. Remote research was carried out – satellite image interpretation for various mountainous regions of the world – to discover other parts of the giant current ripples terrain [1].

Discussion: Emergence of the exotic relief of giant current ripples is connected with outburst of large lakes dammed by glacial or landslide dams. After the outburst, the river faces extremely high intensity of flow for some time, and a terrain in the form of diluvium or flood dunes with height of dozens of meters emerges [2]. Until recently, three areas of giant ripples were thoroughly examined: basin of Columbia River in the north-west of the USA, Altai and Tuva in Russia [2,4]. The age of the ripples in these areas goes back to the end of the late Pleistocene within the range of 7-22 thousand years ago [2]. As for other areas, giant ripples have not been examined, although they play a big role in paleo-hydraulic reconstruction.

Based on the ripples prior research, we have performed remote sensing and surface study in Altai ([5,6], Fig. 1) to find and examine ripples, learn about conditions of its emergence, and clarify its geographic distribution. We have used QuickBird highresolution images published in Google Earth as the main material for the remote study. We have identified search criteria for ripples based on which we have selected and interpreted considerable mountainous areas. High emphasis was placed upon relatively recent forms of ripples that are in better condition than Pleistocene ones. Upon finding the forms of ripples, we have started searching for corresponding terrain forms, e.g. terraces marking the level of former lakes. That is, we have discovered diluvial morpholithologic complexes described in [2]. We have also analyzed publications describing events that may have led to emergence of the ripples on the areas discovered. While carrying out the remote study of the surface, the following circumstances were taken into consideration and the following areas were paid special attention to: -extensive highland valleys with the marks of their blocking; -diluvial dunes and anti-dunes in several terrains across the valley. If giant ripples are discovered in one place, they can usually be found in other places up or down the stream at the distance of several kilometers just like in the Altai and Tuva areas studied; – lake terraces and dropstones. Apart from the western part of the USA, Altai, and Tuva, giant ripples are located in: -the Alsek River valley (St. Elias Mountains, Canada) [4]; -the Yarlung Zangbo river valley (Tibet, China) [4]; -in the upper reach of the Hunza river and farther along the Indus river (north of Pakistan) at the 170-kilometer distance starting from Gilgit City; -in the Indus River valley near Skardu (north of Pakistan); -in the Nubra River valley (Kashmir, India).

Fig.1. The Great Field of Giant Current Ripples in Kuray Basin, Altai, Russia. Picture by A. Rudoy (August 19, 1991)

Fig.2. Giant ripples in the Alsek River valley, St. Elias Mountains, Canada. Picture by S.S. Chernomorets.

Apparently, diluvial dunes in the Alsek River valley are the youngest (Fig. 2). Emergence of these dunes dates to the end of XIX – beginning of XX centuries [3]. Glacial dams have emerged here at least four times due to the Alsek River ponding given surge of the Lowell Glacier. We made a survey of the valley from the helicopter and interpreted clearly defined forms of the relief of the current giant ripples [1]. In addition, we discovered marks of old levels of a dammed lake on the edges of the river valley. It was also established that dunes emerge both upstream of the dam, where still water of the lake starts moving, and downstream of the dam, where the inrushing water comes to. Morphology of the dunes up and down the dike is somewhat different. We have identified peculiar features of valley in place blocked by the glacier, which can be used for analysis of similar objects in other areas in future. Areas that were interpreted as places of possible location of giant ripples were discovered in Tajikistan (two areas –the Murgab River valley (Fig 3) and the Alitchur River valley between the Sassyk-Kul and Yashil Kul lakes), Argentina (the Limay River basin to the south-east of San-Martin-de-los-Andes city, Neuken province, Patagonia), and China (the Dadu River outlet area, Sichuan Province). In those places, there are forms resembling giant ripples that are located in geographic conditions suitable for emergence of ripples. Further interpretation is required, as well as mapping, search for publications on the ripples and interpretation thereof. When analyzing marks of any outburst, it is very important to search for a place of a former dammed dike.

Fig.3. Giant current ripples in Murgab River valley.

Acknowledgements: The study was accomplished with partial support from RFBR projects 07-05-00172 and NATO Science for Peace (Project 982143).

References: [1] Chernomorets S.S., Rudoy A.N. (2009). *Int. Conf. of Mitigation of natural hazards in mountain areas*. Kyrgyz Republic, Bishkek City, 15-18 September 2009, Bishkek: Salam, 24-26. [2] Rudoy, A.N.(2005) Giant Current Ripples: History of Research, Their Diagnostics, and Paleogeographical Signifi- cance. Tomsk, Russia, 223 p. (in Russian, Eng. abs. 134-210). [3] Clague J.J., Rampton V.N. (1982) *Can. J. of Earth Sc.19 (1).* 94-117. [4] Montgomery D.R., Halleta B., Yuping L., Finnegan N., Anders A., Gillespie A., Greenberg H.M. (2004) *Quaternary Res. 62,* 201– 207. [5] Rudoy A.N. (2002). *Quaternary International. 87/1.* 119-140. [6] Rudoy A.N., Baker V.R. (1993) *Sedimentary Geology. 85 (1-4),* 53-62.

Sensitivity of Automatic Determination of Sand Transport Direction and Rate to Dune Morphology in the Namib Sand Sea. S. P. Scheidt[1] and N. Lancaster[1]. [1]Desert Research Institute, 2215 Raggio Parkway, Reno, NV 89512, sscheidt77@gmail.com.

Introduction: Many morphologic dune groups make up the hyperarid Namib Sand Sea, a 120-200 km wide area situated on the Atlantic coast of southern Africa between Walvis Bay and Lüdertz (Figure 1). These dune groups include barchans [1,2,3,4], transverse, linear [5] and complex forms, and some of these dunes have been examined as terrestrial analogue for dunes on Mars and Titan [6,7,8]. Studies suggest that sand transport is taking place on Mars [9,10,11], but actively migrating dunes have not yet been identified on Mars [12,13]. Measuring dune migration and sand flux rates is important to understanding aeolian systems. A number of different approaches have been used in the field [e.g., 14,15,16], but the recent development of the Coregistration of Optically Sensed Images and Correlation (COSI-Corr) algorithm [17] has also afforded a unique remote sensing application for measuring dune migration rates in dune fields [18,19]. Necsoiu et al. [19] were able to use precisely orthorectified, coregistrated SPOT and ASTER satellite imagery to take advantage of the algorithm's ability to determine subpixel correlation between images from different dates, which was related to dune migration rate. These rates are slow compared to the rate of barchan dune sand flux measured in the Bodele region of Chad using COSI-Corr applied to ASTER satellite data [18]. Both studies produced meaningful estimates of dune celerity over time from satellite image data. Vermeesch et al. [18] chose to use simple barchan dune forms to test their techniques in order to avoid second order features of more complex dunes that might cause errors in the application of the correlation algorithm.

Approach: The viability of the COSI-Corr technique for dune studies is established, so our work seeks to test the algorithm's sensitivity to different dune types and evaluate the performance of alogorithm with respect to each. We use locations in the Namib Sand Sea where previous measurements of dune morphologic changes have been measured, including dune migration rates of barchan dunes [2,3] and changes in linear dunes (specifically the crest orientation) [5]. These areas include dunes near (1) Walvis Bay, (2) linear dunes just south of the Kuiseb River and (3) dune groups at the southern margin of the sand sea northeast of Lüderitz (Figure 1). Orthorectified ASTER data from different dates have been acquired that will allow us to study changes between seasons in the same year, as well as incremental and maximal changes between years 2000 and 2009.

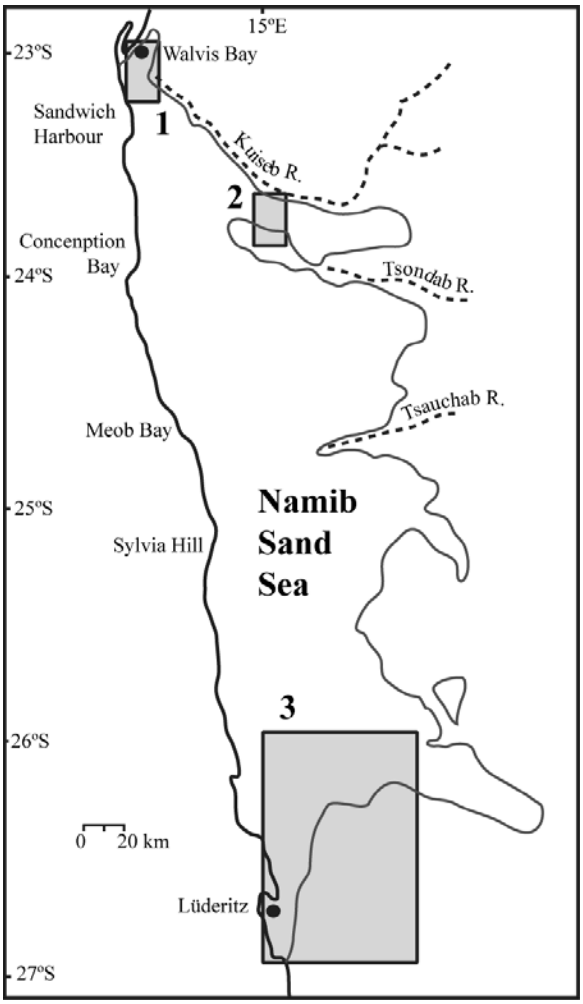

Figure 1. The study location map of the Namib Sand Sea. The numbered, shaded boxes (see text) above show the areas where we are experimenting with the measurement of dune migration and morphologic change using ASTER data and the COSI-Corr algorithm.

Results: A number of different algorithm parameters can be chosen when applying the COSI-Corr algoirthm to determine land surface change, where some of these parameters are set according to the expected magnitude of land surface change (e.g. dune displacement) [17]. For complex dunes and in dune fields with several different dune types, the same parameters are not ideal for each of these areas. Consequently, a variety of questions arise from the results. For example, the sediment transport direction appeared to be esti-

mated correctly according to linear dune defects, but the correct magnitude of transport rate was uncertain. For closely spaced transverse dunes, the offset between 'before' and 'after' satellite imagery appeared to be less than 2 pixels, but the resulting sand transport vectors appeared to be overestimated. In the case of these transverse dunes, we suspect the algorithm (given the set of parameters chosen) determined the correlation between the wrong adjacent dune crests. In areas where transverse dunes are widely spaced, such as the Walvis Bay barchan dunes [2] (Figure 2) and barchan dunes at the southern margin of the Namib Sand Sea (Figure 3), the correct sand transport directions were estimated.

Future Work and Conclusions: Testing of the algorithm continues in order determine seasonal and year to year changes of Namib sand dunes, which will be compared to previously published dune migration rates. We expect the completion of this sensitivity analysis to be useful for future studies that apply COSI-Corr to Mars image data sets to make these types of aeolian measurements. For example, HiRISE data may be used to measure ripple migration rates. The sensitivity analysis should help establish for specific dune types: (1) the ideal time interval between images used in the algorithm, (2) ideal algorithm parameters to avoid errors and (3) the limitations that need to be considered when applying this technique to other aeolian systems on Earth, Mars and Titan.

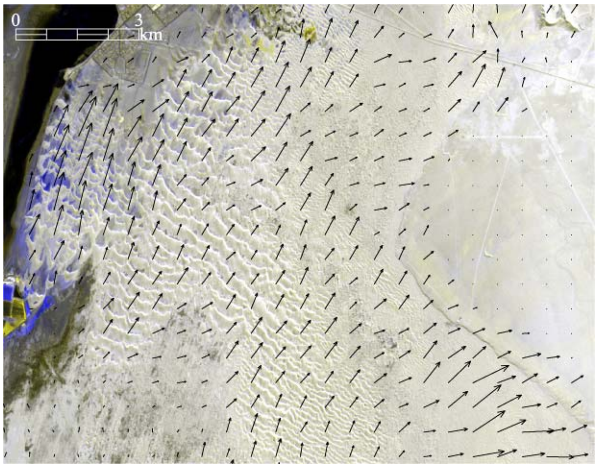

Figure 2: Cosi-Corr dune migration rate vectors are overlain on this color composite image, where both 'before' (May 2003) and 'after' (July 205) ASTER Band 3 are used. Areas of change show as color values here, where gray-scale generally indicates no change. 'Yellow' indicates higher reflectance from 2003 dune faces. 'Blue' indicates the 2005 dune faces. Blue areas on the left margin of the image indicate interdune changes in reflectance, but also indicate the highest rates of barchan dune movement. The direction of the vectors agree with the dune morphology, crest orientations and resultant wind directions for this area.

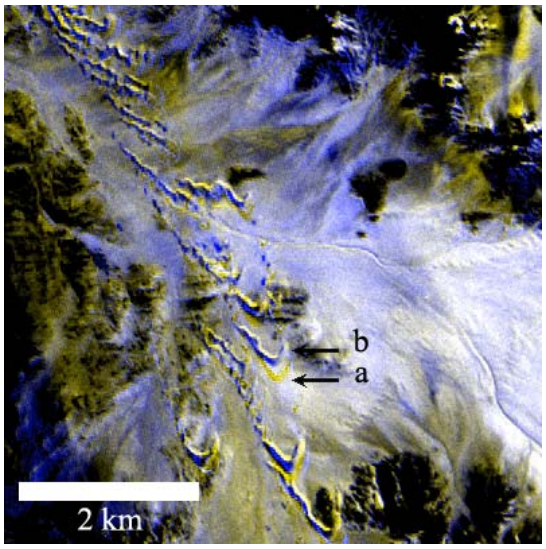

Figure 3. Barchan dunes migrate north-northwest in this area on the southern margin of the dune field. (a) 2003 barchan dune position (yellow). (b) 2005 barchan dune position (blue).

References: [1] Lancaster N. (1989), The Namib Sand Sea: Dune Forms, Processes, and Sediments, 200 pp. [2] Slatterly M.C. (1990), S. Afr. Geogr. J., 72, 5-10. [3] Endrödy-Younge S. (1982), Cimbebasia(A), 5, 257-271. [4] Bourke M.C. and Goudie A.S. (2009), Aeolian Res., 1, 45-54. [5] Bristow et al. (2007), Geology, 35(6), 555-558. [6] Breed C.S. (1977), Icarus, 30(2), 326-340. [7] Radebaugh J. et al. (2008), Planetary Dunes Workshop, Abstract #7034. [8] Wall S.D. et al. (2009), American Astronomical Society, DPS meeting #41, #21.07. [9] Bourke, M.C. et al. (2008) Geomorphology, 94, 247–255. [10] Bourke M.C. et al. (2008) Planetary Dunes Workshop, Abstract #7040. [11] Fenton L.K. (2006), GRL, 33, L20201. [12] Zimbelman, J.R. (2000) GRL, 27, 1069–1072. [13] Schatz V. et al. (2006) JGR, 111, doi:10.1029/2005JE002514. [14] Bristow C.S. and Lancaster N. (2004), Geomorphology, 59, 189-196. [15] Greeley R. et al. (1996), Sedimentology, 43, 41-52. [16] Baas A. (2004), Geomorphology, 59, 99-118. [17] Leprince et al. (2007), IEEE T. Geosci. Remote, 45, 1529-1558. [18] Vermeesch P. and Drake N. (2008), GRL, 35, L24404, doi:10.1029/2008 GL035921. [19] Necsoiu et al. (2009), Rem. Sens. Environ., 113, 2441-2447.

Sand Composition of The Gran Desierto: A Terrestrial Analogue for Thermal Infrared Imaging and Spectroscopy Techniques. S. P. Scheidt[1], N. Lancaster[1], and M. S. Ramsey[2], [1]Desert Reseearch Institute, 2215 Raggio Parkway, Reno, NV 89512, sscheidt77@gmail.com. [2]Department of Geology and Planetary Science, University of Pittsburgh, Pittsburgh, PA.

Introduction: The Gran Desierto in Sonora, Mexico, currently the largest active sand sea in North America, is an important aeolian depositional system wherein a number of possible local- to regional-scale sand transport pathways exist for sources of sand of varied composition. Dune morphology has been extensively studied to explain the history of the dune field [1,2,3,4]. The composition of sands in the Gran Desierto have been studied using geochemical and grain-size analysis at its margins [6] and in other regional aeolian deposits [e.g., 7,8]. These studies suggest that the sands of the Gran Desierto were sourced from the ancestral bed load of the Colorado River [9].

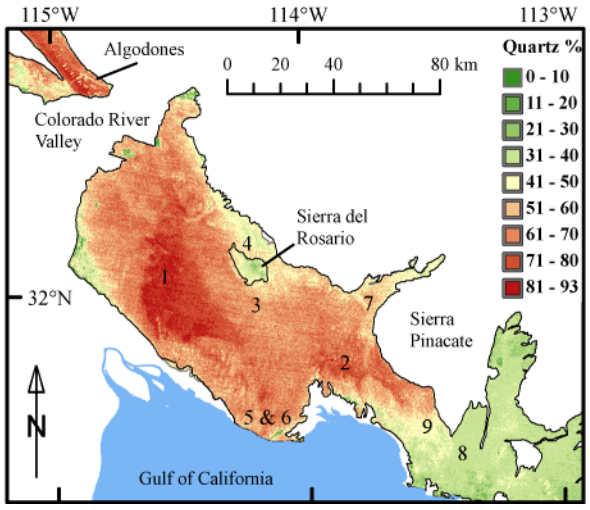

Figure 1. Map of the Gran Desierto dune field showing ASTER derived quartz abundance, which is comparable to the quartz/feldspar ratio. Numbers correspond to laboratory retrievals of different dune areas (see Table 1.)

Determination of surface mineral composition in previous studies of Desierto dunes [9] and other areas using reflectance data were limited due to the spectral complications of VNIR remote-sensing [e.g., 10]. In the thermal infrared (TIR) wavelength region however, mixing of emitted radiant energy is linearly related to the areal abundance of major dune forming minerals (e.g., silicates, carbonates and sulfates), which have diagnostic spectral absorption features [e.g., 11,12]. Linear deconvolution of TIR emission spectra from remote sensing and laboratory spectroscopy has been used as an effective tool for extracting the mineralogical composition of both Mars and Earth surface materials, including sand dunes [e.g., 13,14]. The Advanced Spaceborne Thermal Emission and Reflection Radiometer (ASTER) instrument has high spatial resolution (90m) and multispectral capabilities (5 bands) in the TIR wavelength region (8.125 - 11.65 µm) [15]. Detailed compositional mapping can be achieved using the full spectral capabilities of ASTER, where linear spectral deconvolution of ASTER TIR data alone have been accurate and quantitative [e.g., 16,17,18].

Geologic Setting: The majority of the dune field is located between the Colorado River Valley to the west; the Basin and Range Province to the north/northeast; and the shores of the Gulf of California to the south. East of the main dune field is the Sierra Pinacate volcanic complex, which is dominated by basalts. The center of the Gran Desierto overlies thick sequences of fluvial-deltaic sediments associated with the ancestral Colorado River.

There are several morphologic groups of dunes in the Gran Desierto which are hypothesized to be genetically different aeolian accumulations of different age and composition [1,2]. The major groups of dunes include a central core of star dunes, crescentic dunes that onlap the sand sheets and desert pavement to the west, linear dunes between the Sierra Pinacate and the Basin and Range, compound crescentic dunes north of the Bahia Del Adair, east and south of the Sierra Pinacate, and coastal parabolic and linear dunes to the southeast. Previously undescribed vegetated linear dunes are also distributed as far as 120 km southeast from the Sierra Pinacate along the coastal plain.

Approach: To accurately determine the spatial distribution of mineral composition (to within 3.1% [14]) of sand dunes in the Gran Desierto, this work describes a robust quantitative analysis of bulk mineralogy utilizing spectral deconvolution of both (1) a seamless, multispectral, radiometrically balanced mosaic of the ASTER TIR remote sensing data [18] and (2) high resolution thermal emission spectroscopy of aeolian sand samples using a Nicolet Nexus 670 spectrometer. Several field campaigns provided extensive coverage of surface (< 1 cm depth) sand samples, each representing a point measurement at the sub-pixel scale of the ASTER data. The spectra were acquired at a 2 cm^{-1} wavenumber spectral resolution between 2000

and 400 wavenumber (≈ 5-25 μm wavelength). A detailed description of the instrument and setup are found in [19]. The lab results were used for a detailed, systematic analysis of composition to select spectral end-members for ASTER data. The comparison of high resolution laboratory data to satellite data was critical to assessing accuracy of ASTER composition retrievals. Although of lower spectral resolution than laboratory data, the spatial continuity of mosaicked ASTER TIR data was critical to filling the gaps between the interpolations of field samples.

Results: Spectral end-members determined by laboratory analysis in decreasing order of average areal abundance are: quartz > plagioclase feldspar > potassium feldspar >> carbonate >> ferrohornblende. The interpolated laboratory data provide a moderate spatial resolution, hyperspectral TIR data cube from which the trends in bulk mineral abundance were revealed and comparable to ASTER retrievals of sand composition. Table 1 shows the bulk mineralogy lab results for different dune groups labeled in Figure 1.

Table 1. Normalized bulk mineralogy: quartz (Qt), total feldspar (Ft), plagioclase (Fn) and potassium feldspar (Fk). See Figure 1 for location references.

Region	Qt	Ft	Fn	Fk
(1) Central Dunes	78 ± 5%	22 ± 4%	22 ± 4%	--
(2) Eastern Crescentic	70 ± 4%	30 ± 5%	30 ± 6%	--
(3) Rosario (South)	59 ± 8%	41 ± 8%	38 ± 11%	3 ± 6%
(4) Rosario (North)	52 ± 8%	47 ± 10%	44 ± 13%	3 ± 6%
(5) Coastal (CO_3 rich)	59 ± 15%	41 ± 8%	36 ± 9%	5 ± 8%
(6) Coastal (Siliceous)	68 ± 5%	32 ± 3%	32 ± 3%	--
(7) Northern Pinacate	61 ± 11%	39 ± 11%	39 ± 8%	--
(8) Sonoyta Dunes	38 ± 7%	62 ± 6%	42 ± 12%	20 ± 16%
(9) Crescentic	56 ± 5%	44 ± 5%	34 ± 4%	10 ± 7%

Discussion: The laboratory and ASTER data results suggest that local feldspar-rich sources exert a much greater influence on sand composition than previously reported. The bulk of sand in the Gran Desierto can be described by a two sediment source mixing model between (a) quartz-rich Colorado River source material and (b) feldspar-rich local sources. Carbonate is a significant input for coastal sands. This sand composition model accounts for local feldspathic-rich sand input to dunes at the perimeter of the dune field, especially those close to the Sierra del Rosario and the Sonoyta River. These dunes have a high average feldspar abundance and closely resemble feldspar-rich aeolian sands from the Basin and Range in the Mojave Desert in their bulk composition (Ft > 40%) [7,8,14]. Variation in feldspar content also characterizes the Sonoyta Dunes, which have higher potassium feldspar content than other dunes in the sand sea. In the central portion of the dune field, a gradual compositional transition in the star dunes area can be seen in several remote-sensing datasets but is not detectable in the field. Our studies explained this transition as a gradational 30% increase in the quartz/feldspar ratio over a distance of 10 km from northeast to southwest across the star dune area. The high quartz/feldspar ratio in these dunes indicates a Colorado River sediment source (Qt > 75%) [7,8]. The highest quartz content (> 90%) was found in the western crescentic dunes. The eastern crescentic dunes averaged ~70% quartz.

Conclusions: The bulk mineralogy is characterized by: (1) quartz-rich Colorado River sediments and (2) feldspar-rich local sources. Feldspar-rich sources are similar to immature sands of the Mojave [7,8] supplied by the Basin and Range and the Sonoyta River, creating gradients of feldspar and quartz that reflect sediment transport pathways. These results suggest the importance of combining the advantages of hyperspectral point measurements and moderate resolution imager TIR data for Martian dune studies.

References: [1] Lancaster N. (1992), Sedimentology, 39, 631-644. [2] Lancaster N. (1995), Desert Aeolian Processes, pp. 11-35. [3] Beveridge C. et al. (2006), Sedimentology, 53, 1391-1409. [4] Ewing R. et al. (2007), Eos Trans. AGU, 88, abstract #NG41C-0673. [6] Kasper-Zubillaga J.J. et al. (2007), Earth. Surf. Proc. Land., 32, 489-508. [7] Muhs D. (2004), Geomorphology, 59, 247-269. [8] Zimbelman J.R. and Williams S.H. (2002), GSA Bull., 114, 490-496. [9] Blount G. et al. (1990), JGR, 95, 15463-15482. [10] Hapke B. (1981), JGR, 86, 3039-3054. [11] Thomson J.L. and Salisbury J.W. (1993), Rem. Sens. Environ., 45, 1-13. [12] Ramsey M.S. and Christensen P.R. (1998), JGR, 103, 577-596. [13] Bandfield J.L. et al (2002), JGR, 107, E11, 5092. [14] Ramsey M.S. et al. (1999), GSA Bull., 111, 646-662. [15] Yamaguchi Y. et al. (1998), IEEE T. Geosci. Remote., 36, 1062–1071. [16] Wright S.P. and Ramsey, M.S. (2006), JGR, 111(E8). [17] Katra I. et al. (2008), Geomorphology, 105(3-4), 277-290. [18] Scheidt et al. (2008), Rem. Sens. Environ., 112, 920-933. [19] Ruff et al. (1997), JGR, 102, 14899-14913.

TRANSVERSE AEOLIAN RIDGES AS SEEN IN HIRISE IMAGES. K. M. Shockey[1] and J. R. Zimbelman[1], [1]CEPS/NASM MRC 315, Smithsonian Institution, Washington, D.C., 20013-7012; Shockeyk@si.edu.

Introduction: Recent HIRISE images have allowed us to see surface features on Mars that have not been seen previously at the meter scale, with the highest resolution yet seen from orbit [1], though topographic data outside of HiRISE stereo pairs have yet to reach a comparable resolution. Photoclinometry is a tool that can allow us to derive a topographic profile for certain areas of selected portions of HiRISE images. HiRISE images have significantly influenced the study of transverse aeolian ridges (TARs) [2,3,4], which have been previously interpreted to be either dunes or ripples[5].

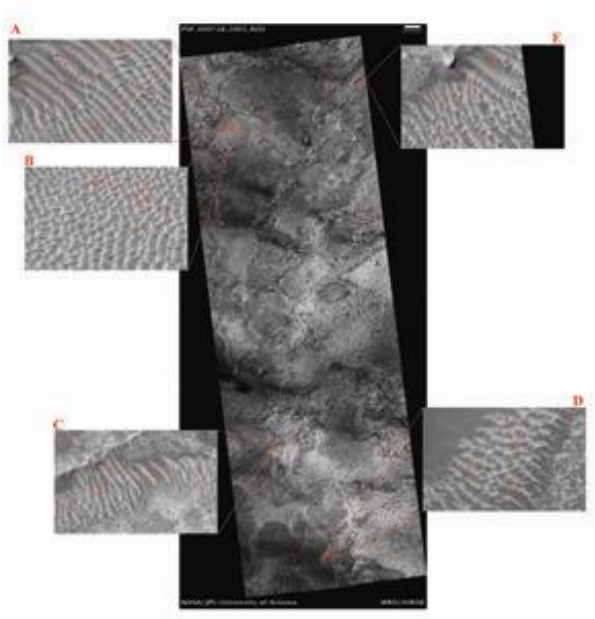

Figure 1: This HiRISE image (PSP-009718-2005) shows various types of TARs as classified by Balme et al. (2008) [4]. In this image, all the TARs would be under the classification of "influenced", which means that they are being affected by a topographic feature, in this case several breaks in slope. All the subsections, with the exception of C, would be under the classification of "networked", which refers to cross-cutting TARs. The subsection C would be under the classification of "forked", which appear to be a mix of linear and networked geomorphology**.**

Background: In our study, photoclinometry was used as a tool to extrapolate topographic profiles from HIRISE images. Before photoclinometry could be used, several assumptions needed to be made about the areas of interest [3]; 1) the albedo of the materials is constant along the entire line, and 2) the photometric properties of the surface materials are considered to be Lambertian, where reflected brightness is solely dependent upon the solar incidence angle to the surface. We also keep profiles relatively short (< 10s of meters) as a way to minimize errors due to possible albedo changes over larger distances.

Several classification systems have been used to describe TARs [2,3,5]. We use the classification system described by Balme (2008) [4] as the primary way to characterize the TARs examined in our study.

To date, we have used seven HIRISE images to create profiles in order to characterize TAR morphology. From these images we have extrapolated 49 individual profiles. Using these profiles, we quantified the width, height, and symmetry of each individual feature, and described the curvature of the TAR crest.

Methods: Figure 1 shows examples of multiple subsections taken of one HiRISE image to create multiple topographic profiles. The lines were consistently drawn from North and/or West to the South and/or East.

Width is measured from the basal break in slope from trough to trough across the TAR. The width would be measured from point A to point E horizontally, as seen in Figure 2. Height is measured from the crest to the midpoint (point C to halfway between A and E), in both the vertical and horizontal direction, between the troughs. This eliminates the need to remove effects of slope from the profile.

We quantified the symmetry by taking the same midpoint between the troughs, as used to measure height, and determined if the crest was directly over this point vertically. If the crest was directly over the midpoint, then the symmetry was assigned a value of zero. If the crest was not over the midpoint, then the horizontal distance between the crest and the midpoint was measured. If this result was negative, then the TAR was classified as left-leaning, with a positive result being classified as right-leaning, though this leaning direction is still somewhat subjective. The absolute value of the symmetry distance was divided by the width to give a scaled ratio. This ratio was used as a means to determine the amount of asymmetry for a TAR. The larger the ratio, the greater the asymmetry. Note that this symmetry analysis does not quantify things like breaks in slope along the sides of a feature.

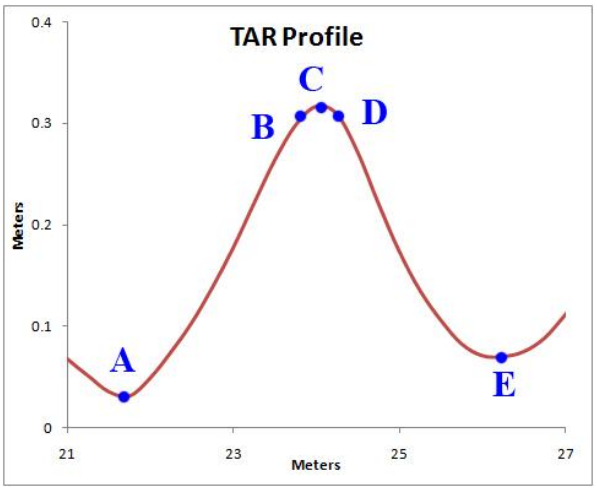

Figure 2: The above red line (left side of the image is pointing North) shows a profile for a TAR from HIRISE image PSP-009604-1725, centered at 7.4°S, 314.8°E. The five points in blue (A-E) indicate the locations on the profile used to determine the characteristics listed in Fig. 3.

$$Width = E_x - A_x$$

$$Height = C_y - \left(\frac{B_y - A_y}{2} + A_y\right)$$

$$symmetry = \frac{abs|C_x - \left(A_x + \frac{1}{2}width\right)|}{width}$$

$$crest\ curvature = \frac{Radius\ of\ Circle_{BCD}}{width}$$

Figure 3: The above equations relate to the points shown on Fig. 2.

To quantify the curvature of the crest of the TAR, three points are needed. The first point was at the crest (Fig. 2, point C). The other two points were to either side of the crest (Fig. 2, B and D), located where crest curvature merged with relatively straight flanks. Each of the two side points was equidistant from the crest. These three points were used to calculate a circle whose radius was then divided by the width of the TAR, which we call the curvature ratio (Fig. 3). The smaller the number, the sharper the crest.

Results: From the 49 profiles that have currently been assessed, we have compiled a summary of their morphologic characteristics. The average width for the TARs is 18.8 m, with a high of 44.75 m and a low of 2.25 m. The average height was determined to be 2.55 m, with a high of 9.68 m and a low of 0.27 m. For the curvatures ratio, an average of 17.7 was calculated. The high curvature ratio was 526.9 and the low was 0.09. A ratio for the symetry yielded an average of 2.2, a high of 2.7 and a low of 0 (perfectly symmetric).

Discussion: These small numbers for our results indicate that we are profiling TARs that were previously too small to characterize geomorpholigically like we are now doing. When compared to profiles of aeolian bedforms measured in the field [7], we hope that the measured Martian profiles will be able to constrain the probable origin of diverse TARs on Mars.

Conclusions: Through the use of HiRISE imagery, we have been able to expand on the work done by Wilson and Zimbelman (2004) [6]. Comparing our geomorphologic results to theirs, it is found that the average wavelength in our study is approximately half of what was obtained previously. This is an indicator that using HiRISE instead of MOC allows us to see features that are much smaller than previously imaged. We were able to further study the shape of the individual TARs and their given characteristics by use of photoclinometry. This gives us the highest resolution topography available.

Expanding on their geomorphologic studies and adding the classification system determined by Balme et al. (2008) [4], we are able to better understand the processes that form these TARs such as the surficial wind directions and how active they are.

Future work will include studying more HiRISE images to have a more comprehensive coverage of the Martian surface. We will also include studies of whether these features are considered to be active or not, as well as how degraded they may be. Pairing our work with these other studies will allow us to asses and understand these features better.

References: [1] McEwen et al. (2007) JGR [2] Shockey K. M. and J. R. Zimbelman (2010) *LPSC XXXXI*, Abstract #1423. [3] Zimbelman J. R. (2009) *Geomorph.*, in press. [4] Balme M. et al. (2008) *Geomorph, 101*, 703-720. [5] Shockey K. M. and Zimbelman J. R. (2008) *LPSC XXXIX*, Abstract #1686. [6] Wilson S. A. and Zimbelman J. R. (2004) *JGR 109*, E10003. [7] Zimbelman J. R. et al. (this volume).
[Supported by NASA MDAP grant NNX08AK90G]

RIPPLE MIGRATION ON ACTIVE DUNES IN NILI PATERA (MARS). S. Silvestro[1], L. K Fenton[2], D. A. Vaz[3], N. Bridges[4] and G. G. Ori[1,5] [1]International Research School of Planetary Sciences, Viale Pindaro 42, Pescara, Italy, [2]SETI Institute, NASA Ames Research Center, CA, USA, [3]Centre for Geophysics, University of Coimbra, Portugal, [4]Applied Physics Laboratory, Laurel, MD, USA, [5]Ibn Battuta Centre, Universitè Cadi Ayyad, Marrakech, Morocco.

Introduction: Recent studies have documented active sand movement Mars. These includes the deflation of several dome-like dunes in the North Polar Erg [1] and in Meridiani Planum [2], and the identification of sand avalanche scars on dark dune slip faces in the Proctor [3] and in the Rabe crater ergs [4]. In contrast, up until this study, definitive evidence of bedform migration was limit to a single observation by the Spirit rover at Gusev crater (~2 cm in 5 martian sols) [5].

Images from the HiRISE camera on the Mars Reconnaissance Orbiter (MRO) have revealed that, as on Earth, wind ripples are common on dune surfaces [6]. In this work we focused our attention on these features and in other subtle changes observed in the shape of several crescentic dunes in Nili Patera (8.6°N; 67°E) in a time span of less than four terrestrial months (between the 30 of June and the 13 October 2007.

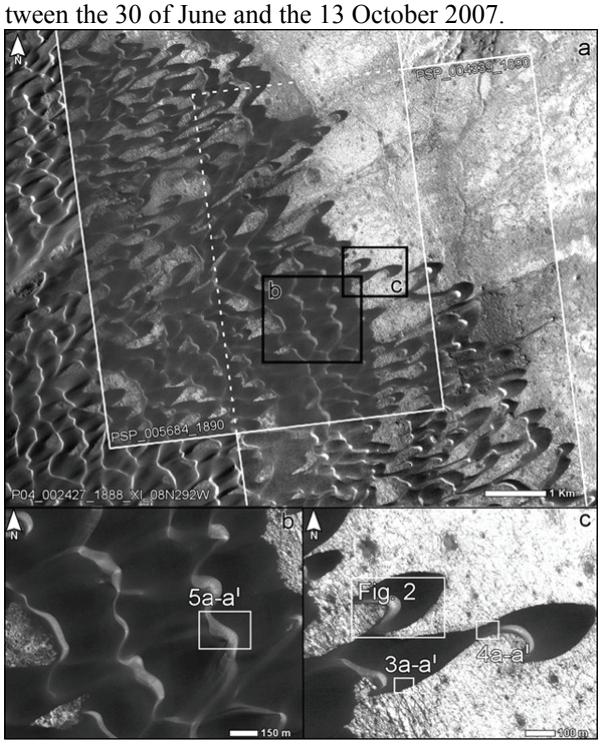

Fig. 1. Location map of the study area

Methods: Two overlapping HiRISE images (PSP_004339_1890 and PSP_005684_1890) were processed and co-registered with the CTX P04_002427_1888_XL_08N292W (Fig. 1) into a Geographic Information System (GIS) environment. The HiRISE have been acquired the 30 June and 13 October 2007 at Ls=267.5° (late autumn) and Ls= 330.0° (winter), respectively. A semiautomatic algorithm for ripple identification was used to extract ripple crests and to search for changing ripple patterns [7, 8, 9] (Fig. 2).

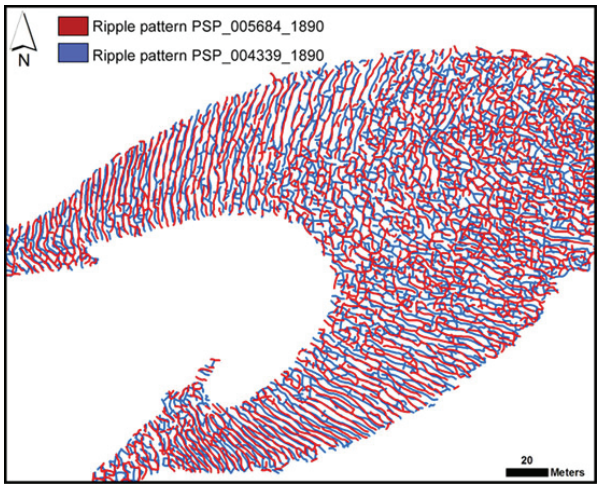

Fig.2. Examples of ripple patterns extracted by using the semiautomatic algorithm

Results: the results of our mapping suggest that widespread ripple migration occurred in the study area (Fig. 2). In particular, such movement is best evidenced in displacement of the Y junctions at the ripple crest terminations (Fig. 3a - a^{I}). Ripple crests are outlined in yellow and major modifications in blue. Assuming that the displacement of the ripple crests would be less than one crest wavelength, we calculated a migration of ~2 m toward the WSW.

Fig. 4a – a^{I} shows a significant change of albedo in the two images, highlighted by the red circles. We interpret this albedo variation to be due to the removal of the dark sand that saltates downwind suggesting that these dunes are undergoing major modifications of their shape.

Fig. 5a - a^{I} shows the variation of the rectilinear streaks over the dune slip face (see Fig. 1 for location). We interpret these features as new grainflow events [10] suggesting consistent dune activity between late autumn and winter.

Discussion: The changes in the position of the Y junctions and in the edges of the study dunes (Figs. 3, 4), indicate that sand transport occurred in the study

area. The ripple migration was likely forced by the same ENE winds affecting the whole dune field suggesting high stress winds blowing between late autumn and winter.

The capability of sand to move on the Martian surface has been discussed by [5] as a factor controlled by the pervasive indurations of the regolith and the frequency of wind events having sufficient energy to saltate sand. Ripple migration at this site suggests that dune surfaces are not heavily crusted or indurated and that saltation events, possibly caused by high-energy atmospheric phenomena like dust storms, are frequent enough to prevent the formation of a thick stabilizing crust.

The occurrence of new grainflow scars on dune slip faces in Nili Patera indicates that not only ripples, but also the whole dunes, are actually migrating.

Collectively, our results, indicate that sustained sand saltation occurred in the study area and that dark dunes in Nili Patera are active in present day atmospheric conditions.

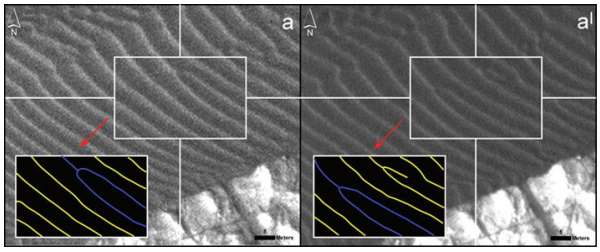

Fig. 3. Modifications of the ripple pattern in the study site. Ripples are outlined in yellow. Major changes in the ripple pattern are outlined in blue. HiRISE PSP_004339_1890; a^I, b^I, c^I) HiRISE PSP_005684_1890

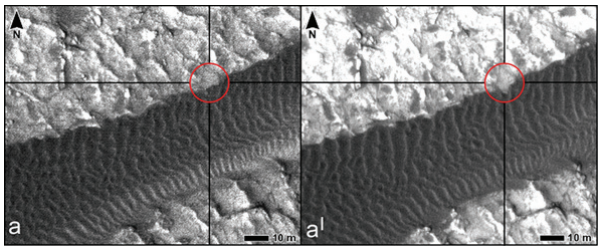

Fig. 4. Dune edges modifications. Major albedo change outlined by the red circles

Future work: a global searching for ripple movement and dune slip face avalanching is planned to better constrain the migration rate of the wind ripples and the geographical distribution of the active dark dunes and seasonal wind pattern on Mars.

References: [1] Bourke M. C. et al. (2008) *Geomor., 94,* 247-255. [2] Chojnacki M. et al. (2010) 41 LPSC, [3] Edgett K. S. and Malin M. C. JGR, 105, 1623-1650. [4] Fenton L. K. (2006) *GRL, 33,* L20201, doi:10.1029/2006GL027133. [5] Sullivan R. et al. (2008), *JGR, 113,* E06S07, doi:10.1029/2008JE003101. [6] Bridges N. T. et al. (2007) *GRL, 34,* L23205, doi: 10.1029/2007GL031445. [7] Pina P. et al. (2004), *L PS XXXV,* Abst. #1621. [8] Soille P., (2002). *Morphological Image Analysis- Principles and Applications, 2nd Ed.*, Sringer-Verlag, Berlin, 391 pp. [9] Vaz D. A. et al. (2008) *LPS XXXIX,* Abst. #1058. [10] Hunter R. E. (1977), *Sedimentology 24*, 3, 361-387.

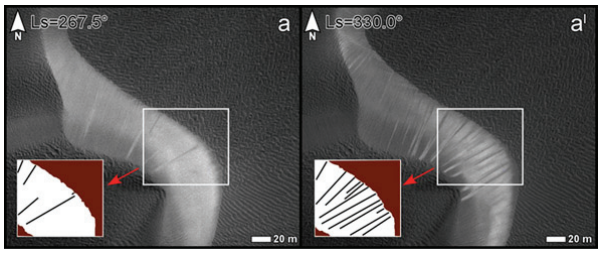

Fig. 5. Modifications occurred over dune slip faces. Several new grainflows (in black) occurred over the dune slip face (in white). Dune stoss side in brown. a) PSP_004339_1890; a^I) PSP_005684_1890.

Acknowledgments: We would like to thanks R. L. Kirk (USGS) and G. Di Achille (LASP) for their useful advices and comments.

MARS EXPLORATION ROVER OBSERVATIONS OF SAND SALTATION AND SAND-SIZED DUST AGGREGATES. R. Sullivan[1], P. Geissler[2], K. Herkenhoff[2], G. Landis[3], and A. Vaughan[2], [1]308 Space Sciences, Cornell University, Ithaca NY 14853 rjs33@cornell.edu. [2]U.S.G.S.-Flagstaff, AZ pgeissler@usgs.gov, kherkenhoff@usgs.gov, afvaughan@usgs.gov. [3]NASA-Glenn Research Center, Cleveland, OH geoffrey.a.landis@nasa.gov.

Introduction: Evidence for current sand movement on Mars is rare, compared with routine and regular dust lifting [1-8]. More examples of sand movement should be expected as the temporal span of our highest resolution observations continues to increase, but the overall picture likely will remain that downwind migration of dune crests is rare compared with dust raising [9]. However, wind tunnel experiments show that wind should initiate movement of sand-sized grains more easily than dust [10,11], so it has been paradoxical that winds routinely raising dust hardly seem to affect bedforms of more easily moved sand-sized grains. We address this issue by combining MER in situ evidence for sand saltation (including ripple migrations), observations revealing airfall dust as fragile sand-sized aggregates, observations of pervasive regolith cohesion (under mantles of loose dust aggregates where present), and histories of dust accumulation and clearing at both MER landing sites.

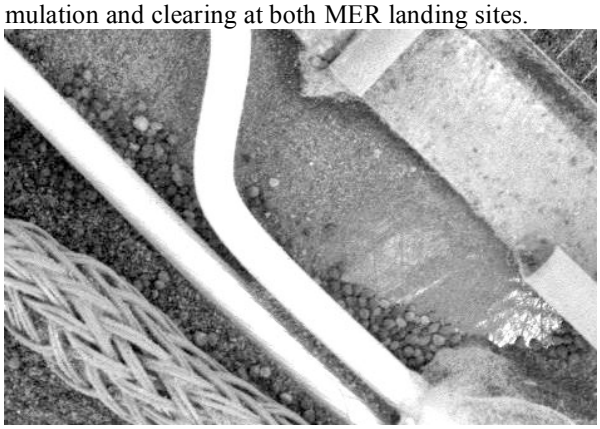

Figure 1. Spirit MI image of rover deck taken in shadow, showing sand grains up to 0.3 mm diameter. Area shown is 1 cm high.

MER Observations of Active Sand and Dust: Both rovers have observed evidence of sand mobility. Sand grains up to 0.3 mm diameter were recognized in MER Microscopic Imager (MI) views of the Spirit rover deck (Fig. 1), indicating saltation heights of at least 0.7 m [9,12]. Opportunity's pause at a dark wind streak outside Victoria crater revealed changes in drifts of ~0.1 micron sand [13]. Repeated imaging of Gusev soils during strong wind events associated with the 2007 dust storm showed ripple migration (Fig. 2)[9], redistribution of sand around rocks, and obliteration of sandy tracks nearby. Opportunity MI images acquired on sols 551 and 552 show movement of sand grains. Indirect evidence for recent saltation in the current surface environment is indicated by: (1) ripples of clean mafic sand on the floor of Eagle crater that are misaligned with indurated plains ripples outside the crater, but aligned with (i.e., perpendicular to) the transient wind streak extending from the crater's rim; and (2) the ripple field El Dorado at Gusev crater consists of sands with almost no cohesion which have remained considerably less dusty than surrounding terrain.

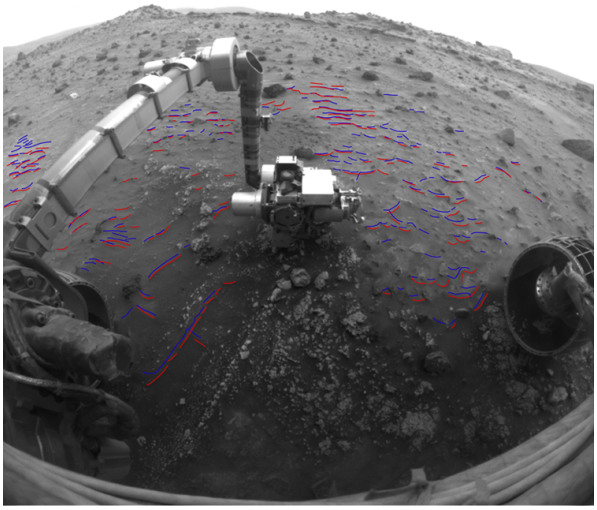

Figure 2. Front hazcam view showing 2 cm of ripple migration between sols 1260 (blue crests) and 1265 (red crests) at Gusev crater (image acquired sol 1265).

Dust particles suspended in the martian atmosphere typically are <4 μm in diameter [14,15], much smaller than MI resolution of ~31 μm/pixel. However, MI views show that dust mantling the surface commonly occurs as fragile, sand-sized aggregates of irregular shape, superficially resembling tiny popped corn (Fig. 3). The large size and low density of these aggregates should make them much easier to entrain than either <4 μm air fall dust, or hard (saltation-capable) sand-sized grains [9]. We have proposed that dust aggregates like those seen in MI views are widespread across dusty regions of Mars, and that they are the primary means—the "low-hanging fruit"—for wind to raise dust directly into the atmosphere [9]. Implicit in these ideas is that once the dust aggregates are entrained, they contribute to the suspended dust load by shedding suspendable smaller grains, perhaps breaking up completely into their <4 μm constituent particles.

The impressions of fragility in MI images suggest that these aggregates partially or totally disaggregate back into their clay-sized constituent grains during the violence of entrainment by a passing dust devil or a strong wind event (including disintegration from high-speed impacts with the ground). Tensile strengths of martian dust aggregates likely are much less than even the tiny magnitudes of the compressive pressures of MER Mössbauer touches, which easily crush and re-mold the aggregates into extremely high-fidelity castings [9, 16-17]. We therefore suggest that dust devils seen by Spirit—and by analogy dust devils elsewhere on Mars—must be raising a substantial fraction of their dust opacity by the relatively easy raising and rupturing of these fragile dust aggregates [9].

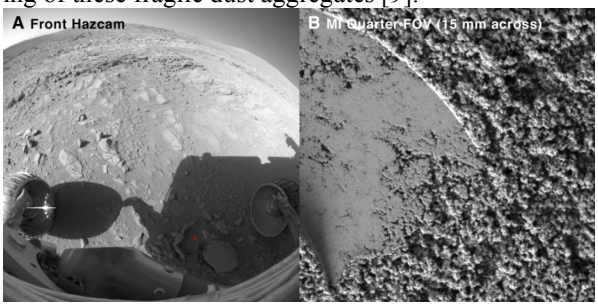

Figure 3. Mössbauer contact plate impression into dust mantle at Gusev crater. (A) front hazcam with red dot showing MI image location; (B) quarter-frame excerpt of MI image, ~15 mm across. Large, well-developed dust aggregates blanket the regolith. MI view shows where the Mössbauer contact ring touched the ground with ~1 N of force, completely and easily crushing the aggregates into ultrafine, unresolved particles that allow a high-fidelity casting of the smooth metal surface of the contact plate. (After Fig. 20 of [9])

A Dust Particle Cycle On Mars: The MER observations suggest that a dust particle cycle operates on Mars, in which <4 μm dust grains alternate between suspension as individual grains, and as components within very loosely-bound, much larger aggregates at the surface. How might individual dust grains migrate between these two states? Aggregate growth has been observed in wind tunnel experiments involving dust "rolling up" across the surface downwind [Rod Leach, personal comm., 1980s], and similar behavior has been observed on the MER Spirit rover deck [12]. On Mars it is unclear whether aggregate growth might initiate earlier, between <4 μm particles "colliding" while still suspended, due to electrostatic attractions (perhaps affecting fall-out rate). Some circumstantial evidence for this comes from wind tunnel experiments in which dust aggregates were observed to form from suspended dust in a martian environmental wind tunnel [18]. We speculate that dust aggregate growth would continue on the ground, facilitated by "jostling" of the growing aggregates by minor wind turbulence that is otherwise too weak to move the dust aggregates enough to destroy them. This scenario suggests that on the ground, the maximum dust aggregate size at any given place and time would be a function of: (1) local dust fall-out rate; (2) time interval between disturbances (e.g., between dust devil passages, and/or regional wind events); and (3) very local aerodynamic protection characteristics of the setting (e.g., exposed, sloping rock surfaces vs. small ground patches sheltered by surrounding rocks). At the surface, then, dust aggregate size and growth rate might change with time and overall size, perhaps approaching a limiting maximum diameter governed by inherent electrostatic bond fragility and the local conditions of dust abundance (functions, in turn, of local fall-out rate and time interval since the last major wind disturbance).

Conclusions: On a planet where hard sand grains are found at the surface along with fragile sand-sized dust aggregates, we should expect winds to be more successful mobilizing the dust (in its weakly aggregated form) than moving the sand. This is consistent with what has been observed repeatedly from orbit (lots of dust raised, not many dune movements).

Dust raising therefore seems much easier than suggested by the classic Iversen & White relationships [10] that have been applied to hard <4 μm dust particles, or to indirect raising of these dust grains by saltation of hard, sand-size grains. If the appropriate grain characteristics (sand-sized diameters and very low densities) are applied, however, the Iversen and White relationships and their successors predict much lower dust threshold-of-motion wind speeds.

References: [1] Zurek and Martin (1993) *J. Geophys. Res.*, *98*, E2, 3247-3259. [2] Cantor et al. (2002) *J. Geophys. Res.*, *107*, E3, 3-1 to 3-8. [3] Zimbelman (2000) *Geophys. Res. Lett.*, *27*, 7, 1069-1072. [4] Malin and Edgett (2001) *J. Geophys. Res.*, *106*, E10, 23,429-23,570. [5] Fenton (2006) *Geophys. Res. Lett.*, *33*, L20201. [6] Bourke et al. (2008) *Geomorph.*, *94*, 247–255. [7] Chojnacki et al. (2010) *LPSC XVI* #2326. [8] Silvestro et al. (2010) LPSC XVI #1820. [9] Sullivan et al. (2008) *J. Geophys. Res.*, *113*, E06S07. [10] Iversen and White (1982) *Sediment.*, *29*, 111-119. [11] Greeley and Iversen (1985) *Wind as a Geological Process*, Cambridge, pp. 76-82. [12] Vaughan et al. (2010) in preparation. [13] Geissler et al. (2008) *J. Geophys. Res.*, *113*, E12S31. [14] Pollack et al. (1995) *J. Geophys. Res.*, *100*, E3, 5235–5250. [15] Wolff et al. (2006) *J. Geophys. Res.*, *111*, E12S17. [16] Herkenhoff et al. (2004) *Science*, *305*, 824 – 826. [17] Herkenhoff et al. (2006) *J. Geophys. Res.*, 111, E02S04. [18] Merrison et al. (2007) *Icarus*, *191*, 568-580.

SPECTRAL ANALYSIS OF DARK DUNES IN KA'U DESERT (HAWAI'I): INITIALLY ALTERED TERRESTRIAL ANALOGS TO DARK DUNES ON MARS. D. Tirsch[1], R.A. Craddock[2], and R. Jaumann[1,3] [1]German Aerospace Center, Institute of Planetary Research, Rutherfordstrasse 2, 12489, Berlin, Germany. (Daniela.Tirsch@dlr.de); [2]Center for Earth and Planetary Studies, National Air and Space Museum, Smithsonian Institution, Washington D.C.; [3]Institute of Geological Sciences, Free University Berlin, Berlin, Germany.

Introduction: Unlike on Earth, dark basaltic dunes represent the majority of Martian eolian bedforms. There are only few places where basaltic dunes can be found on Earth, including New Zealand, Iceland, the western USA, Peru, and Hawai'i [1]. Is has been suggested that the Marian dunes sands are volcanic in origin because their mineralogical composition consists of pyroxene and olivine [e.g. 2, 3, 4]. The dark dunes in Ka'u Desert on the Big Island of Hawaii are located on the western flank of Kilauea volcano. The dark sands are derived from volcanic ash and reworked pyroclastic material [e.g. 1, 5, 6]. Thus, the Hawaiian dark sand dunes are an adequate analog to Martian dunes, particularly for testing the hypothesis of volcanic origin and to determine basic spectral characteristics that may be associated with differences in grain size and chemistry indicative of maturity and transport distances.

Methods: Samples of different dark dunes in Ka'u Desert were collected during a field trip in summer 2009. Several samples were taken from a large, dark vegetated parabolic dune (Fig. 1, sample 6), a falling dune (Fig. 2, sample 1), and a large dark climbing dune (Fig. 3, sample 2). The sand samples have a dark grayish color and are of fine- to coarse-grained sand sizes. We measured the samples with an ASD field spectrometer [7] in a laboratory. For each sample, we took 10 reflection spectra from 0.5 to 2.5 µm each consisting of 50 single measurements and created an average spectrum, which best reflects the mineralogical composition. We compared the terrestrial spectra with typical OMEGA [8] near-infrared spectra of different Martian dark dune fields.

Results and Discussion: Fig. 4 presents a comparison between spectra of Martian and terrestrial dark dunes and library spectra. The Martian OMEGA spectrum (black curve) reflects the basaltic composition of the dark dunes as it is typical for Martian dunes [cf. 10]. The spectrum shows a deep broad absorption band at 1 µm (slightly shifted to shorter wavelengths due to the mineral mixture) and a broad shallower band around 2 µm. Both bands result from Fe^{2+} in the minerals and are indicative of a mixture of olivine and pyroxene. The terrestrial spectra (sample 1, 2, 6) strongly reflect the olivine content of the dark sands as indicated by the deep broad absorption band at 1 µm. A pyroxene absorption around 2 µm is less obvious in sample 1 and 6 and seems to be overlapped by other features, although it still exists. The increase of the spectra to higher wavelengths, results from the alteration of these silica materials. Sample 2 strongly exhibits a narrow 2.2 µm-band, probably related to bending metal-OH-bounds, and a further absorption at 1.9 µm, which is generated by molecular H_2O in the minerals. Thus, a beginning aqueous alteration is obvious in the spectral shape of sample 2. The coarser grain size (1-3 mm) of this sample results in the decrease of the reflectance intensity and an increase of the absorption band depths [e.g. 11, 12]. We compared our sample spectra with library spectra (USGS and RELAB spectral database) of olivine, pyroxene, and iddingsite. The latter is a common alteration product of olivine on Earth, comprising phyllosilicates, iron oxides, quartz and calcite [13, 14]. However this library spectrum represents a sample which is in its initial alteration phase, as indicated by the lack of the 1.4 µm band and the weakness of the 1.9 µm water associated absorption band [14]. However it represents a good intermediate stage between unaltered and altered olivine-rich material.

Conclusions: The overall spectral shape of the terrestrial spectra reflects a basaltic composition of the sands similar to that of Martian dunes. The rock-forming minerals olivine and pyroxene form as the lava cools, and are commonly found in basaltic volcanic ash. The correlation in mineralogical composition of terrestrial and Martian dunes hints to a similar origin of the dark sands on Mars and Earth. The sources of the Ka'u Desert dune sands are ashes erupted from the volcanoes in the vicinity and lava disintegration particles [e.g. 1, 5, 6]. A similar volcanic ash origin for Martian dunes has been suggested by [4], who found dark layers of fine-grained materials exposed in impact craters and a material transport to the dark intra-crater dune fields. Based on the mineralogical similarities and the morphological evidence, the sources of the dark material on Mars are probably layers of volcanic ash [4]. Our initial analyses of the Ka'u Desert's dark dune sands support these findings. Since the terrestrial spectra show a beginning aqueous alteration of the dark sands these samples could be used to analyse alteration features of Martian dark dunes.

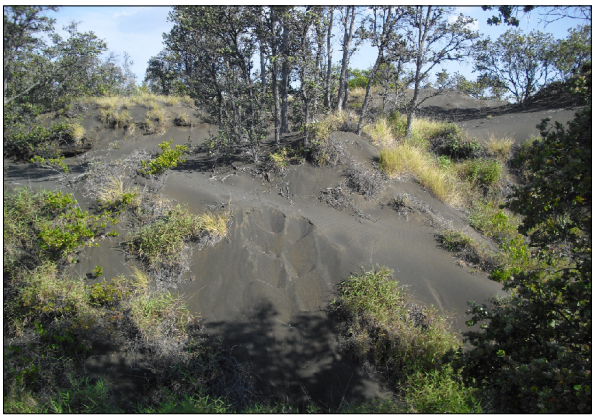

Fig. 1: Dark parabolic dune located off the Footprints trail at 19°21'17.52"N, 155°21'51.59"W (sample 6).

Fig. 2: Dark falling dune located off the Ka'u Desert trail at 19°19'29"N, 155°21'51.15"W (sample 1).

Fig. 3: Dark climbing dune located at the base of a small pali along the Mauna Iki trail at 19°20'39.43"N, 155°18'26.56"W (sample 2), (see also [9]).

Acknowledgements: This research has been supported by NASA's Mars Fundamental Research Program, Grant NNX09AC27G (Smithsonian Institution) and by the Helmholtz Association through the research alliance 'Planetary Evolution and Life'. We thank Edward Cloutis for friendly providing the RELAB laboratory spectrum of iddingsite.

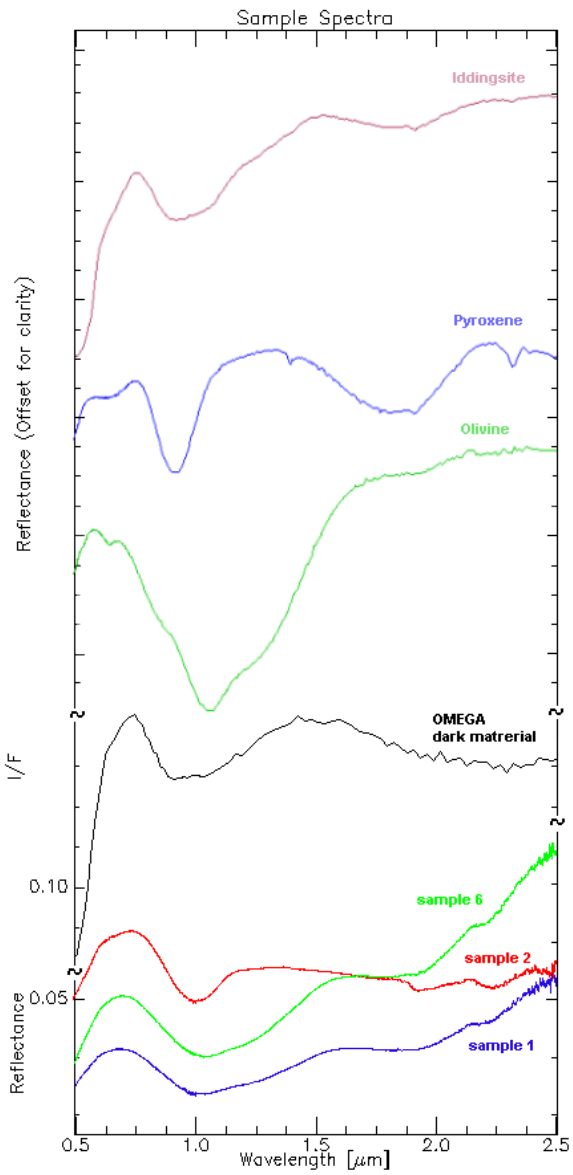

Fig. 4: Comparison of library, Martian and terrestrial spectra.

References: [1] Edgett, K.S. and Lancaster, N. (1993) J. Arid Eniron 25, 217-297.[2] Hoefen, T.M. et al. (2003) Science, 302, 627-630. [3] Bandfield, J. (2002) JGR,107, 10.1029/2001JE001510. [4] Tirsch, D. (2009) LPSC XL ,abst. #1004. [5] Stearns, H.T. (1925), Bull. Volcan., 2, doi: 10.1007/BF02719505. [6] Powers, H.A., (1948) Pacific Sci., 2, 278-292. [7] ASD (2000) FieldSpec® Pro User's Guide, Analytical Spectral Devices, Boulder, CO, USA. [8] Bibring, J.-P. et al. (2004), ESA Special Publication, 1240, 37-49. [9] Craddock R.A. et al. (2010) LPSC XLI, abst. #2164. [10] Tirsch, D. (2008) LPSC XXXIX, abst. #1693. [11] Gaffey, S. J. et al. (1993), in: C. Pieters and P. A. J. Englert (Ed.) Remote Geochemical Analysis: Elemental and Mineralogical Composition, pp. 43-77. [12] Poulet, F.et al. (2007), JGR, 112, doi: 10.1029/2006JE002840. [13] Orofino et al. (2006) PSS, 54, 784-793. [14] Cloutis, E.A. et al, (2004), LPSC XXXV, abst. #1265.

THERMAL INERTIA CHARACTERIZATION OF POSSIBLE NIVEO-AEOLIAN FORMATION IN OLYMPIA UNDAE, MARS. T. N. Titus[1] and G. E. Cushing[1], [1]U.S.G.S., Astrogeology Science Center, 2255 N. Gemini Dr., Flagstaff, AZ 86001, ttitus@usgs.gov.

Introduction: With the detection of a widespread water-ice table in the Mars polar regions [1,2] and the landing of the Phoenix Polar Lander, it is important to understand the thermal inertia and hydration states of both the north polar ice table and the top layer of soil that covers the H_2O ice table (hereafter referred to as ice table).

The presence of hydrated minerals, most likely gypsum, has been identified within part of Olympia Undae by the Mars Express (MEX) near-infrared imaging spectrometer OMEGA [3]. The Mars Reconnaissance Orbiter (MRO) Compact Reconnaissance Imaging Spectrometer for Mars (CRISM) has also mapped out these features [4].

During the site-selection process for the Phoenix Polar Lander, several studies estimated the depth to the ice table at the proposed landing site to be ~1 to ~10 cm [5]. In one of these studies, Bandfield [6] used multiple Mars Odyssey Thermal Emission Imaging System (THEMIS) observations to estimate depths to the ice table at high spatial resolution (~100 m); Bandfield found large variation of ice table depths at the 100 m scale.

Feldman et al. [7] have used both the Mars Odyssey Neutron Spectrometer (NS) and the Mars Global Surveyor (MGS) Thermal Emission Spectrometer (TES) observations to further constrain the ice composition distribution of Olympia Undae. They found Olympia Undae to be consistent with a 2-layer model where the bottom layer has 30% Water-Equivalent Hydrogen (WEH) and a desiccated top layer that is 9 g/cm^2 thick (6 cm if one assumes a density of 1.5 g/cm^3).

In this study, we use MGS TES temperature observations immediately following the springtime disappearance of seasonal CO_2 to estimate the depth to the ice table and the thermal inertia of both the soil and ice table within the Olympia Undae and the region of Vastitas Borealis south of Olympia Undae. The methodology used in this study is similar to that used by Feldman et al. [7], except we include temperatures from both the day and night, as well as temperatures from the season immediately following the disappearance of CO_2 ice. Feldman et al. [7] excluded the temperatures from both the daytime and the earlier seasons to minimize systematic errors caused by variations in surface and atmospheric conditions, such as dust opacity and albedo. However, by including these additional observations, we can estimate the underlying ice table thermal inertia.

KRC Model and TES Data: We used the MGS TES thermal bolometer brightness temperatures and solar albedo observations (Fig. 1) to constrain the depth of the soil overburden covering the ice table. We use a thermal model originally written by Hugh Kieffer, KRC [8], to fit the rise in both the 2 a.m. and 2 p.m. brightness temperatures following sublimation of seasonal CO_2 frost. This approach has proven successful in detecting both the presence of exposed H_2O ice and estimating the overburden for buried H_2O ice [9].

Several thermal models are generated for a range of soil depth, soil thermal inertia, and ice table thermal inertia values. We then use a least-squares best-fit approach to match the brightness temperatures with the model that provides an estimate of both the depth and thermal inertia of the soil and the thermal inertia of the ice table.

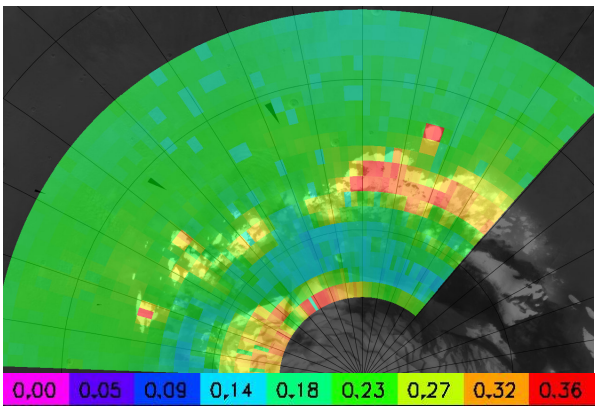

Figure 1: TES albedo overlaid on a MOC image of the Mars north polar region.

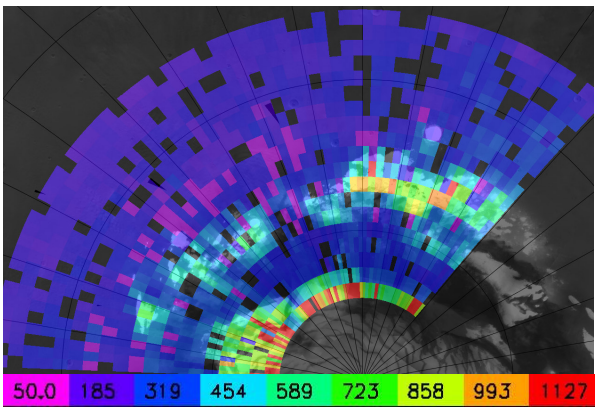

Figure 2: Model Results - Top layer thermal inertia.

Results: Estimates of the depth and composition of the soil and ice table, derived from the diurnal and seasonal temperature trends, are generally consistent with prior thermal and high-energy (neutrons and gamma rays) studies [10, 11, 12].

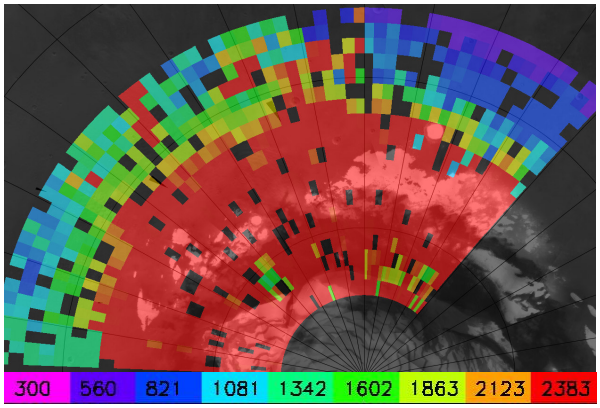

Figure 3: Model results - Bottom layer thermal inertia.

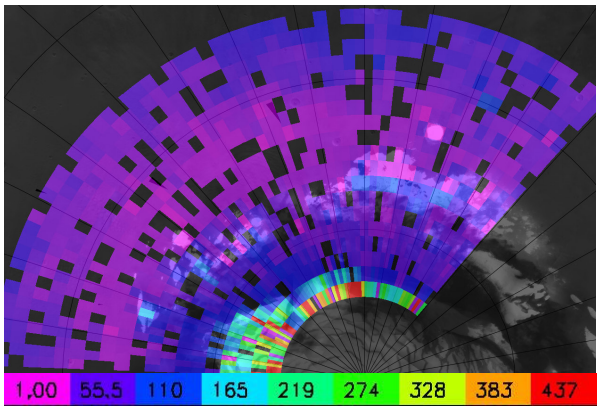

Figure 4: Model Results - Depth of the top layer in millimeters.

Thermal Edge of the Ice Table: Based on the results from the analysis of Phoenix Region B [12], the thermal edge of the ice table is approximately where the lower layer thermal inertia drops below 600 $Jm^{-2}K^{-1}s^{-1/2}$. Based on this criterion, the thermal edge of the ice table is ~67ºN latitude for the longitude range 140ºE-220ºE.

Thermal Properties of Olympia Undae: The thermal inertia of the top layers of Olympia Undae appears to be similar to that of lower latitudes within Vastitas Borealis which is ~200 $Jm^{-2}K^{-1}s^{-1/2}$. The depth of this top layer is generally thicker than the latitude zone just south of the polar erg with a depth of ~5-10 mm. This thicker, low-thermal inertia top layer of Olympia Undae is located near the same location that the NS observed a drop in Water Equivalent Hydrogen (WEH), which is consistent with a thicker desiccated top layer. The thermal inertia estimate of the lower layer is ~2400 $Jm^{-2}K^{-1}s^{-1/2}$, which is quite high, even for pure H_2O ice. NS results indicate that the lower layer is only 30% ice, which may suggest that the lower layer is sand cemented together with a briny ice, as opposed to pure water ice.

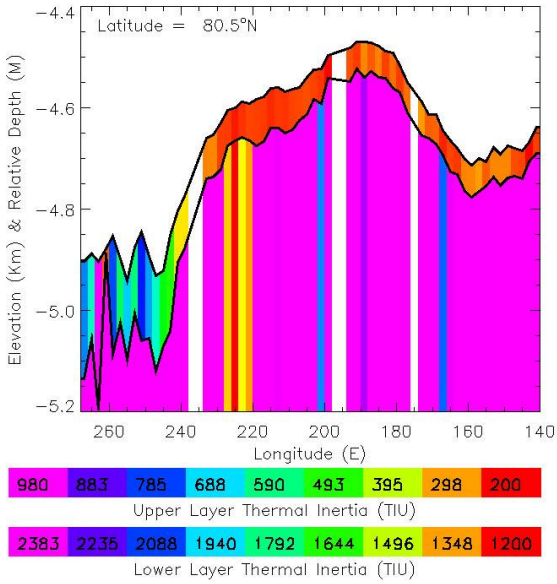

Figure 5: A cross-section profile of the topography, layer depth and layer thermal inertia, at latitude 80.5ºN. The topography is shown in km and the top layer depth is shown in meters. Notice that the thermal inertia of the two layers has different color bars.

Future Work: TES observations will be used to fit this two-layer model to the entire northern polar region. The variations in depth and thermal inertia will be compared to results from NS. The possibility that Olympia Undae is a niveo-aeolian feature will be explored, as well as the possibility of sand grains being cemented together with frozen brines.

References: [1] Boynton, W.V. et al. (2002) Sci., 297, 5578. [2] Feldman et al. (2002) Sci., 297, 5578. [3] Langevin et al. (2005) Sci., 307, 1584. [4] Roach et al. (2007) LPSC XXXVIII, Abstract #1970. [5] Mellon et al. (2008) JGRE, 113, CiteID E00A25 [6] Bandfield, (2007) Nature, 447, 64. [7] Feldman et al. (2008) Icarus, 196, 422-432. [8] Kieffer, H.H. (1977) JGR, 82, 4249-4291. [9] Titus, T. et al. (2003), Sci, 299, 1048-1051. [10] Titus et al. (2005) AGU Fall Meeting, Abstract #P31A-0197 [11] Titus et al. (2006) LPSC XXXVII, Abstract #2161 [12] Titus et al. (2007) LPSC XXXVIII, Abstract #1338.

Sand Sources and Transport Mechanics on Titan

Graham Vixie and Jason W. Barnes
University of Idaho, Department of Physics

Introduction

We are using *Cassini*'s Visual and Infrared Mapping Spectrometer (VIMS) to study Titan's sand. Specifically, we are constraining the sand's composition, how it is formed, and how it moves. The precise composition of the sand is still unknown. Water ice has been ruled out, leaving atmospherically-derived hydrocarbons as the best fit. The precise superposition of phases the compound is remains a mystery. Many dry lake beds have been found near and around the poles of Titan via *Cassini*'s RADAR [1]. Capitalizing on tidally driven global winds that are present on Titan [2], we present a new possible mechanism for creation and distribution of the sand.

Sand Sources

The sand itself is thought to be created out of hydrocarbons [3, 4]. Our proposed mechanism posits that sand could be formed in lake beds similar to the sand-formation process at White Sands, NM. As the methane/ethane [5] lakes dry out seasonally [6, 7], the crust of the leftover lakes begin to erode into smaller and smaller particle sizes until saltation is possible, giving birth to sand. As pointed out by Lorenz et al. [8], the winds are strong enough to carry sand-sized particles across the globe. The low gravity of Titan and density of the air help in bringing the required threshold of wind carrier speed down. Dry lake beds could quite possibly not be the only source of sand on Titan, given how much sand there is in the equatorial belt, but they could certainly contribute. The channels and fans present on Titan also put the erosion of lithified hydrocarbons into play as another sand source.

Sources of sand can be evaluated by matching the pure sand spectrum from Barnes et al. [4] to candidate terrains. We consider an area to be a sand source candidate if the spectral type for a given terrain matches the spectral unit for a known sandy area. We are evaluating several locations at present using publicly available data from the NASA Planetary Data System (PDS).

Substrates

The sand seas reside in the equatorial region of Titan. The longitudinal nature of the large expanses of dunes are evidence of the winds that shape Titan's middle. Tidally driven and seasonal winds are thought to be a mechanism by which the sand is brought from the polar regions to the equatorial.

The existence of different compositional substrates within this equatorial region raises several questions. First, why do the sand seas only reside at the equator and why don't they take up the whole equatorial region? Second, could the dunes be covering up the same bright terrain that makes up Xanadu, for instance? Are the darker albedo regions sand sinks, where the sand gets semi-permanently sequestered and forms a new type of hydrocarbon substrate? Also, within the sand dunes, there are sections of icy-substrates that lead in to darker dunes, acting as an intermediary from bright spectral types to dark. The global map of Titan using the VIMS-Visible data shows distinct boundaries between albedos.

Techniques

The map we present (Figure 1) uses three methane windows, 0.754μm, 0.827μm, and 0.937μm, from the VIMS-Vis channels to create a global scale RGB map using blue, green, and red to the respective wavelengths. Using part of an algorithm developed by Perry et al. [9] and employed in Stephan et al. [10], we create a map of pure haze using 9 channels from VIMS-Vis and divide this by our first optical wavelength map of Titan to remove the haze. The resulting map reveals just as much major surface contrast as IR maps as well as provides distinct boundaries between spectral types. Furthermore, the vis maps allow easy identification of water-ice dune substrates due to the greater spectral contrast between dunes and water ice at visible wavelengths.

With the aid of this map, we can use the contrast to match the dark areas of the sand seas in the equatorial belt to other place on Titan. The light blue spectral types may be areas that are producing sand that is then moved by the winds. Such locations may be southeast of Shangri-La, around Tsegihi, and south of Adiri. Other dark spots scattered over Titan may be active places of sand formation. Some active sites may include those north of Fensal, north of Belet, north of Xanadu, and also around Tsegihi.

Conclusion

Is the sand we see all that exists, or is that sand part of an ongoing, active near-surface hydrocarbon sand cycle

2

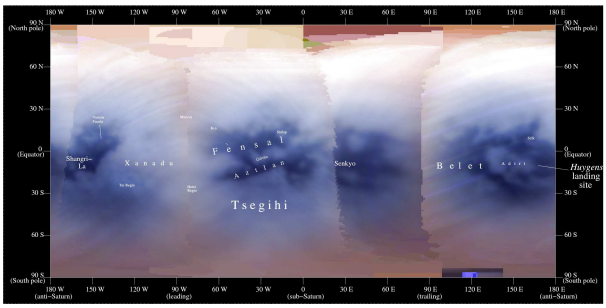

Figure 1: This is a global map of Titan done using an algorithm to "divide" out the atmospheric haze component. In doing so, the surface features and spectra of Titan become more pronounced. Removing some of the haze also brings out the striping effects that are inherent to the VIMS-V system. The differing colors represent different spectral types, allowing for identification of the icy substrates.

wherein sand is continuously being produced by erosion or wind? Then, from the active dunes in the equatorial region of Titan, does the sand become isolated and sink in the giant belt of the sand seas, get covered by blankets of ejecta, or get carried away by fluvial means? The winds are certainly strong enough to allow sand sized particles to circumvent Titan. Further VIMS coverage of the polar regions will aid in determining dry lake locations and spectral properties as well as provide most substrate comparison. This work is funded by a grant to JWB by the NASA Outer Planets Research program.

References

[1] E. R. Stofan, C. Elachi, J. I. Lunine, R. D. Lorenz, B. Stiles, K. L. Mitchell, S. Ostro, L. Soderblom, C. Wood, H. Zebker, S. Wall, M. Janssen, R. Kirk, R. Lopes, F. Paganelli, J. Radebaugh, L. Wye, Y. Anderson, M. Allison, R. Boehmer, P. Callahan, P. Encrenaz, E. Flamini, G. Francescetti, Y. Gim, G. Hamilton, S. Hensley, W. T. K. Johnson, K. Kelleher, D. Muhleman, P. Paillou, G. Picardi, F. Posa, L. Roth, R. Seu, S. Shaffer, S. Vetrella, and R. West. The lakes of Titan. *Nature*, 445: 61–64, January 2007. doi: 10.1038/nature05438.

[2] T. Tokano and F. M. Neubauer. Tidal Winds on Titan Caused by Saturn. *Icarus*, 158:499–515, August 2002. doi: 10.1006/icar.2002.6883.

[3] L. Soderblom, R. L. Kirk, J. I. Lunine, J. A. Anderson, K. H. Baines, J. W. Barnes, J. M. Barrett, R. H. Brown, B. J. Buratti, R. N. Clark, D. P. Cruikshank, C. Elachi, M. A. Janssen, R. Jaumann, E. Karkoschka, S. Le Mouèlic, R. M. Lopes, R. D. Lorenz, T. B. McCord, P. D. Nicholson, J. Radebaugh, B. Rizk, C. Sotin, E. R. Stofan, T. L. Sulcharski, M. G. Tomasko, and S. D. Wall. Correlations between Cassini VIMS Spectra and RADAR SAR Images: Implications for Titan's Surface Composition and the Character of the Huygens Probe Landing Site. *Planet. Space Sci.*, page Published online 2007 April 27, 2007.

[4] J. W. Barnes, R. H. Brown, L. Soderblom, C. Sotin, S. Le Mouèlic, S. Rodriguez, R. Jaumann, R. A. Beyer, B. J. Buratti, K. Pitman, K. H. Baines, R. Clark, and P. Nicholson. Spectroscopy, morphometry, and photoclinometry of Titan's dunefields from Cassini/VIMS. *Icarus*, 195:400–414, doi:10.1016/j.icarus.2007.12.006, May 2008. doi: 10.1016/j.icarus.2007.12.006.

[5] R. H. Brown, L. A. Soderblom, J. M. Soderblom, R. N. Clark, R. Jaumann, J. W. Barnes, C. Sotin, B. Buratti, K. H. Baines, and P. D. Nicholson. The identification of liquid ethane in Titan's Ontario Lacus. *Nature*, 454:607–610, July 2008. doi: 10.1038/nature07100.

[6] A. Hayes, O. Aharonson, P. Callahan, C. Elachi, Y. Gim, R. Kirk, K. Lewis, R. Lopes, R. Lorenz, J. Lunine, K. Mitchell, G. Mitri, E. Stofan, and S. Wall. Hydrocarbon lakes on Titan: Distribution and interaction with a porous regolith. *Geophys. Res. Lett.*, 35:9204–+, May 2008. doi: 10.1029/2008GL033409.

[7] O. Aharonson, A. G. Hayes, J. I. Lunine, R. D. Lorenz, M. D. Allison, and C. Elachi. An asymmetric distribution of lakes on Titan as a possible consequence of orbital forcing. *Nature Geoscience*, 2:851–854, December 2009. doi: 10.1038/ngeo698.

[8] R. D. Lorenz, S. Wall, J. Radebaugh, G. Boubin, E. Reffet, M. Janssen, E. Stofan, R. Lopes, R. Kirk, C. Elachi, J. Lunine, K. Mitchell, F. Paganelli, L. Soderblom, C. Wood, L. Wye, H. Zebker, Y. Anderson, S. Ostro, M. Allison, R. Boehmer, P. Callahan, P. Encrenaz, G. G. Ori, G. Francescetti, Y. Gim, G. Hamilton, S. Hensley, W. Johnson, K. Kelleher, D. Muhleman, G. Picardi, F. Posa, L. Roth, R. Seu, S. Shaffer, B. Stiles, S. Vetrella, E. Flamini, and R. West. The Sand Seas of Titan: Cassini RADAR Observations of Longitudinal Dunes. *Science*, 312:724–727, May 2006. doi: 10.1126/science.1123257.

[9] J. E. Perry, A. S. McEwen, S. Fussner, E. P. Turtle, R. A. West, C. C. Porco, B. Knowles, D. D. Dawson, and The Cassini Iss Team. Processing ISS Images of Titan's Surface. In S. Mackwell & E. Stansbery, editor, *36th Annual Lunar and Planetary Science Conference*, volume 36 of *Lunar and Planetary Inst. Technical Report*, pages 2312–+, March 2005.

[10] K. Stephan, R. Jaumann, E. Karkoschka, J. W. Barnes, R. Kirk, M. G. Tomasko, E. P. Turtle, L. Le Corre, M. Langshans, S. Le Mouèlic, R. Lorenz, and J. Perry. Mapping Products of Titan's Surface. In R. H. Brown and J. Lebreton and J. H. Waite, editor, *Titan from Cassini-Huygens*, pages 489–510, 2009.

Subsurface thermal effects of dune migration on Mars: Implications for ground ice stability. Stephen E. Wood[1], Stephen D. Griffiths[2], and Mary C. Bourke[3], [1]Dept. of Earth and Space Sciences, University of Washington, Box 351310, Seattle, WA 98195-1310 (sewood@ess.washington.edu), [2]Dept. of Applied Mathematics, University of Leeds, Leeds, LS2 9JT, UK (sdg@math.leeds.ac.uk), [3]Planetary Science Institute, 1700 E. Ft. Lowell, #106, Tucson, AZ 85719-2395 (mbourke@psi.edu).

The formation and migration of dunes on Mars may play an active role in modifying the state and distribution of water ice and salts in the regolith. Unconsolidated (loose) sand at typical Martian surface pressures has a thermal conductivity of ~0.03 W/m/K (the corresponding thermal inertia is 200 in MKS units, close to the Martian surface average). Estimates for the present-day planetary heat flux in the Martian crust range from 10 - 25 mW/m^2 [1,2]. Therefore the geothermal gradient in a sand dune – beneath the depth of the seasonal thermal wave (~1m) - could be as large as 0.8 K/m. Given that measured dune heights on Mars range up to 90m or more [3], this implies dunes moving over a surface could raise the temperature by up to 70K, depending on their speed or residence time. In areas where ground ice is present, this warming effect will tend to sublimate the ice and drive upward diffusion of water vapor into the dune where it may recondense. If hygroscopic/deliquescent salts with low eutectic temperatures are present within or beneath the dune sand - such as the perchlorate discovered by the Phoenix Mars Lander in soil at 68 N [4] – then the increased temperature and humidity could also lead to formation of liquid brines.

The rates of dune migration on Mars are unknown: theoretical modeling suggests they are potentially faster than on Earth [5] but the presence of ice in dunes may limit sediment transport through crusting and induration [6]. There is evidence of significant sand mobility in the current climate, even at high latitudes where three small dome dunes were observed to shrink or disappear over a period of 5 Mars years [7].

We will present results from a 1-D cryo-thermal model for the evolution of subsurface temperatures and ice content representing the scenario described above for a range of dune heights, migration speeds, and interior heat flux values.

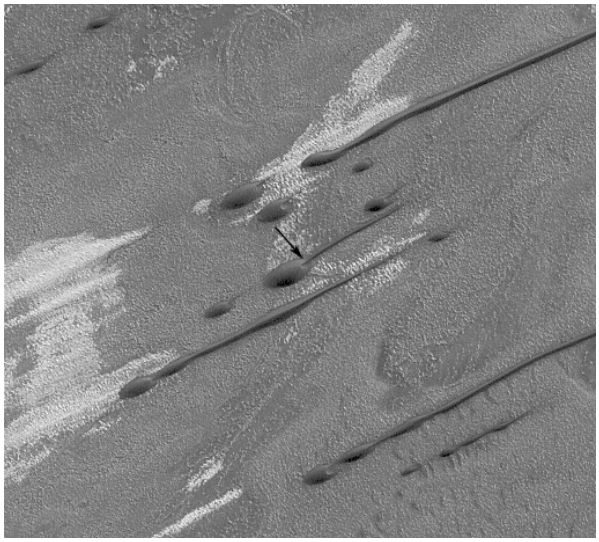

Figure 1. Rounded barchans and rectilinear dunes on Mars in Chasma Boreale near the north polar ice cap (83.9 N, 40.5W) – subframe of MGS MOC image E01-00104. Some barchans retain their "horns" which indicate sand transport direction is from the lower left to upper right. White patches on the surrounding surface are likely water ice.

References:

[1] Hauck, S. A. and R. J. Phillips (2002) *JGR,* 107, 5052. [2] Phillips, R. J. *et al.* (2008) *Science 320,* 1182. [3] Bourke, M. C. *et al.* (2006) *Geomorphology* 81, 440-452. [4] Hecht, M. H. et al. (2009) *Science* 325, 64-67. [5] Parteli, E. J. R. and H. J. Hermrmann (2007) *Phys. Rev. E* 76, 041307. [6] Bourke, M. C. *et al.* (2009) *Geomorphology* 109, 148-160. [7] Bourke, M. C. *et al.* (2008) *Geomorphology* 94, 247-255.

CROSS-SECTIONAL PROFILES OF RIPPLES, MEGARIPPLES, AND DUNES: A METHOD FOR DISCRIMINATING BETWEEN FORMATIONAL MECHANISMS. J. R. Zimbelman[1], S. H. Williams[2], and A. K. Johnston[1], [1]CEPS/NASM MRC 315, Smithsonian Institution, Washington, D.C. 20013-7012, zimbelmanj@si.edu, [2]Ed. Div., NASM, MRC 310, Smithsonian Institution, Washington, D.C. 20013-7012.

Introduction: The distinction between ripples and dunes, two very common aeolian landforms in desert environments, is a consequence of differing processes active in the generation and propagation of both features. Here we present topographic profiles of sand ripples, megaripples, and small sand dunes, measured perpendicular to the crest of each feature. This information provides a useful method for discriminating between ripples and dunes for transverse aeolian bedforms observed on other planets.

Methodology: Several procedures were used to measure topography for features whose dimensions range over more than three orders of magnitude. A simple but elegant procedure for generating detailed profiles of sand ripples [1] was used to document active sand ripples with wavelengths of ~10 cm at Great Sand Dunes National Park and Preserve (GSDNPP) in central Colorado (Fig. 1). Megaripples, with wavelengths up to several meters, were measured relative to a laser line projected above the feature (Fig. 2); we measured megaripple profiles at GSDNPP and several locations throughout the Mojave Desert region in the southwestern U.S. [2-7]. For sand dunes, we used Differential Global Positioning System (DGPS) [8, 9] surveys to measure profiles across active (Fig. 3) and stabilized (Fig. 4) transverse dunes throughout the western U.S. [7]. Precision varies with each method but in general, the shadow measurement technique [1] provides horizontal and vertical locations to better than ~0.2 mm, the laser profiling technique provides horizontal and vertical locations to better than ~0.5 cm, and the DGPS points are reproducible to <2 cm horizontal and <4 cm vertical [8, 9].

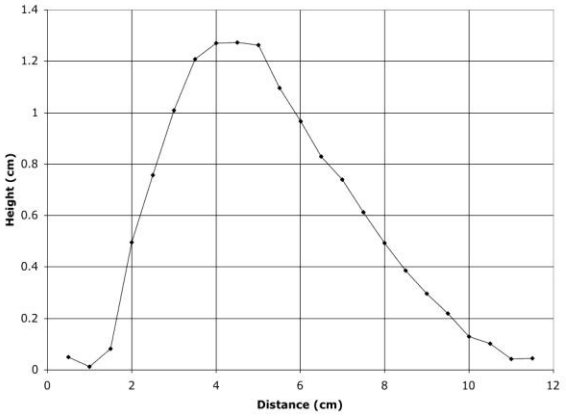

Figure 1. Profile across a sand ripple at GSDNPP, 9/18/03. Wind from the right. V.E. = 6.0X.

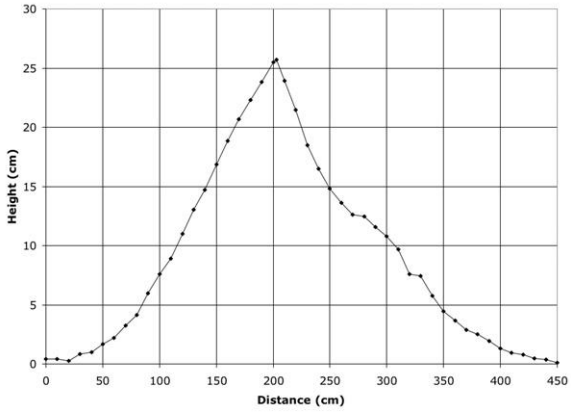

Figure 2. Profile across a megaripple coated with very course sand, GSDNPP, 9/20/02. Wind from the left. V.E. = 10.5X.

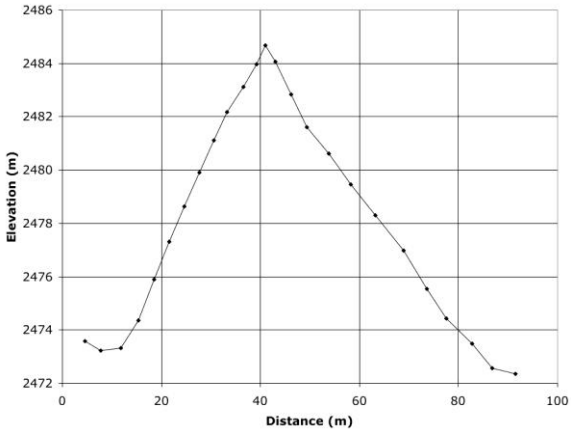

Figure 3. Profile across an active reversing sand dune, GSDNPP, 7/30/09. V.E. = 5.4X.

Results: The measured cross-sectional profiles show interesting similarities and differences between sand ripples, megaripples, and dunes. When all profiles (both distance and height scales) are normalized by the width of the feature (defined to be the breaks in slope at the base of either side of the feature crest), the shape of each profile is preserved while allowing for comparison of features of greatly different scale [10]. Sand ripples have a much broader, more rounded profile than profiles of either megaripples or dunes. The scaled height of megaripples is half that of either sand

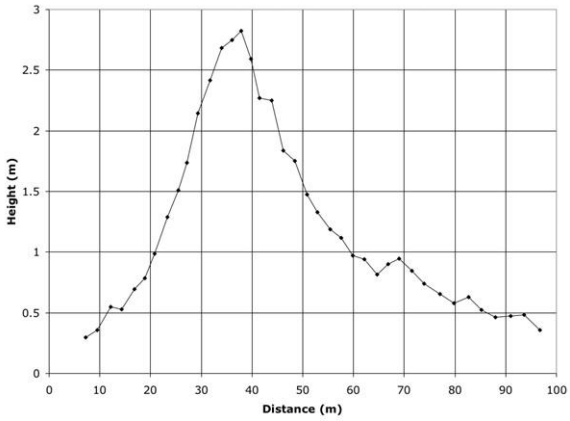

Figure 4. Profile across a stabilized transverse sand dune near Parker, AZ, 2/19/03. Wind from the left. V.E. = 24X.

ripples or dunes, and the megaripple profiles tend to be more symmetric than the profiles of either ripples or dunes (with the exception noted below). Dunes can have diverse profiles depending on the type of dune being studied; transverse dunes tend to have rounded overall shapes, stabilized transverse dunes have scaled heights that are half that of megaripples (and a quarter that of sand ripples or other dunes), and reversing dunes are the only dune type that yields profiles as symmetric as the profiles of megaripples.

Application to Mars: Measured field profiles were compared to profiles obtained through photoclinometry along transects from HiRISE images [10, 11] using the same width-scaling procedure described above [10] (Fig. 5). The HiRISE data reveals that Martian trans

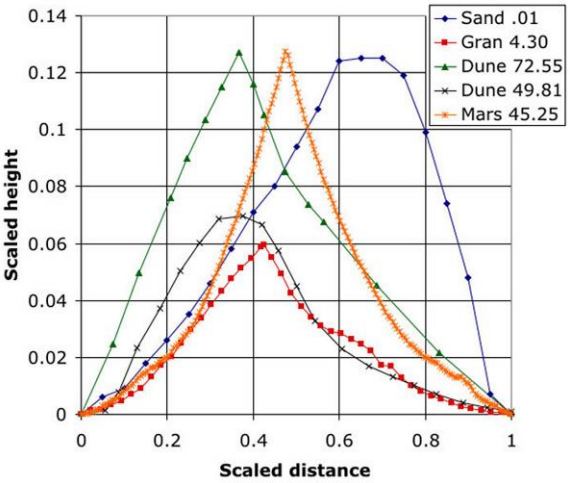

Figure 5. Profiles scaled by the width of the feature (widths, in m, indicated in inset box). 'Sand' is a sand ripple, 'Gran' is a granule-coated megaripple, 'Dune' (green) is a reversing dune, 'Dune (black) is an active transverse dune, 'Mars' is a TAR on Mars [10].

verse aeolian ridges (TARs) have incredibly symmetric profiles [10, 11]. TARs with (unscaled) heights <0.5 m most closely match the profiles of megaripples, while TARs with (unscaled) heights >1 m are closely matched to profiles of reversing dunes [10, 11]. Additional measurements of TARs from HiRISE images are underway [12], and it is hoped that the additional data will help to clarify where large megaripples and small reversing dunes may be distinguished on Mars.

Conclusions: Measurements of the cross-sectional profiles of sand ripples, megaripples, and small sand dunes provides a useful tool for attempting to discriminate between formation by ripple and dune processes. HiRISE images of Mars are sufficiently detailed that it now seems likely that most TARs on Mars can be distinguished as either megaripples or reversing dunes.

References: [1] Werner B.T. et al. (1986) Geology 14, 743-745. [2] Williams S.H. et al. (2002) LPS 33, Abs. 1508. [3] Wilson S.A. et al. (2003) LPS 34, Abs. 1862. [4] Zimbelman J.R. and Williams S.H. (2005) Spring AGU, Abs. P32A-4, JA363. [5] Zimbelman J.R. and Williams S.H. (2006) LPS 37, Abs. 2047. [6] Zimbelman J.R. and Williams S.H. (2007) GSA Aba Prog. 39(6), Abs. 218-5. [7] Zimbelman J.R. and Williams S.H. (2007) in The Geology of Mars (M. Chapman, Ed.), Cambridge Univ. Press, 232-264. [8] Zimbelman J.R. and Johnston A.K. (2001) in Volcanology in New Mexico, NM Mus. Nat. Hist. Sci. Bull. 18 (L.S. Crumpler and S.G. Lucas, Eds.), 131-136. [9] Zimbelman J.R. and Johnston A.K. (2002) NM Geol. Soc. Guidebook, 53rd Field Conf., 121-127. [10] Zimbelman J.R. (2009) 7th Int. Conf. Geomorphology, Melbourne, Aust., \Papers\236.pdf. [11] Zimbelman J.R. (in press), Geomorphology, doi: 10.1016/j.geomorph.2009.05 .012. [12] Shockey K.M. and Zimbelman J.R. (this volume).

[Supported by NASA MDAP grants NNG04GN88G and NNX08AK90G]

NOTES